POLITECNICO DI MILANO

Facoltà di Ingegneria Meccanica

Master of Science in

Mechanical Engineering

Application of Li-ion cell ageing models on automotive electrical propulsion cells

Supervisor: Prof. Francesco Braghin

Co-supervisor: Davide Tarsitano; Ferdinando Mapelli

MSc Thesis of:

Zhi Zhang ID. 780987

Academic Year 2012 - 2013

CONTENT

List of Figures

List of Tables

Abstract:

Nowadays power is a very important characteristic for the vehicle and large-capacity batteries can produce higher power for the electrical vehicle in which the speed or the maximum load of the electrical vehicle will be increased absolutely. But most lithium-ion batteries are produced in small format with a capacity range from 100mA to 10A. They are applied in daily use such as cellphone and very few large format lithium-ion batteries have been researched. With the increasing demand of the electrical vehicles, large-capacity batteries are becoming more and more accepted by car-marking factories.

The extensive use of batteries in hybrid electric vehicles (HEVs) today requires establishing an accurate model of battery aging and life. During a battery's lifetime, its performance slowly deteriorates because of the degradation of its electrochemical constituents, they experience power and energy fade associated with impedance rise and capacity loss, respectively. Capacity decrease and power fading do not originate from one single cause, but from a number of various processes and their interactions. Moreover, most of these processes cannot be studied independently and occur at similar timescales, complicating the investigation of ageing mechanisms. Identification of key aging parameters in lithium ion battery models can validate degradation hypotheses and provide a foundation for State of Health (SOH) estimation. Battery manufacturers usually provide aging data that will show this degradation. However the data they provide result from steady state tests, in which the battery is discharged and charged thousands of times with constant current profiles (or cycles). The current and the Depth of Discharge (DOD) in the vehicles will depend completely on the real application. Using these data many aging models have been developed that relate the maximum number of battery cycles to the DOD of the current profile used.

The identification of aging and degradation mechanisms in a battery in real-life operation has been a long-desired yet challenging goal in battery and practical

applications. Most of Li-ion ageing mechanisms have been experimentally identified and described in literature. Nevertheless, Li-ion ageing mechanisms are complex and can interact with each other resulting in different evolution shapes for capacity loss and power fade. Battery aging and degradation often encounter multiple complex and coupled physical‐chemical processes in complicated operating conditions, including dynamic duty cycles, temperature/thermal effects, time between operations, and other environmental factors. To quantify aging and degradation effect accurately is not a simple task either. Even if a vigorous test plan can reveal how much capacity is lost in a life cycle test, the result is insufficient to either provide detailed information on degradation mechanism or predict how much loss will occur under a different regime.

This thesis has performed a Life Cycle Assessment (LCA) of a 60Ah lithium-ion (TS-LFP60AHA (A)) battery which is expected as the power source for hybrid electrical vehicles (HEVs) or full electrical vehicles (FEVs). The simulation tool MATLAB is employed to examine the behaviors of batteries and control the running of other electrical devices. To complete the test, a discharge-charge system will be designed to perform the cycling. The test bench will include battery charger, discharge system, data acquisition system, battery and computer. All the cycles will be in the constant-current (CC) situation. The stations assembled can charge and discharge the battery automatically. At the end of each cycle, test parameters (time, temperature, Voltage, current) will be saved in the computer with the name of the cycle number. The effects of test parameters were investigated and described in the following steps.

Several battery models are built to simulate the behavior of the battery and predict battery performance of cycles. The increasing resistance is widely accepted as a judgment for the aging of battery. From the trend of the discharge curve, the dynamic equivalent circuit model can be built, and the increasing resistance of the battery can be monitored as important parameter for aging. Secondly, the EIS (Electrochemical Impedance Spectroscopy) is also a method for detecting the aging of the battery any of the mechanisms responsible for battery decay and ageing can be monitored and investigated non-destructively by the use of impedance spectroscopy. In the Nyquist

Plot, data collected in the EIS test can reflect that the curve of the impedance respected frequency becomes narrow. In my work, capacity and capacitance analysis are used to detect and predict the phenomenon of aging. During aging, capacity fade can be measured easily and the capacitance is inverse proportional to the slope of the discharge curve. So the model can be built easily and reflect directly the trend of the aging. The models are validated through comparison with real datasheet performance and with experimental data. After finishing building the models, these models will be used to predict the life of the battery by assuming a suitable end of life (80% of the initial capacity).

Most numerical models are built based on the small size lithium-ion batteries and my work is applying these models on the automotive electrical propulsion cells which have a higher capacity. In this scenario, various studies have attempted at investigating the effects of current/power demand and cycle life, as well as estimating the residual life of the batter. A set of computing processes are running concurrently to address power capability, efficiency of the battery, and capacity retention, which are represented by cumulative Ah-throughput. The objective of this project is to utilize data originally collected with the intent of analyzing aging of the high capacity battery to create an algorithm for predicting capacity retention for the purpose of predicting high-capacity battery life. The battery life predictions made by this algorithm should be reasonably accurate. Moreover, large amount of data collected in this the experiment can be regarded as the reference of the following experiments. Following tests will base on the influence of the temperature, evaluation of mechanical stress and vibration on battery behavior and life internal stress. This work will bring a good start for the research of lithium-ion for electrical vehicles in Polytechnic of Milan.

Keywords: *Lithium-Ion Batteries, Aging, Cycling, EV*

1. Introduction and Research Background

1.1 Outline of the thesis

In the first chapter, a general introduction of the electrification of transportation was given in addition to some information on different types of battery applications. After comparison of all the type of batteries, we show the reason for study on Li-ion battery. At the end of the first chapter, the important parameters (SOC, DOD, Life Definition and Efficiency) of Li-ion battery are discussed generally.

In Chapter 2, we show the research aim, aging phenomenon, as well as the influence of aging on the battery capacity and internal resistance. From the point of the chemistry, we explain the change of the cathode, anode, and the electrolyte of the battery during aging. Furthermore, the factors which have influence on the aging and life prediction from aging were also given. A brief literature review introducing the model and methodologies was given. For example, aging detection from the equivalent circuit model and electrochemical impedance spectroscopy, calendar aging and Shepherd empirical model. Some boundary condition and international standard of experiment are also introduced in the second chapter.

In the third chapter, we present the battery experimentation hardware and software structure as well as described some of the challenges in battery testing. The battery testing systems (charger, discharger, data acquisition system, and computer) that were described are used for the battery model coefficient identification which was used in later chapters to schedule the coefficients on the single cell battery models. The work that was done to develop the testing stations is believed to be a contribution in and of it and is thus archived in this thesis.

At the beginning of Chapter 4, measured information (current, voltage and temperature) will be extracted from the saved MAT data in the system. After identification of each phase in the cycle, the important parameters such as SOC, DOD, battery efficiency and capacity can be identified respectively in each cycle. In the

second part, we derived an analytical solution to the battery cell models to define the trend of the battery. 2 numerical models which based on the capacitance and capacity are built to fit for the data known. From the result of the fitting we can have a better understanding that whether the models are suitable for the large-capacity cells. With the built models residual life can be predicted and numbers of cycles needed to reach the end of life (EOF).

1.2 EVs and EVBs background

As part of the efforts to control anthropogenic greenhouse gas emissions, the replacement of internal combustion engine vehicles by electric vehicles (EV) stirs much scientific, political, and public interest. Depending on the electricity mix used, these vehicles harbor the potential for substantial emission reductions. In these automotive applications, batteries are capable of delivering tens or hundreds of kilowatts, hence necessitating large battery packs composed of multiple series strings of cells, and often involve multiple strings in parallel to increase the pack capacity as well as to decrease the aging severity of the current seen by each cell. The present study investigates several Li-ion batteries and highlights their environmental tradeoffs.

Figure 1 Electric Vehicle

1.3 Comparison between batteries

Lithium-ion batteries will play an important role in our mobility because of various advantages over other battery technologies such as the high specific energy and the high specific power, which are very important for HEV and FEV applications. In spite of these advantages there are some improvements (cycle life, calendar life and high degree of the safety) needed in order to make the lithium-ion technique more competitive in particular in terms of costs and lifetime. The ability to predict the lifetime of batteries is essential for the market introduction of lithium batteries in the electric vehicle market. But this key challenge is very complex because in this electrochemical system a number of aging processes take place parallel due to different stress factors which are caused by the varied operation conditions of the battery related to the drivers requirements.

Battery types	Advantages	Disadvantages
Lead - Acid	Can be designed for high power Inexpensive Safe Reliable	Poor Cold temperature Performance Short Calendar and Cycle Life
Nickel-Cadmium	High Specific Energy Good Cycle life compared with lead acid	Does not deliver sufficient power
Nickel-Metal Hydride	Reasonable Specific Energy Reasonable Specific Power Much longer cycle life than lead acid Safe Abuse-tolerant	High Cost Heat Generation at High Temperatures Low cell efficiency Need to control Hydrogen Losses
Lithium Ion	High Specific Energy High Specific Power High Energy Efficiency Good High temperature performance Low Self-Discharge	Needs Improvement in: Calendar and Cycle life Abuse Tolerance Acceptable Cost Higher degree of Battery safety
Lithium Polymer	High Specific Energy Has potential in providing high specific power Safe Good Cycle and Calendar Life	Only viable if: The cost is lower dramatically Specific Power is increased

Table 1 General Battery Differences [14]

1.4 Important parameters

In spite of intensive investigations on various positive and negative electrode chemistries, these aging phenomena are not yet well understood nor quantified, and the combined impacts of temperature (T), state-of-charge (SOC), depth of discharge (DOD), and current intensity (I) still remain difficult to quantify and manage. Accurate estimation of batteries life is also a great challenge in particular for lithium-ion batteries in traction applications because these batteries experience a very irregular pattern of charge and discharge cycles depending on the driver's driving and recharging habits. The requirements of the driver (power and energy demand) determine the operating conditions of the battery like current and voltage. But also other factors like the temperature distribution within the battery, the depth of discharge (DOD) and the state of charge (SOC) of the battery must be taken into account in the lifetime estimation. These operating conditions determine the stress factors which induce the aging and the rate of aging. A successful lifetime prediction requires knowledge of the aging processes, the stress factors and their relationships.

1.4.1 DOD and SOC Definition

DOD is defined as the amount of Amp-hours (Ahs) removed from a battery cell expressed as a percentage of the rated capacity. DOD is the opposite of State of Charge (SOC). For example, the removal of 25 Ah from a fully charged 100 Ah rated battery results in a 25% depth of discharge. Extensive research has been done in trying to relate the cycle life of a battery to the DOD the cycle achieves [19].

Assuming the cell to be fully charged at the time t=0, the cell capacity is Q_C, the extracted charge, $Q_e$is defined as:

$$Q_e(t) = \int_0^t I(\tau)\, d\tau \tag{1}$$

The State of charge (SOC) is:

$$\mathrm{SoC} = 1 - \frac{Q_e}{Q_c} \tag{2}$$

The Depth of Discharge (DOD) is:

$$\mathrm{DoD} = \frac{Q_e}{Q_c} \tag{3}$$

1.4.2 Battery Life Definition

The most common definition of battery life is as cycle life. This is easy and meaningful when the load history of the battery is regular, so that a "cycle" is always the same. However, in HEVs, the battery is not cycled on a regular basis, because the current history depends on the driving path. Thus, the definition of life as number of cycles would imply the designation of a "standard" or "equivalent" cycle, which would lead to non-intuitive results. For this reason, in this work the battery life $\mathrm{L_{tot}}$is expressed as a total amount of charge that can be drawn from the battery. The charge life of a battery can be derived from the cycle life using the following equation [19]:

$$\mathrm{L_{Ah}} = \mathrm{L_{cyc}} * \mathrm{DoD} * \mathrm{Ah_0} \tag{4}$$

$\mathrm{L_{Ah}}$ is the life expressed in Ah, $\mathrm{L_{cyc}}$ is the life expressed as number of cycles at the depth of discharge DOD, and $\mathrm{Ah_0}$ is the nominal capacity of the battery.

For example, for a 6.5 Ah battery,

$$L_{Ah}(DOD-10\%) = 5400cycles * \frac{10}{100} * (6.5Ah) = 3510Ah$$

$$L_{Ah}(DOD-20\%) = 2700cycles * \frac{20}{100} * (6.5Ah) = 3510Ah$$

$$L_{Ah}(DOD-30\%) = 1500cycles * \frac{30}{100} * (6.5Ah) = 2925Ah$$

1.4.3 Efficiency

A battery, as an electro-thermal system, encounters the same efficiency losses as all systems that deal with the laws of thermodynamics. When a battery is being discharged, the current seen at its terminals is downstream of all the electro-thermal losses encountered, starting from the charge migration from deep inside the plates, to the plate-electrolyte interface, through the electrolyte to the terminals, and out through wire of a certain gage. Therefore, to have the battery reach the same state of charge as before one started, one must put back more current than one pulled out.

Conventional wisdom (such that comes from mechanics and mechanic-oriented websites) states that automotive batteries should be recharged with 110% as much charge for the battery to reach the original state of charge. This efficiency that penalizes charging current from fully contributing to state of charge is called the Coulombic or calorimetric efficiency [43]. It is, however, sometimes neglected in computation if a reliable method to determine state of charge is not extant to determine this value empirically, and if it has not been provided by the manufacturer [7].

The efficiency will be

$$\eta = \frac{E_d}{E_c} \quad (5)$$

E_d: $Discharged\ Energy$

E_c: $Charged\ Energy$

2. Literature Review

2.1 Reasons for aging

Aging on cycling is often described as the result of degradation of active materials reversibility, especially the positive, coming from phase transformations during lithium insertion. This is beyond the scope of this paper to describe these mechanisms, which are extensively studied and published for many materials. In some cases, the fading rate may exhibit an inflexion point, where the capacity loss starts to increase, instead of decreasing [23]. When dismantling the cells, a large deposit of Li metal was observed, this was the reason for rapid capacity decay. In the same time, a strong increase in cell resistance is observed. There would be a specific point exhibiting a change in the slope of the capacity or resistance curves, probably when Li starts to plate significantly.

When induced, lithium plating itself will produce more deposit, and aggravates the phenomenon, which explains the increasing of capacity fading rate. Indeed, the electrode porosity is recognized as one of the first-order parameters controlling the capacity fade on cycling [24].

2.2 Aging Effect

The charging rate has obviously a strong influence on this behavior. Temperature decrease would accelerate the fading rate, lowering the limit at which the Li plating will occur, and for the same reasons increasing temperature in some limits would be beneficial. This is a tradeoff effect between lithium corrosion rate, which accelerates reduction of active area (negative effect of temperature), and concentration gradients producing high local current density (positive effect of temperature) [23].

2.2.1 Electrolyte

It is widely known from literature, that electrolyte decomposition and the corresponding formation of solid electrolyte interphase (SEI), is the dominant aging process in most graphite-based lithium-ion batteries during storage leading to capacity decline (due to loss of active lithium) and impedance rise (due to increase in film layer thickness). Theoretical derivations of the time dependency of the SEI growth rate are quite opposing [20]. Overcharging and over-discharging the battery leads generally to electrolyte decomposition. This results in a decreased electrolyte conductivity, which leads to an increase of internal resistance [27].

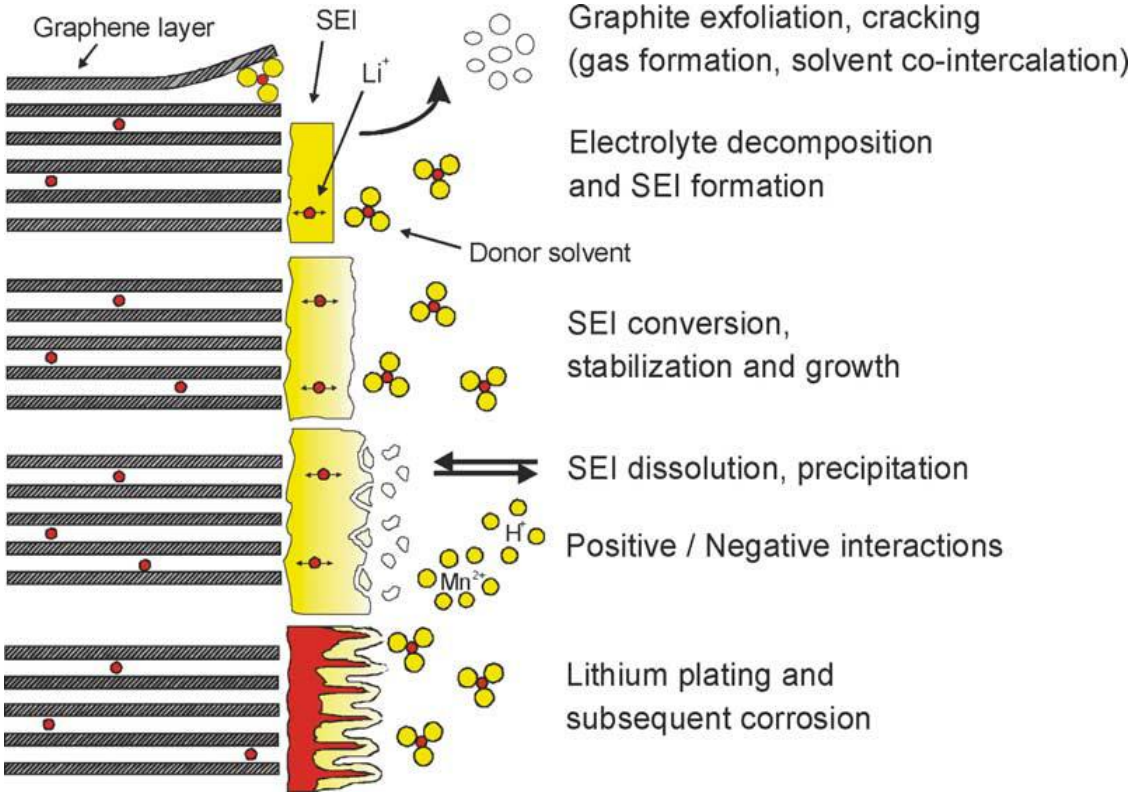

Figure 2 Changes at the anode/electrolyte interface

Changes at the electrode/electrolyte interface due to reactions of the anode with the electrolyte are considered by many researchers to be the major source for ageing of the anode. It is well known that lithium-ion battery anodes operate at voltages that are outside the electrochemical stability window of the electrolyte components. Hence, reductive electrolyte decomposition accompanied by irreversible consumption of lithium ions takes place at the electrode/electrolyte interface when the electrode is in the charged state. The decomposition products build up “protective layers” that cover the electrode’s surface. This process occurs mainly (but not exclusively) at the beginning of cycling, especially during the first cycle [2].

2.2.2 Negative electrode (Cathode)

The cathode was made of LiFePO4, a polyvinylidenefluoride (PVDF) binder and carbon black in slurry mixed with the solvent Nmethyl-2-pyrrolidone which was spread on an aluminum foil. The solvent NMP was dried off. NMP is volatile, flammable, expensive, easily absorbed by the skin and suspected to cause genetic and reproductive

damage. In the model it was assumed that no NMP is emitted to the environment [17].

2.2.3 Positive electrode (Anode)

The anode is generally made of graphite coated on copper foil about 14 mm thick. In addition a binder is needed. As with the cathode, the LCA data used for the anode ingredients was found in the Ecoinvent database. For the anode made with water a styrene butadiene latex binder was used. It was approximated with ABS, acrylonitrile butadiene styrene, from the Ecoinvent database. [13]

Chemical reaction happens on the positive electrode:

For Charging:

$$\mathrm{LiFePO_4} - xLi^+ - xe^- \rightarrow xFePO_4 + (1-x)LiFePO_4$$

For Discharging

$$\mathrm{FeP}O_4 + xLi^+ + xe^- \rightarrow xLiFePO_4 + (1-x)FePO_4$$

An additional SEI formation mechanism results from insertion of lithium into graphite layers. This causes an increase of the lattice volume. The surface film can be stretched and even destroyed. This damage is repaired by a chemical reaction that irreversibly consumes lithium, but thereby battery capacity decreases. In the case of lithium metal negative electrodes, growth of dendrites at small discharge currents can be observed. This leads to an increase of self-discharge. The probability of internal short circuit becomes higher [27].

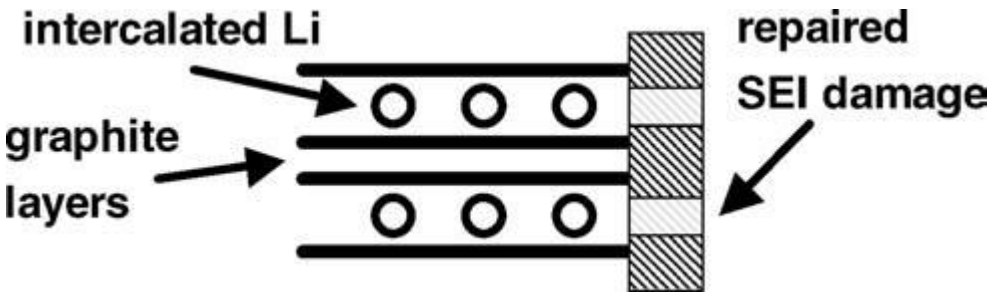

Figure 3 Surface film formation on graphite electrodes

2.3 Aging Models

2.3.1 Resistance Increasing in ECM

Between the low-level chemical modeling and the input-output heuristic-level modeling exists a compromise. It is possible to understand the chemical processes in the battery, and approximate their effects as the behavior of a lumped-model network of higher-level physical systems. In this section, we review a number of ways to reduce complex chemical phenomena to well-understood and well-behaved electrical-level circuit elements in creating a model.

In [31], many of the short-time and long-time processes inside batteries are identified and modeled. Figure 5 both lists the major dynamic processes inside batteries, and shows typical time scales on which they operate. An appreciation of these scales will be very useful when creating and using battery models.

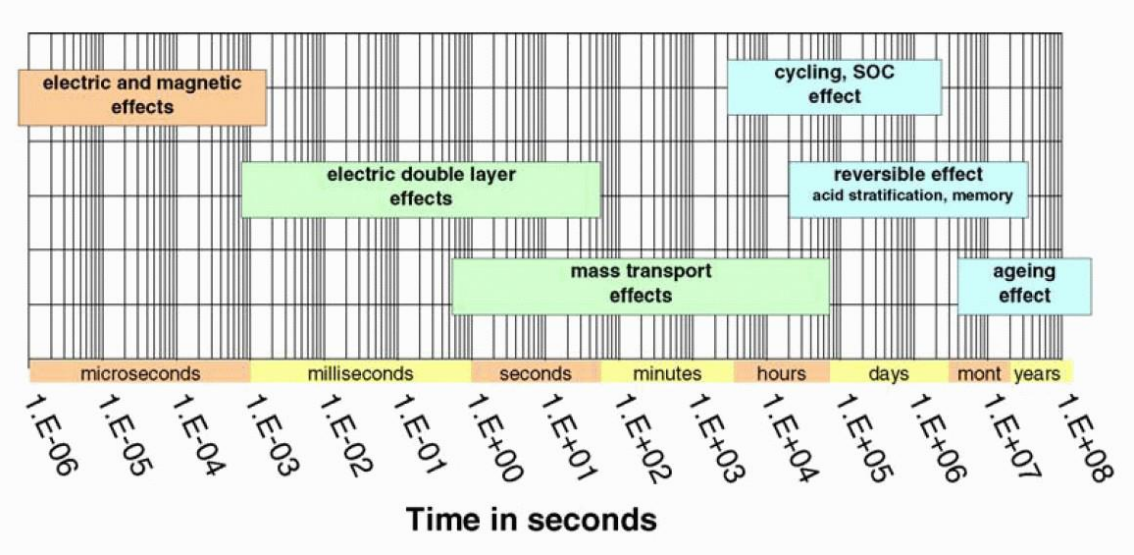

Figure 4 A listing of the major dynamic processes in batteries and their average time constants

The long-term processes such as irreversible aging, some reversible effects such as minor sulfation or acid stratification, and cycling processes vary greatly from battery to battery due to their dependence on how the battery is used. These effects are desired to be quantified for aging and prognostics studies of batteries and therefore must be

domain-specific. The model proposed, however, is not directly intended to model these effects but instead the shorter-time processes of mass transport, electric double-layering and charge storage, and electromagnetic processes. The technique of electrochemical impedance spectroscopy (EIS) was used here to observe these processes. This technique is another major topic of ongoing research for it may yield not only excellent battery models but may also allow predictive estimation of the states of the battery with respect to aging and other extremely long-term effects (viz., [19]). The technique has excellent primers elsewhere ([32]), but a briefly, the technique involves performing a frequency sweep of a complex system to compute its complex impedances using the amplitude and phase differences of the input and output signals. These complex impedances are then fit to a number of possible circuit models using least-squares, etc.

Diffusion processes occur in the active mass, the porous electrode, and in free electrolyte. They can be modeled using RLC elements either as a series of T-circuit ladders, as shown in Figure 5 and whose mathematics can grow unwieldy, or can be lumped into a Warburg impedance.

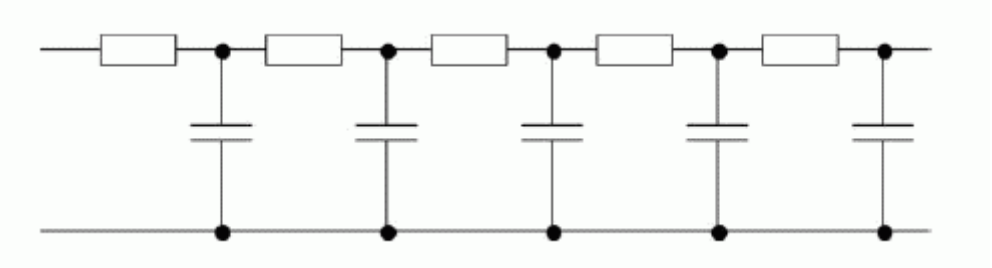

Figure 5 The RLC equivalent circuit needed to model diffusion effects

On a faster level is the double-layer capacitive effect, which many models stop at. This useful idea derives from the fact that charge must move from the solid electrode to the liquid electrolyte by crossing a charge-free region. This naturally warrants a capacitive description. A single layer turns out to be overly simplistic, as generally more than one of these capacitive layers form side-by-side: one right at the electrode-electrolyte interface and another beyond it.

This effect can be reduced to a simple electrical equivalent circuit. The parallel

circuit parameters vary by state of charge and temperature, and even battery age and current levels. (The series element is an ohmic resistance, discussed shortly.) Additional effects happen in this range when an electrode is porous (to maximize surface area, as is the case in automotive lead-acid batteries). During the following modeling, the ECM will be discussed in detail, so I just give a general introduction here.

2.3.2 Aging Detecting From Electrochemical Impedance Spectroscopy

Electrochemical techniques are very helpful for evaluation of batteries and cells during charge and discharge, and in service, as the nature of chemical and electrochemical processes occurring in these devices may be determined. Both traditional and an accelerated screening test method are necessary to analyze and compare battery properties, to obtain kinetic information, and to predict the likelihood of failure [16]. EIS maintains a high potential for 'on-the-fly' onboard vehicle battery assessment since it is relatively fast. The process can eventually be used as an approximation for reserve capacity and aging assessment to aid in prediction of future battery performance.

2.3.2.1 First Order Randle Model

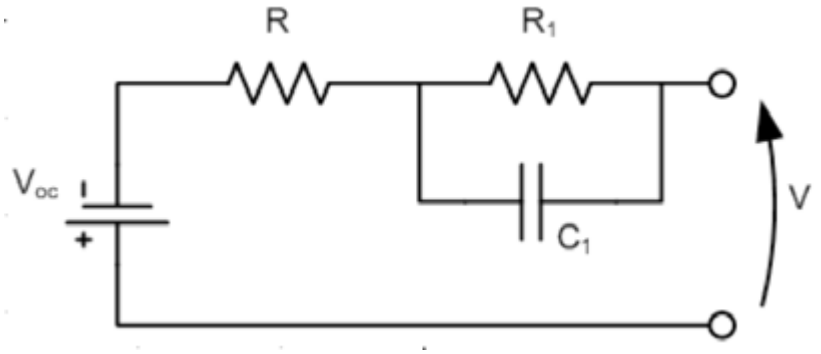

Figure 6 Equivalent circuit of 1st order Randle model

Assume the current going through resistance R_1 is i_R,

$$i_R = \frac{V_c}{R_1} \tag{6}$$

And the current on the capacitance C_1 is i_c

$$i_c = \frac{dV_c}{dt} * C_1 \tag{7}$$

The total current in the circuit will be:

$$\mathrm{i} = i_C + i_R \tag{8}$$

After the Laplace Transform, we can get the equation:

$$V_c(s) = \frac{R_1}{1 + C_1 * R_1 * s} * I(s) \tag{9}$$

So the final expression for the total circuit will be:

$$\mathrm{V(s)} = \mathrm{I(s)} * \left(R_0 + \frac{R_1}{1 + C_1 * R_1 * \mathrm{s}}\right) \tag{10}$$

So the transfer function between current and the voltage would be:

$$\text{Tranfer function} = \left(R_0 + \frac{R_1}{1 + C_1^2 * R_1^2 * \mathrm{w}^2}\right) + \frac{-C_1 * R_1^2 * \mathrm{w}}{1 + C_1^2 * R_1^2 * \mathrm{w}^2} * i \tag{11}$$

Assume that:

$$\mathrm{x} = R_0 + \frac{R_1}{1 + C_1^2 * R_1^2 * \mathrm{w}^2} \tag{12}$$

$$\mathrm{y} = \frac{-C_1 * R_1^2 * \mathrm{w}}{1 + C_1^2 * R_1^2 * \mathrm{w}^2} \tag{13}$$

The mathematic result of the model should be:

$$(\mathrm{x} - R_0)^2 + y^2 = R^2 \tag{14}$$

$$\mathrm{R} = \frac{R_1}{\sqrt{1 + C_1^2 * R_1^2 * w^2}} \tag{15}$$

When we increase the frequency of the system, we can witness the decreasing of the radius, if the frequency reach infinite, the radius is 0, oppositely, if the frequency were 0, the radius become the maximum that is R1. With the frequency range from the negative infinite to the positive infinite, the plot will be as the follows:

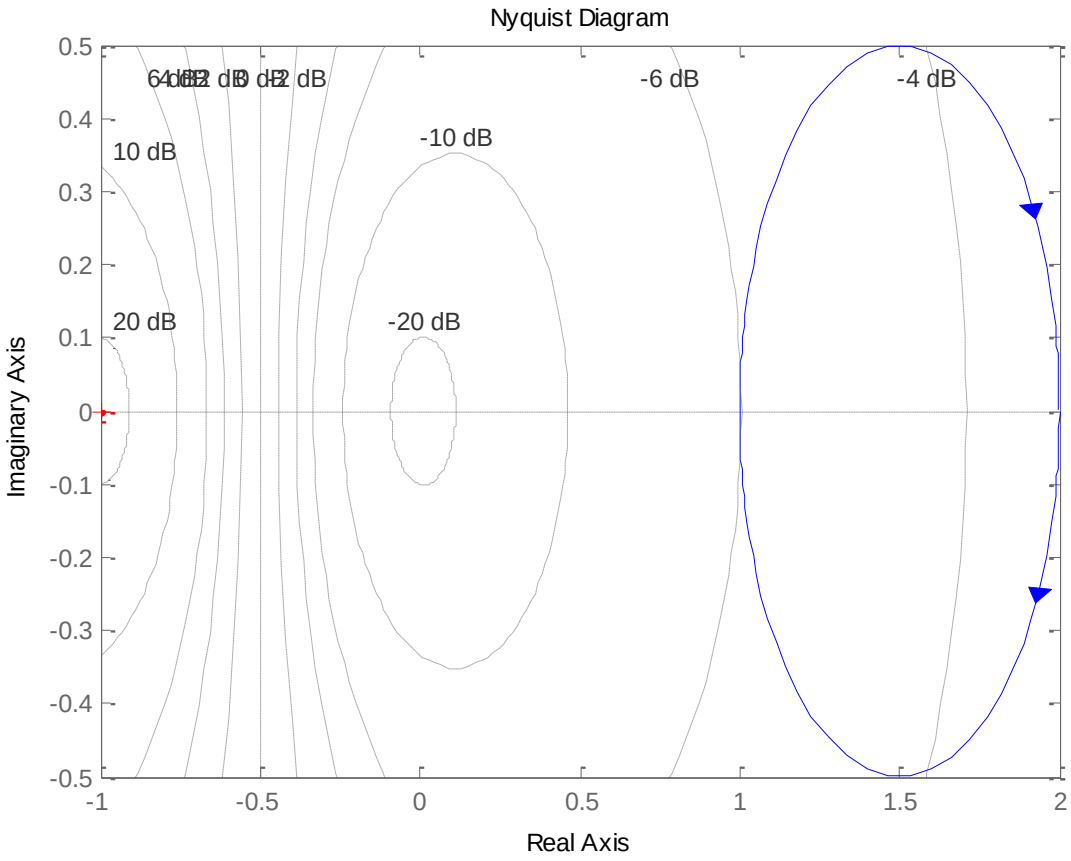

Figure 7 mathematic model of the first order of the impedance

2.3.2.2 First order with WARBURG impedance

The Warburg impedance is defined as an electrical component by:

$$Z_w = \frac{1}{\sigma * (i * w)^p} \qquad (16)$$

Where T is the length or magnitude and p is the angle in the complex plane. If p is 0.5, then the equation changes to:

$$Z_w = \frac{1}{\sigma * \sqrt{i * w}} \qquad (17)$$

And the angle is 45°. T corresponds to the diffusion of charge based on the material thickness [12]. The characteristics of this kind of impedance can be read easily from the relationship between Z_w and w,

1. Nonlinear impedance to model diffusion
2. Mainly present in low frequency region
3. Very difficult to model in time domain

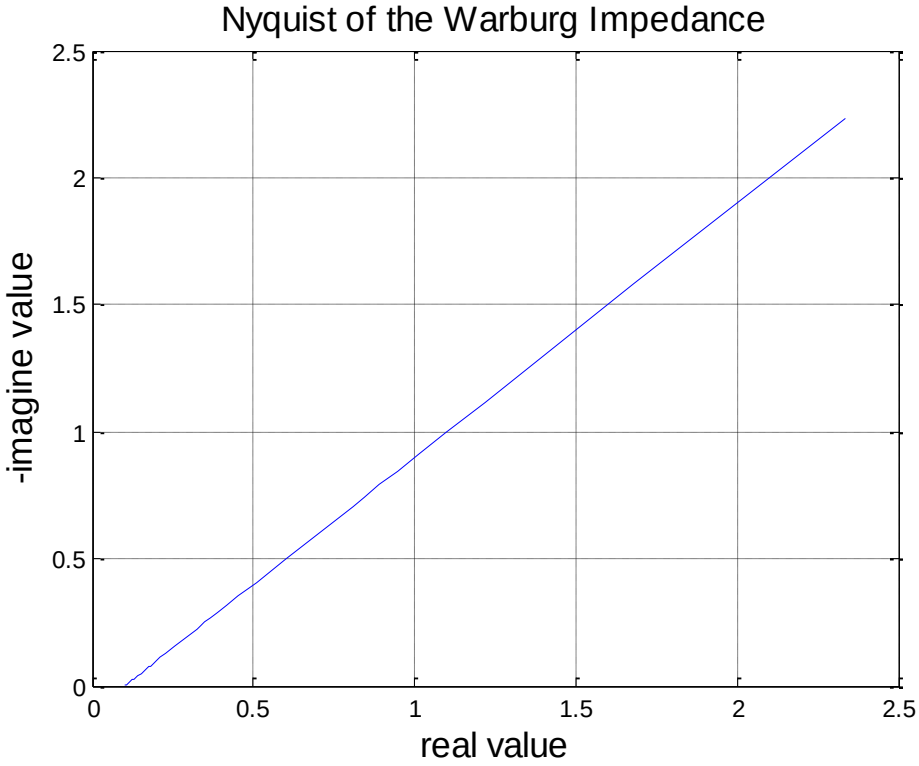

Figure 8 Nyquist diagram of the Warburg Impedance

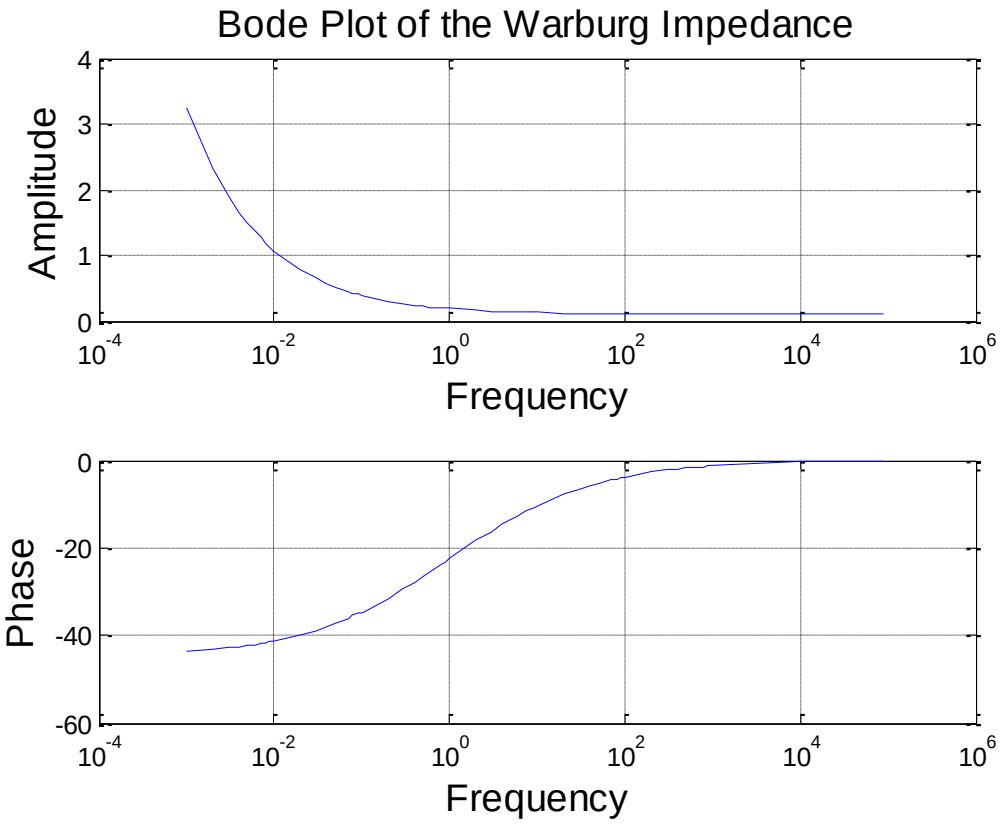

Figure 9 Bode plot of the Warburg Impedance

The equivalent circuit model would be as follows:

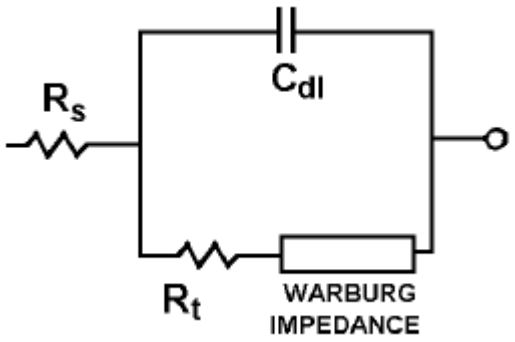

Figure 10 ECM with Warburg impedance

Because of the adding of the Warburg Impedance, the current on the branch of the resistance will be changed. The new current going through will be:

$$i_R = \frac{V_c}{R_1 + Z} \tag{18}$$

The transfer function will be

$$\mathrm{TF} = R_0 + \frac{1}{C_1 * s + \frac{1}{R_1 + (\sigma * s^{0.5})^{-1}}} \tag{19}$$

$$\mathrm{s} = \mathrm{w} * \mathrm{i} \text{ and } \mathrm{i}^{0.5} = \frac{2^{0.5}}{2} * (1 + \mathrm{i}) \tag{20}$$

The real part would be

$$\mathrm{Real} = \frac{R_1 + \frac{2^{0.5}}{2 * \sigma * w^{0.5}}}{\left(1 + C_1 * \frac{w^{0.5}}{2^{0.5} * \sigma}\right)^2 + \left(C_1 * R_1 * w + C_1 * \frac{w^{0.5}}{2^{0.5} * \sigma}\right)^2} + R_0 \tag{21}$$

The imagine part would be

$$\mathrm{Imag} = \frac{C_1 * R_1^2 * w + \frac{C_1}{\sigma^2} + \frac{1}{\sigma * (w * 2)^{0.5}} + \frac{2^{0.5} * w^{0.5} * C_1 * R_1}{\sigma}}{\left(1 + C_1 * \frac{w^{0.5}}{2^{0.5} * \sigma}\right)^2 + \left(C_1 * R_1 * w + C_1 * \frac{w^{0.5}}{2^{0.5} * \sigma}\right)^2} \tag{22}$$

If we assume the $\frac{1}{\sigma}$ reaches a value very close to 0.Then the final result will be completely the same as that of 1st order Randle model without Warburg impedance.

2.3.2.3 High orders with or without Warburg impedance

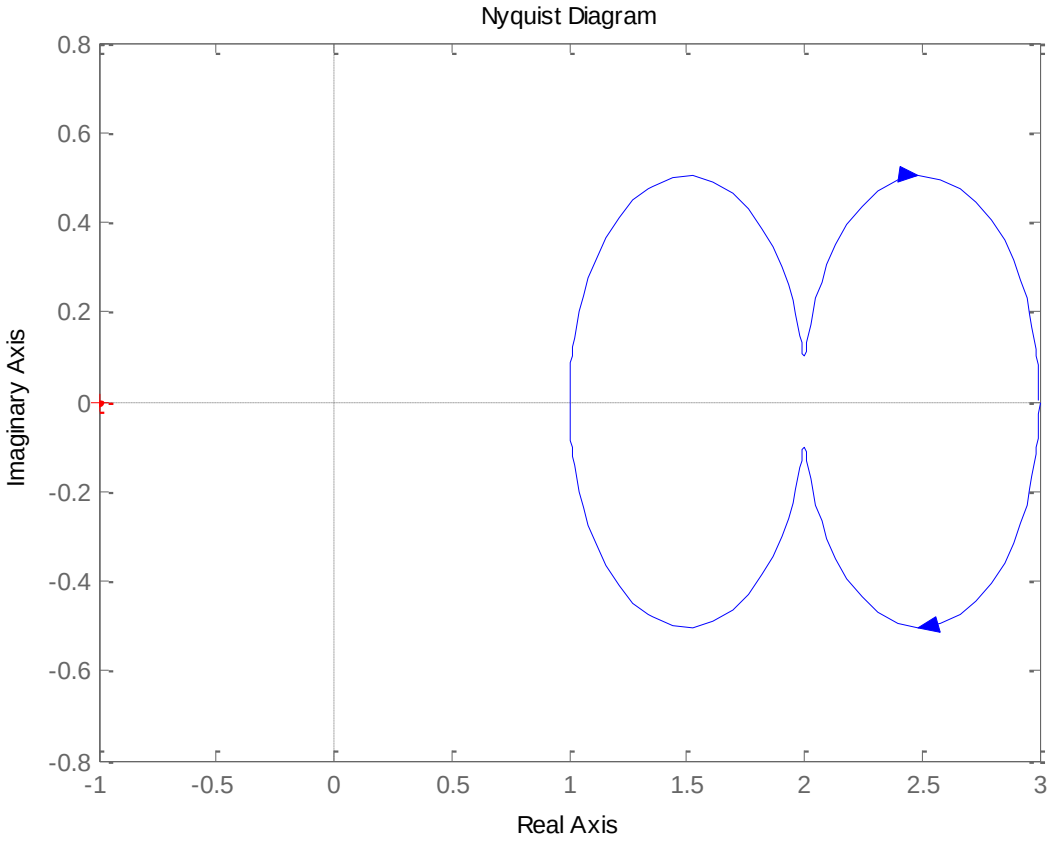

Figure 11 Nyquist diagram of the Second order without Warburg Impedance

For the orders which is larger than 1, the equation of the result will be like this

$$\mathrm{V(s)} = \mathrm{I(s)} * \left(R_0 + \frac{R_1}{1 + R_1 * C_1 * s} + \cdots + \frac{R_n}{1 + R_n * C_n * s}\right) \qquad (30)$$

The n is the number of the orders will be modeled during the experiment. Actually, the real number of orders will not be higher than 4.

2.3.3 Calendar Aging Model

For HEV, PHEV and EV passenger cars applications, the battery packs spend more than 90% of the time in the calendar mode. During the parking mode, no current intensity flows in the battery pack. Thus, two stress factors impact the battery lifetime during this mode namely the temperature (T) and the state of charge of the system (SOC). To quantify the impact of these two aging factors on power and capacity fade, a parametric study is performed to simulate a 10-year storage period in three different regions of the world.

Based on the above mentioned simulation results for power and capacity loss, management strategies can be discussed to mitigate the aging of the system during the parking mode. According to the model predictions, drastic reduction of aging could be achieved by storing the battery at low SOC and low temperature.

The following figure done by E. Prada, shows clearly the influence of the temperature and state of charge. After a 10-year storage period at 100% SOC, the capacity loss in Dubai is 25.5% whereas in Moscow the value is 11.5%. The second interesting simulation result is related to the impact of SOC. As can be observed in the figure, the higher the SOC, the higher the capacity loss. For the case of Dubai, between 10 and 35% SOC, the capacity loss varies strongly from 1% to 20%. From 35% to 100%, one can notice the presence of two plateaus corresponding to the shape of the thermodynamic potential of the graphite negative electrode [1]. For the first plateau between 35% and 70% SOC, the capacity loss is around 23%. For the second plateau, above 75% SOC, the capacity loss is around 25%.

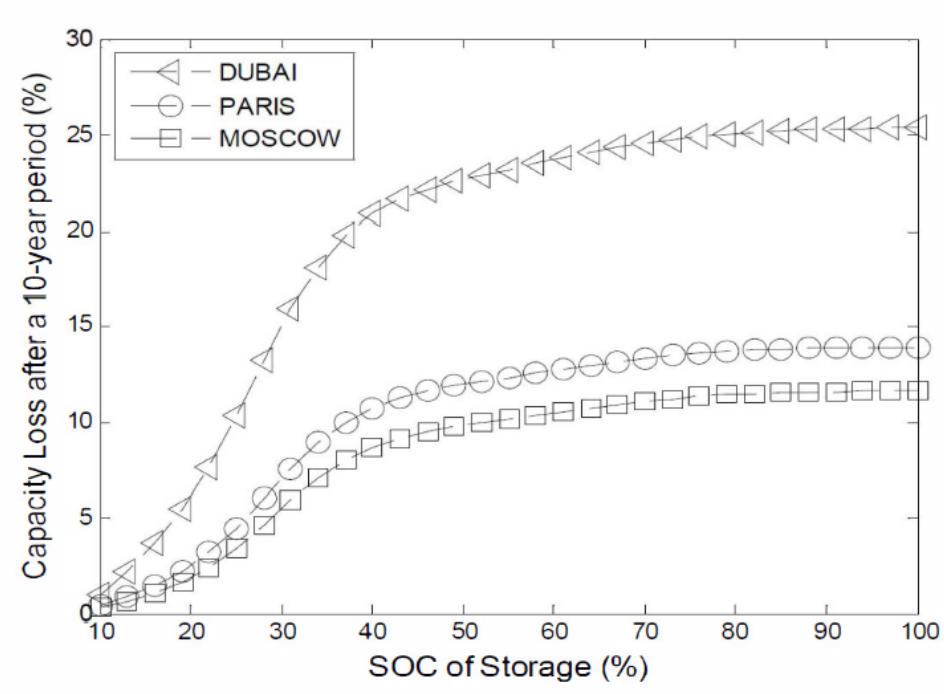

Figure 12 Model predictions for the capacity loss after a 10-year storage period at different SOC for the three cities

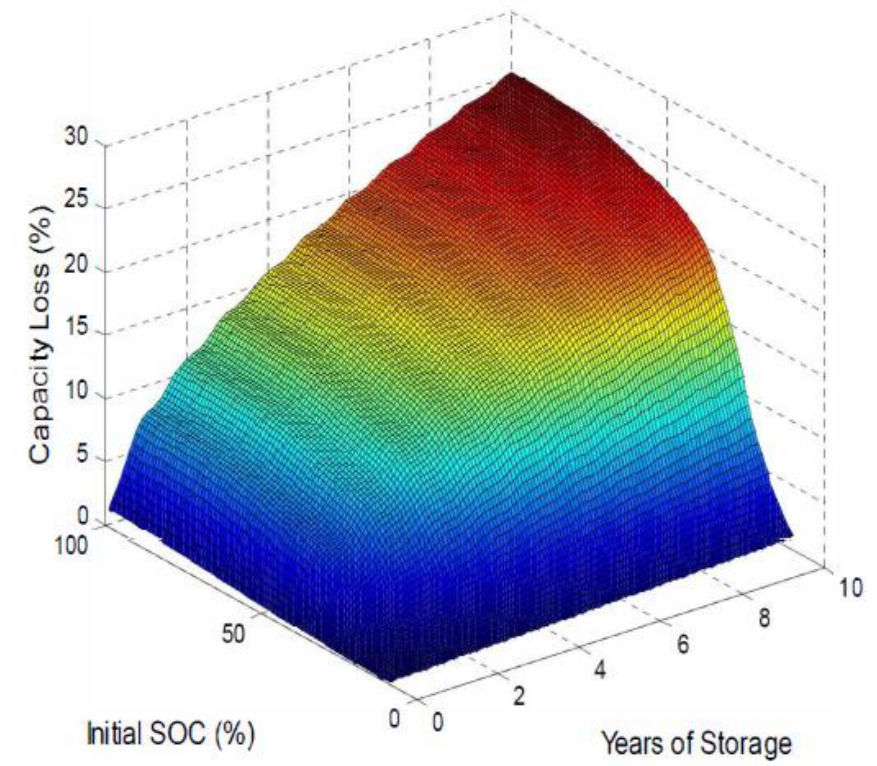

Figure 13 Capacity loss predictions as a function of the SOC of storage in Dubai

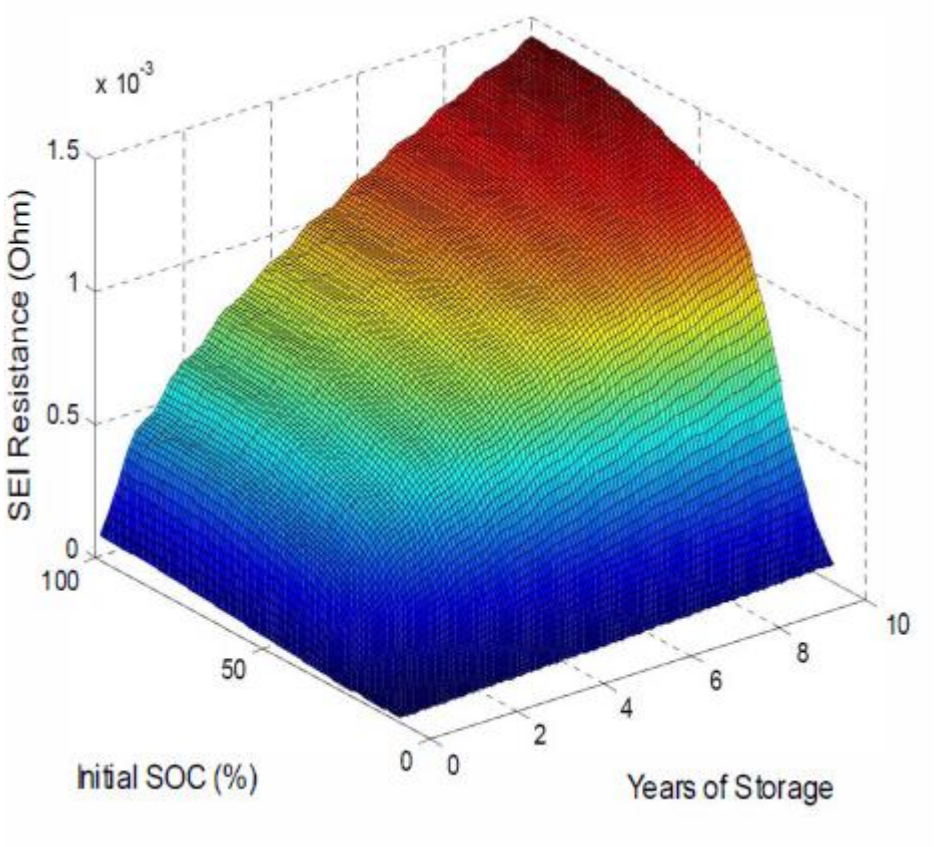

Figure 14 SEI resistance increase predictions as a function of the SOC of storage in Dubai

Based on the abovementioned simulation results for power and capacity loss, management strategies can be discussed to mitigate the aging of the system during the parking mode. According to the model predictions, drastic reduction of aging could be achieved by storing the battery at low SOC and low temperature. This battery management strategy could have sense for PHEV and EV applications for instance.

This model is a helpful tool to shed light into possible mechanisms leading to the battery end-of-life and a promising candidate for simulation studies, design specification purposes and BMS applications.

2.3.4 Cycle Life Aging Model

2.3.4.1 Capacitance Retention

Constant current–constant voltage (CC–CV) charging and constant current (CC) discharging are the most common schemes for LIB cycle life performance tests. For practical use, LIBs are charged by a charger that usually adopts the CC–CV charging scheme [37]. It is well known that LIBs significantly deteriorate with deeper DOD [35-36]. Therefore, DOD is one of the most important parameters for cycle life testing of LIBs. DOD is usually defined as the ratio of the discharged capacity to the rated capacity, and LIBs are cycled using CC discharging, with which the discharged capacity is invariably constant in every charge–discharge cycle.

Figure 15 shows the typical discharge curve trend of cell 1 during capacitance measurement. As the number of cycles increased, the curve slope steepened because of aging. Because the voltage slope during CC discharging is inversely proportional to the capacitance (dV/dt = I/C), the resultant discharge curve trends reflect capacitance fade due to aging.

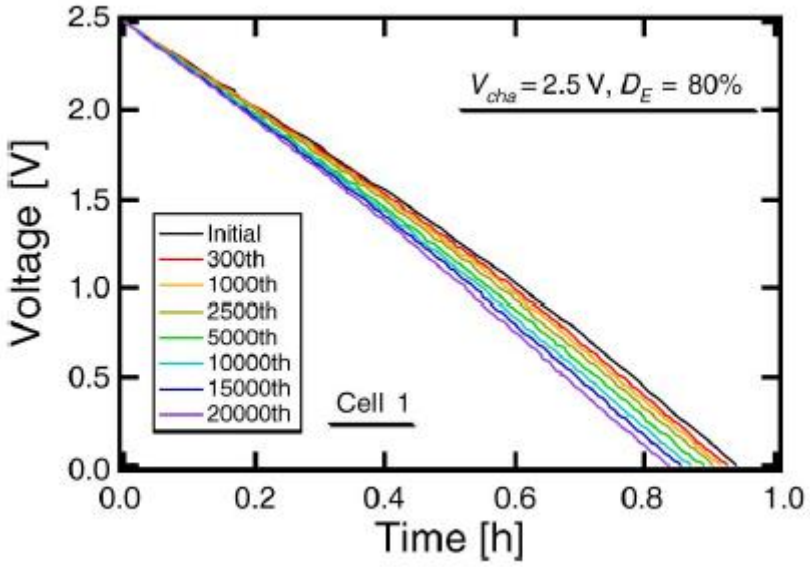

Figure 15 Typical discharge curve trend during capacitance measurement

Figure 16 redraws the capacitance retention trends of battery as a function of the square root of the number of cycles. It is empirically accepted that the retention trends of LIBs can be linearly extrapolated using the square root of the number of cycles or testing time as the x-axis [38], [39], [40].

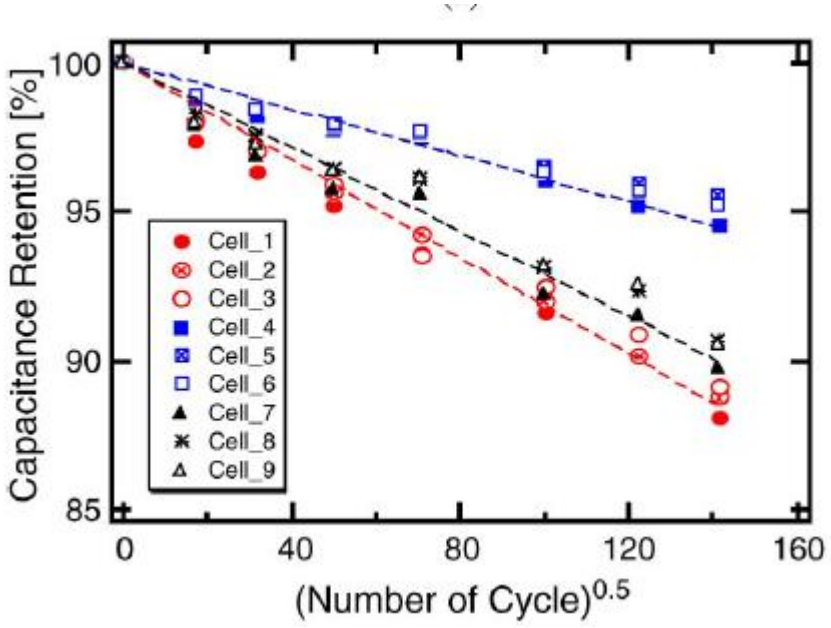

Figure 16 Capacitance retention trends as a function of square root of number of cycles.

The degradation Rate can be extrapolated by using:

$$D_T = d_T * \sqrt{N} \tag{23}$$

Experimental retention trends and extrapolation curves agreed well for all temperature conditions, indicating that the extrapolation using (5) can be used to predict cycle life performance of LIBs at a given temperature for alternative battery applications.

In accelerated stress tests for electrolytic capacitors and semiconductor devices, an Arrhenius model is generally used to express temperature dependence of life. The calendar degradation rates of the secondary batteries under the float conditions can be also expressed by the Arrhenius equation [38], in which the rate of a chemical reaction K is given by

$$D_T = A_D * \exp\frac{-E_a}{R * T} \tag{24}$$

The acceleration factor for every 10 ℃ increase, i.e.,α is defined as

$$\alpha = \left(\frac{T - T_{ref}}{10}\right) * \sqrt{\exp\left(\frac{E_a}{R} * \left(\frac{1}{T_{ref}} - \frac{1}{T}\right)\right)} \tag{25}$$

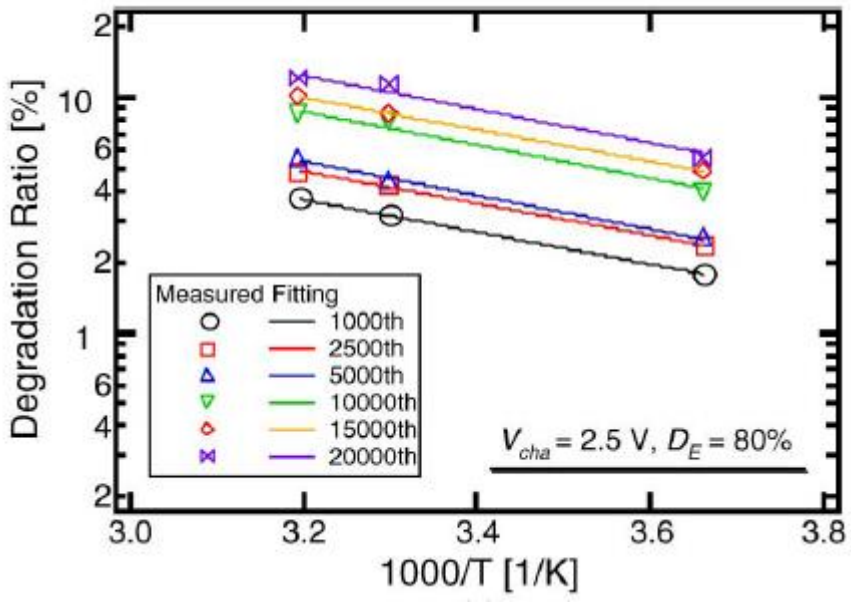

Figure 17 Arrhenius plot trends of cycles

Figure 17 shows the resultant Arrhenius plot trend at each cycling condition. The results showed good linearity in all conditions, implying that the degradation rate was dominated by the ambient temperature in alternative battery applications in which the cell temperatures are considered to be almost equal to the ambient temperatures because of negligible heat generated during cycling.

2.3.4.2 Capacity Fade

Capacity characterization data were used to quantify the capacity fade rate for the model development. As an example, Figure 18 shows the discharge curves obtained at a C/2 rate (after different number of cycles) for the cells cycled under the following conditions: A, 90% DOD, C/2, 0 ◦C; B, 90% DOD, C/2, 45 ◦C; and C, 90% DOD, C/2, 60 ◦C. As cells age upon cycling, the measured capacities decrease steadily, while the shape of discharge profiles remained unchanged. These cycle number dependent capacity loss data were collected for the cycle life model development. The functional form of the life model can be expressed as:

$$Q_{loss} = \mathrm{f}\,(\mathrm{t}, \mathrm{T}, \mathrm{DOD}, \mathrm{Rate}) \quad (26)$$

Where t is the cycling time, T is the test temperature, DOD is the depth-of-discharge, and Rate is the discharge rate for the cycle testing.

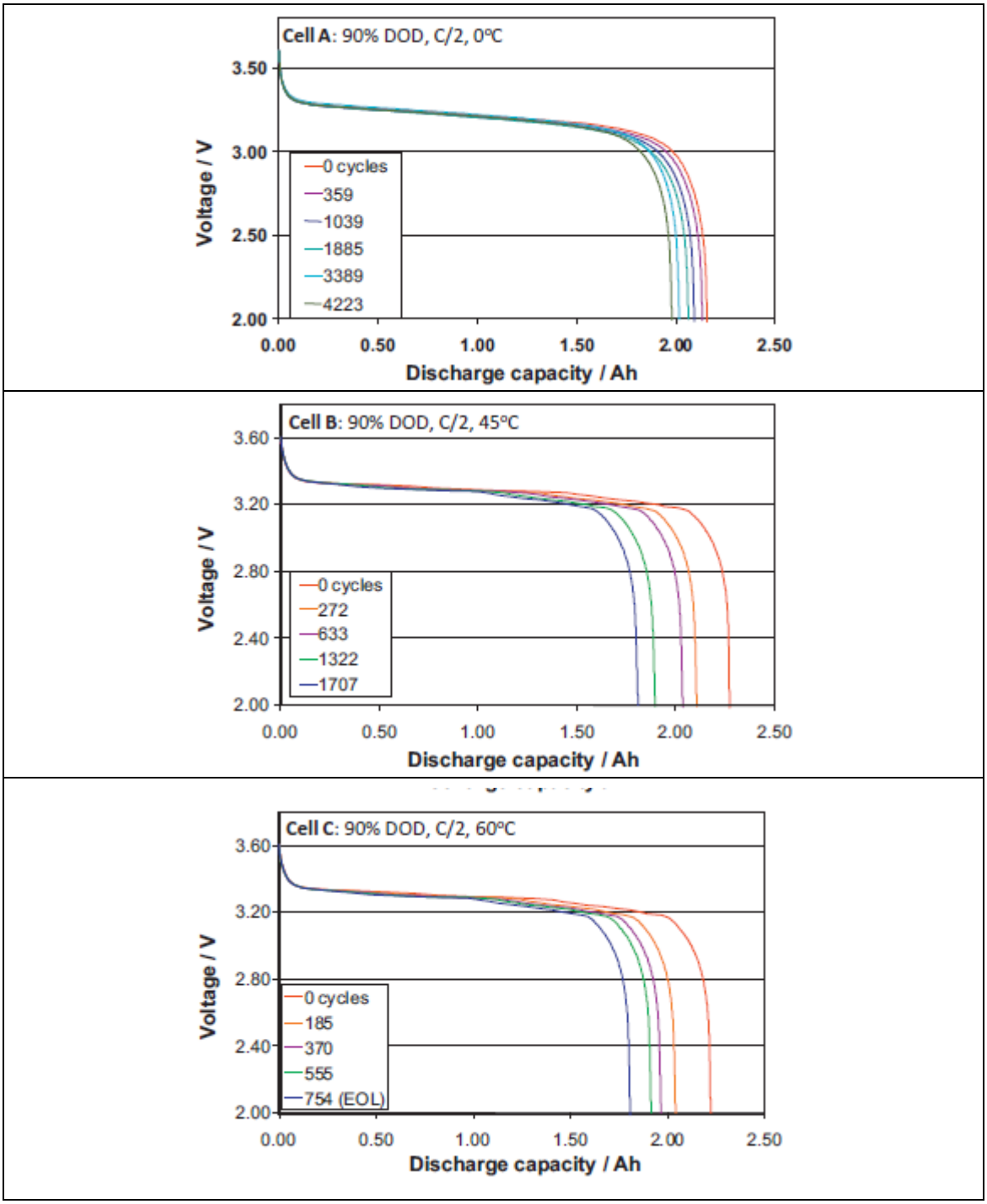

Figure 18 Discharge curves of the battery cells cycled at three different conditions: (Cell A) 90% DOD, C/2, 0 ◦C; (Cell B) 90% DOD, C/2, 45 ◦C; and (Cell C) 90% DOD, C/2, 60 ◦C.

At a given C-rate, cells cycled at DODs greater than 50% were shown to reach the defined end of life condition sooner than those cycled at lower DODs (<50%). After eliminating DOD, capacity fade can only be affected by time (t) and temperature (T). In this case, we adopt the following battery life model [33]:

$$Q_{loss} = B * e^{\frac{-E_a}{R*T}} * t^z \quad (27)$$

To determine the fitting parameters, we implemented a single step optimization process using Equation 4 with a slight rearrangement of the terms. The graphical representation of this method is shown in Fig. 6 where ln(Q_{loss}) + E_a/RT is plotted as a function of ln(A-h). The activation energy E_a was obtained from the intercept values of the best-fit nonlinear regression curves. Applying the experimental data from 15, 45 and 60 ◦C at C/2 discharge rates, E_a was found to be close to 31,500 J/mol. Previous reports have indicated that this square-root of time relationship with capacity fade represents the irreversible capacity loss due to solid electrolyte interface (SEI) growth that consumes active lithium and is often controlled by a diffusion process.

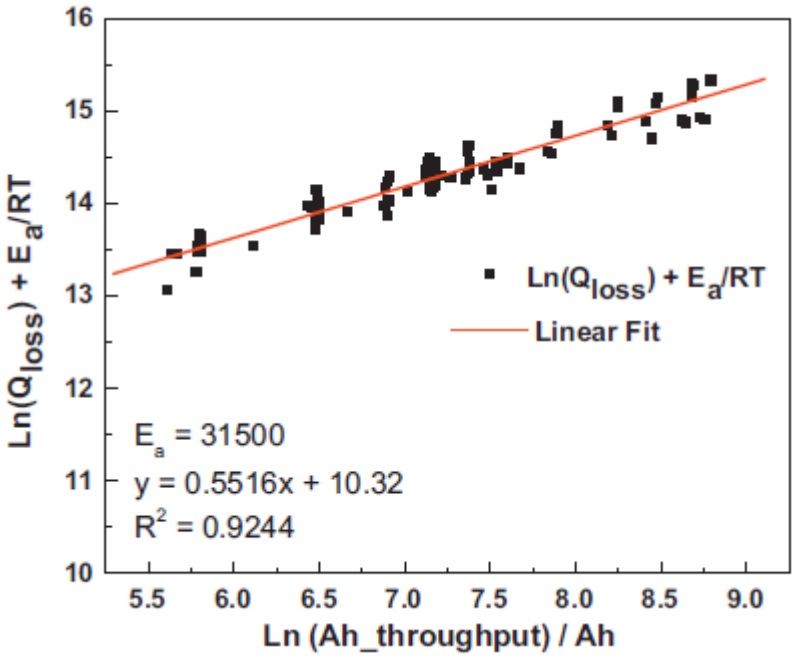

Figure 19 Fitting Plot

2.3.5 Shepherd Empirical Model

The simulation model, which predicts the charge-discharge phenomena, is that proposed by Shepherd. This model presents the relation between voltage, current and the battery state of Charge Q as follows:

In discharge (I<0):

$$\mathrm{U(t)} = U_d - g_d * I * \frac{t}{C} + R_d * \left(1 + M_d * I * \frac{t}{C * (1 + C_d) - I * t}\right) \quad (28)$$

In charge (I>0):

$$\mathrm{U(t)} = U_c - g_c * \left(1 - I * \frac{t}{C}\right) + R_c * I * \left(1 + M_c * I * \frac{t}{C * (1 + C_c) - I * t}\right) \quad (29)$$

Where U is the battery output voltage, g is the coefficient with characterize$\Delta \mathrm{U} = \mathrm{f(Q)}$, C the capacity, R the internal resistance, I the current, t the time, T the temperature, M the slope of the U=f(t, I, Q) characteristic, SOC the state of charge (1-(Q/C)), DOD the deep of discharge (Q/C) and c, d are the indices of charge and discharge, respectively.

Thus the obtained model of aging is the following in discharge:

$$C_d = -0.005 - 0.0012 * t \quad (30)$$

$$U_d = (2.175 - 0.0001 * D^2) - 0.036 * \log(0.25 * t + 1) \quad (31)$$

$$M_d = 0.065 + 0.011 * \log(0.75 * t + 1) \quad (32)$$

$$g_d = 0.210 + 0.0473 * \log(0.33 * t + 1) \quad (33)$$

$$R_d = (0.0053 + 0.0008 * D) * \frac{20 - 0.5 * D}{\sqrt{(20 - 0.5 * D)^2 - t^2}} \quad (34)$$

In charge:

$$C_C = 1.15 + 0.0004 * t * (t + 30) \quad (35)$$

$$U_c = (2.01 + 0.00013 * D^2) + 0.0266 * t * \log(t + 1) \quad (36)$$

$$M_C = 0.55 + 0.053 * \log(0.25 * t + 1) \quad (37)$$

$$g_c = 0.25 - 0.078 * log(0.125 * t + 1) \quad (38)$$

$$R_c = (0.011 + 0.001 * D) * \exp\left(\frac{-t}{t - 20 + 0.5 * D}\right) \quad (39)$$

Where D is the battery age (in months), t is the time variable (in hours). The values at origin (t=0) indicate the new state of the battery [21].

Figure 20 and Figure 22 shows the results of charging and discharging of the Shepherd

model. It is easy to find the model predict correctly the trend of the voltage variation during charging and discharging.

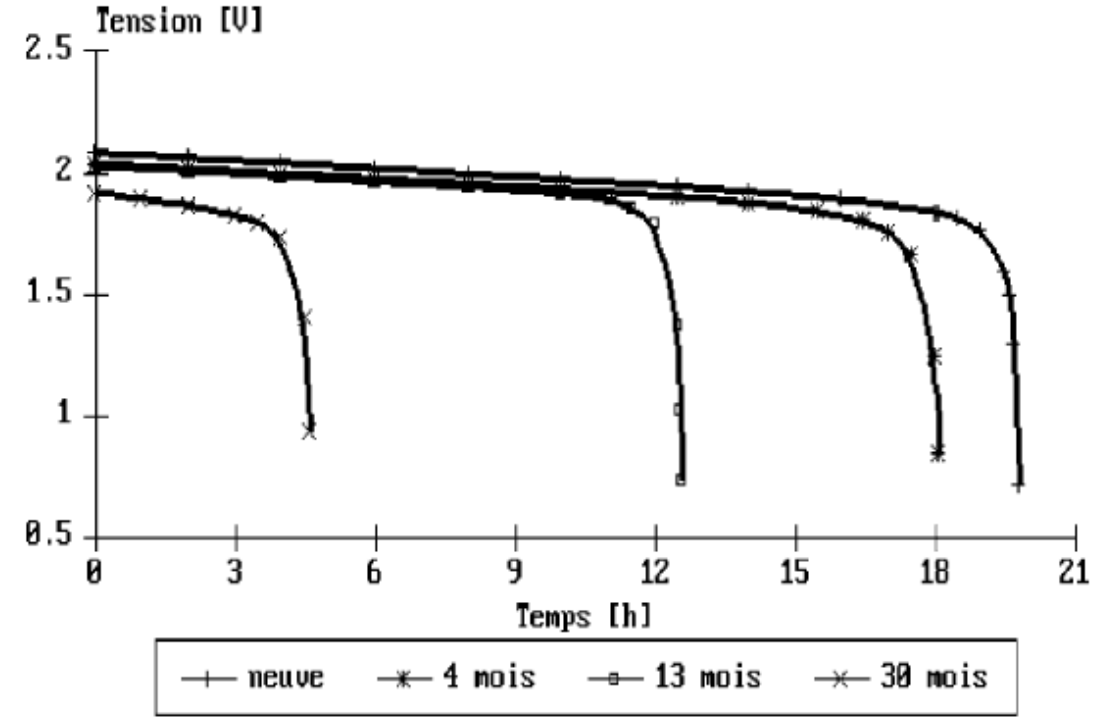

Figure 20 Discharge Voltage Variation for 4 states of ageing

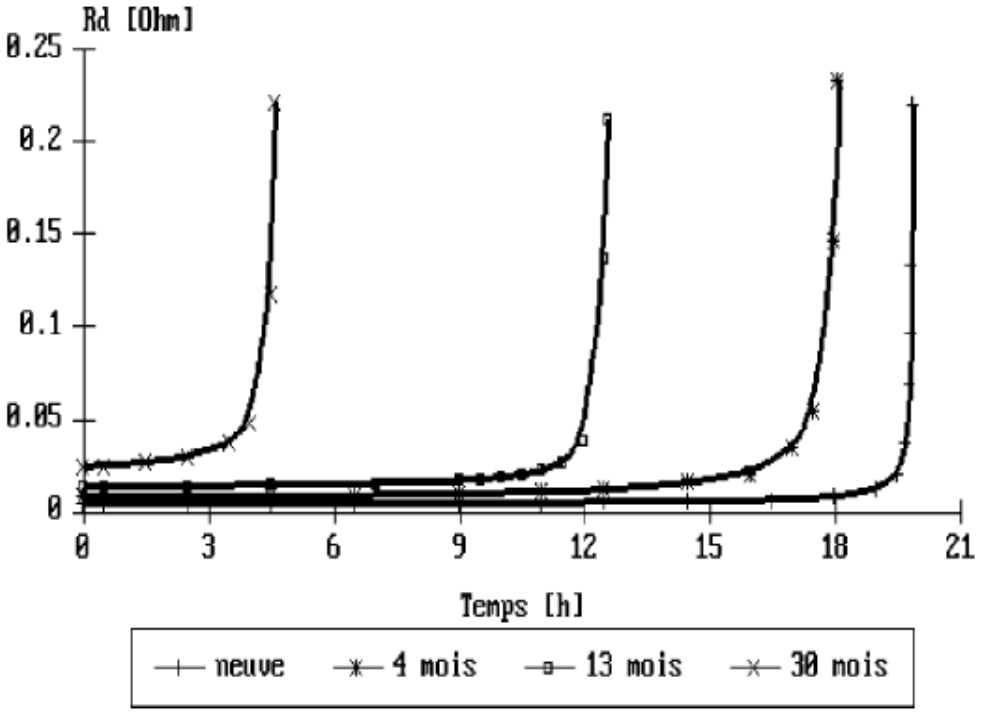

Figure 21 Variation of Discharge Resistance for 4 states of aging

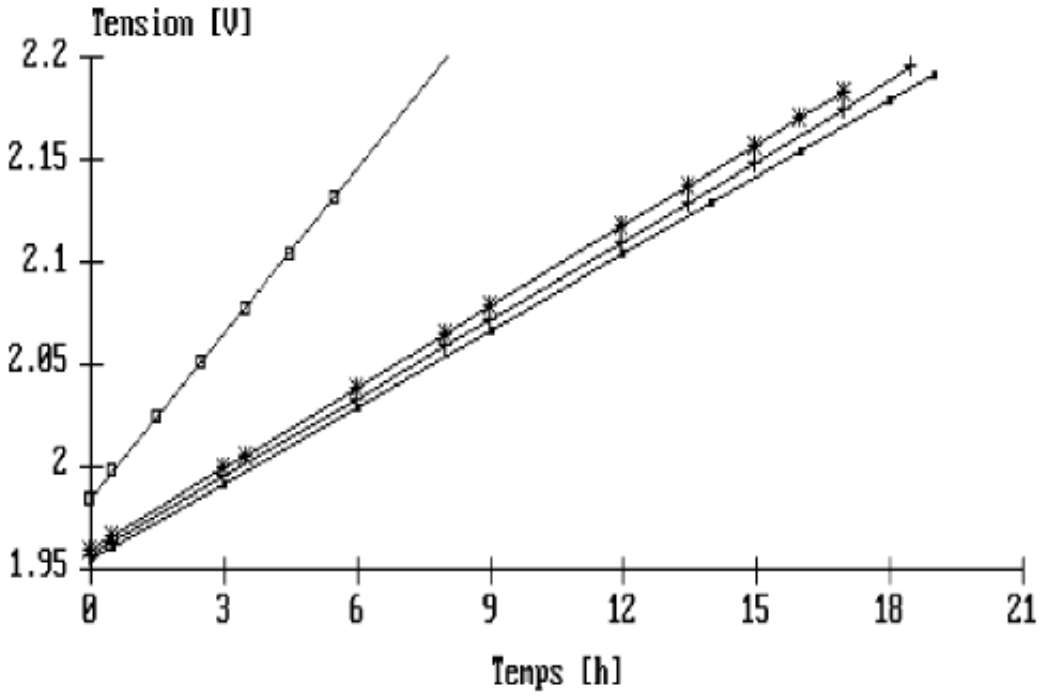

Figure 22 Charge Voltage Variation for 4 states of ageing

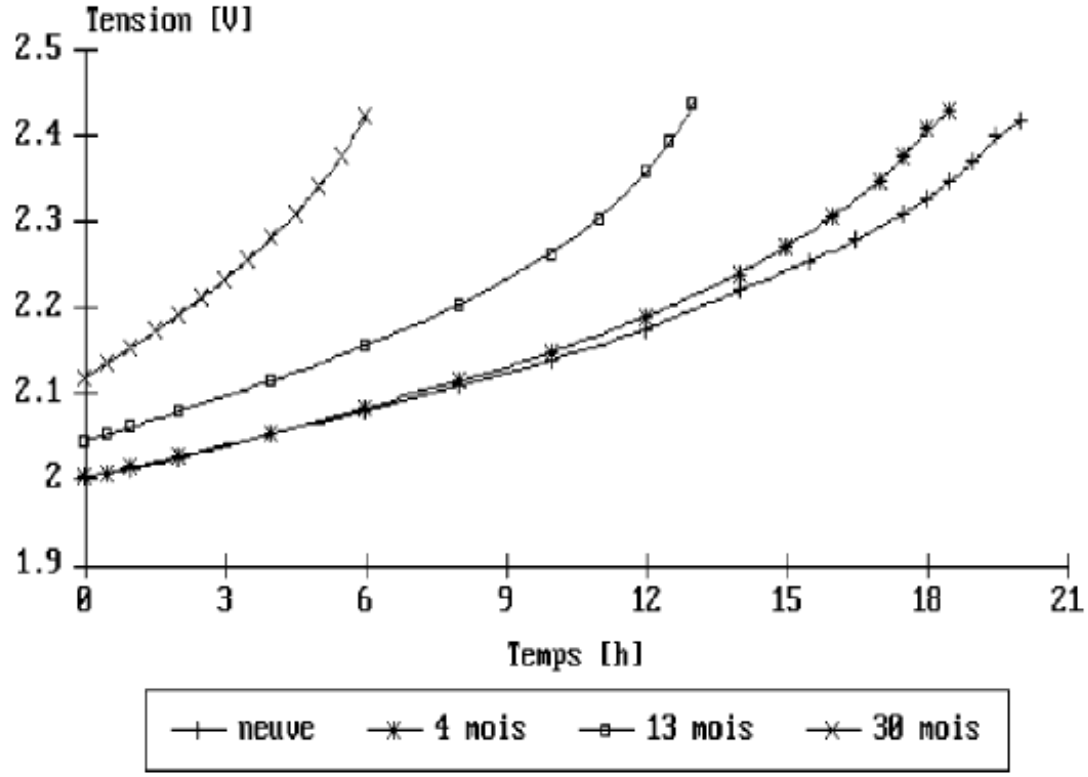

Figure 23 Charge Voltage Variation for 4 states of ageing

In this paper, the author has identified the temporal model of a lead-acid battery.

Moreover, he demonstrated how the battery aging affects all parameters of the Shepherd model. This variation is most remarkable with dynamic solicitations (in current and load consumption). However, in nominal functioning conditions, the aging affects slightly the output voltage and is not significant before the first year. To protect the battery from deep discharges and irreversible corrosion, the load request and the power consumption must be limited and controlled. To avoid deep discharge, the voltage output must be fixed in function of the discharge current. Finally, the battery regulator in insufficient to reduce aging consequences and thus must be assisted by an optimal management and monitoring of the PV plant.

2.4 Battery Life Prediction from Aging

Battery lifetime is one of the largest barriers preventing widespread adoption of lithium ion battery chemistries in automotive, as well as stationary applications. Sauer and Wenzl explain that all battery systems are affected by a wide range of aging processes in Comparison of different approaches for lifetime prediction of electrochemical systems [11]. They explain that many of these processes occur due to different stress factors and operating conditions imposed on the battery. Some of these factors include the number of charging cycles a battery has experienced, the battery state of charge at which cycling occurs, frequency of battery operation, and wide ranges of temperatures during operation[10]. For this project, we are not concerned with calendar aging, but with the aging that occurs as a result of the amp hour throughput experienced by the battery. In this paper, a large number of cells were aged across a wide range of conditions and the aging effects displayed by each battery were analyzed with respect to each battery's experienced amp hour throughput. The experiments were designed to gather data that could be used to analyze the severity of capacity degradation while aging batteries in fringe areas of their operating regions. The methods represent procedures that can be used in real time to predict the remaining life of a battery, which is what this work hopes to accomplish.

2.4.1 First Method (based on Resistance Growth)

The first life prediction method calculated estimates for the predicted growth of internal resistance based directly on the local slope values identified using the resistance growth dynamic model. This was accomplished by utilizing a sliding window method similar to what was used when averaging calculated resistance values and identifying local slope values. The predicted resistance growth was determined by averaging a set of 20 identified slopes together. Upper resistance growth estimates were created by calculating the standard deviation of the group of values being considered and adding this value to the average. Lower life predictions were created by mirroring the upper prediction. This was done to prevent the lower life estimate from ever producing

unreasonable resistance growth predictions or those with a negative slope, which was possible if the lower growth estimate was calculated using the same method as the upper growth estimate by subtracting the standard deviation from the average growth rate [10].

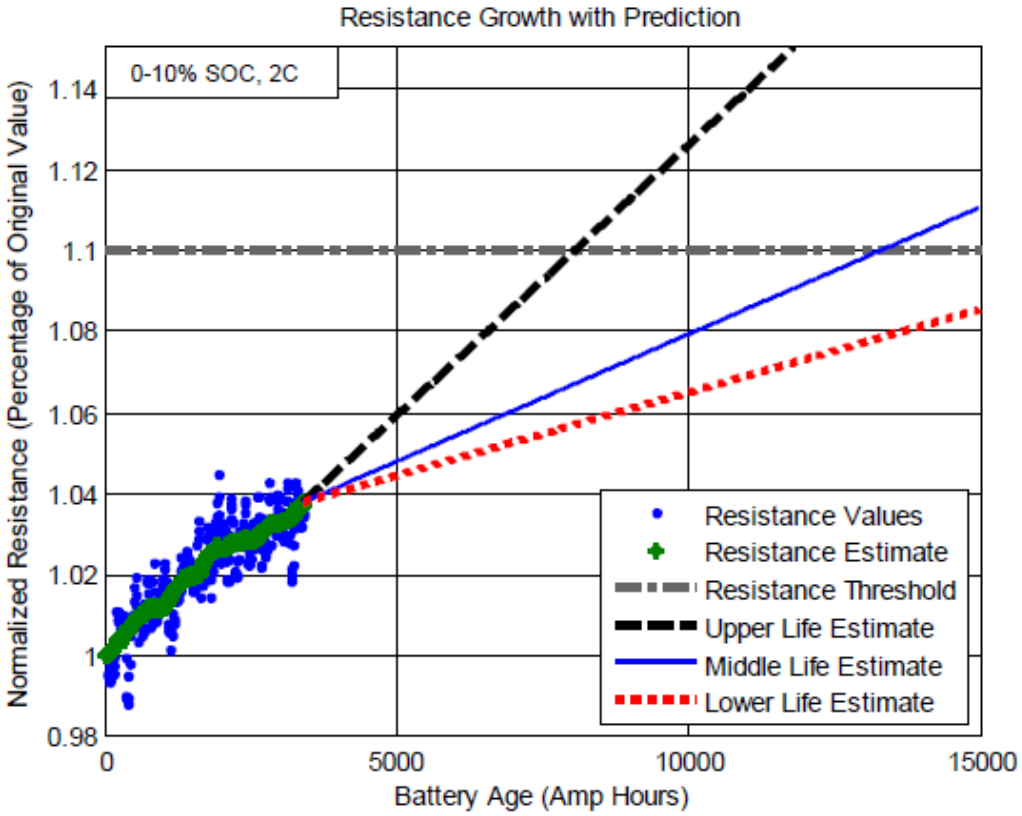

Figure 24 Example of Life Prediction Using Method 1 at 3500 Amp Hours

By extrapolating the lines of predicted resistance growth to a threshold value of normalized resistance, a life prediction could be made in terms of amp hours. A threshold of 10% growth was chosen for the purpose of making life predictions simply for illustrative purposes, although other threshold values could be chosen. For Instance, because resistance growth is directly related to power loss, this threshold could be set so that life predictions would forecast the amp hours remaining in a battery pack's life until it could no longer meet performance requirements in a vehicle. Each prediction was made at the battery age shown on the x-axis and included the mean predicted life, the lower life estimate based on the worst case, and the best expected life which was chosen to be the same distance from the mean prediction as the worst case [10].

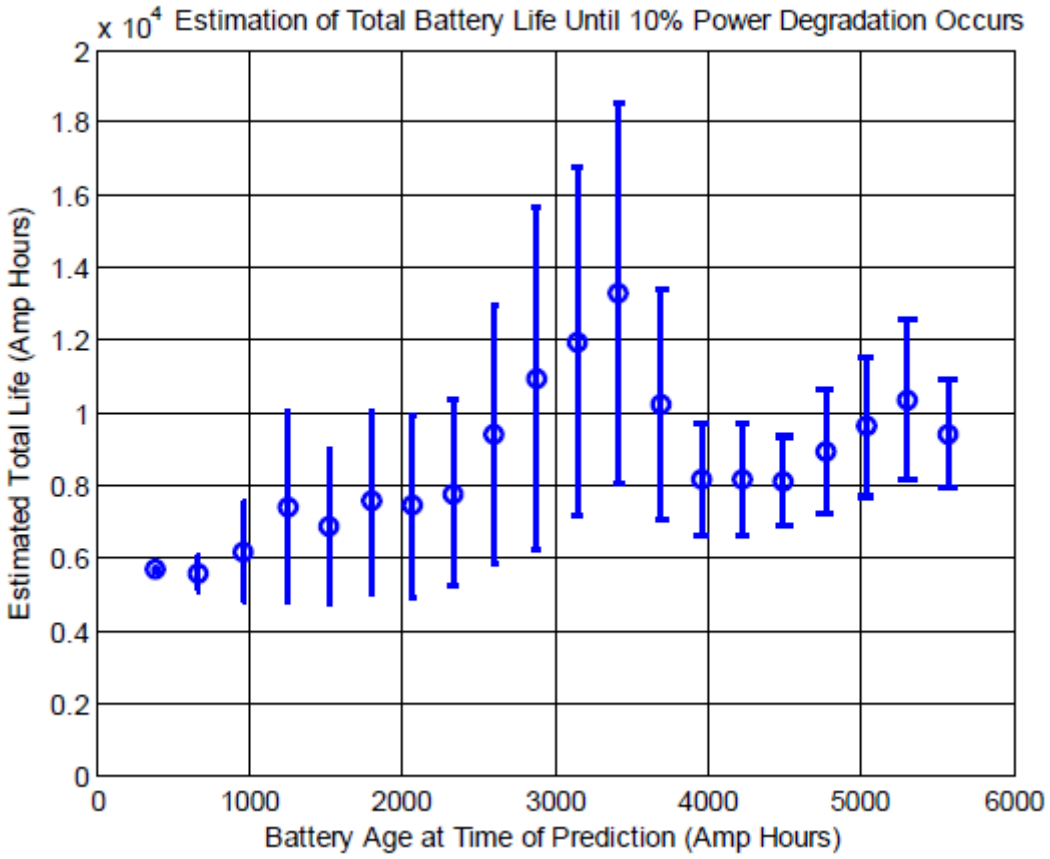

Figure 25 Prediction of the life from the resistance

Although the life predictions made using method 1 provided some level of insight into the remaining life of the battery being tested, they were not ideal. The large error bars indicated low levels of precision and confidence in the estimates and the fact that the mean estimate never converged to a single value causes the accuracy of the method to be questioned. Although more trials were run using this method, their results were no better than those displayed in this example. For this reason, additional methods of life prediction were developed.

2.4.2 Second Method (based on Capacitance Retention)

By combining extrapolation and acceleration factor discussed in the previous sections, a cycle life prediction model can be yielded as:

$$C_T = 100 - d_{ref} * \alpha^{\frac{T-T_{ref}}{10}} * \sqrt{N} \qquad (40)$$

This cycle life prediction model suggests that capacitance retention, C_T, at a given cycle number and a given temperature can be predicted by determining α and d_{ref}.

Figure 26 shows the capacitance retention trends predicted by the derived cycle life prediction model. The experimental and predicted retention trends were in good agreement, verifying that the cycle life prediction model is appropriate for batteries in alternative battery applications [41].

Batteries were cycled under various cycling conditions for 5000 cycles. The resultant capacitance retention trends were mainly influenced by temperature, and other conditions such as DOD and charge voltage were found to have only minor effects on the degradation. The experimental retention trends could be extrapolated linearly with the square root of the number of cycles as the x-axis.

The cycle life prediction model was derived from the combination of extrapolation and acceleration factor. The experimental and predicted capacitance retention trends were in good agreement, verifying that the derived prediction model is appropriate for SCs in alternative battery applications.

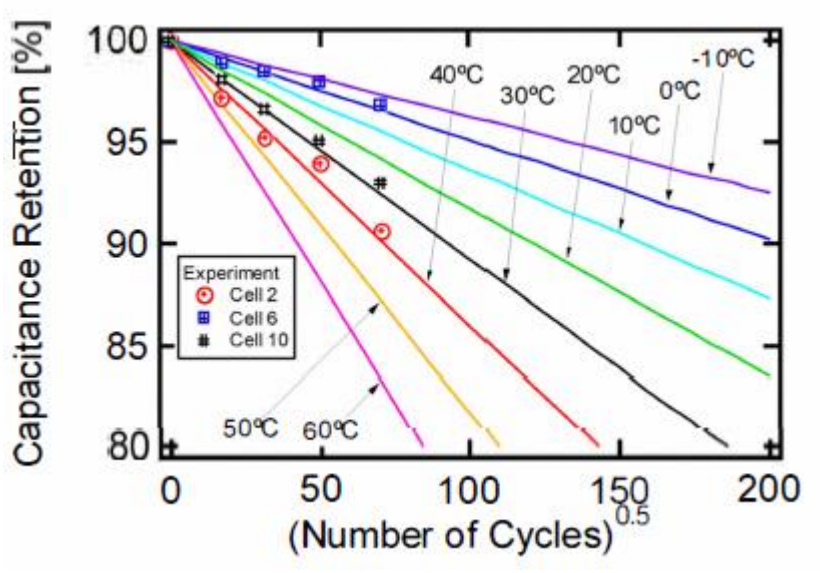

(a) As a function of number of cycle.

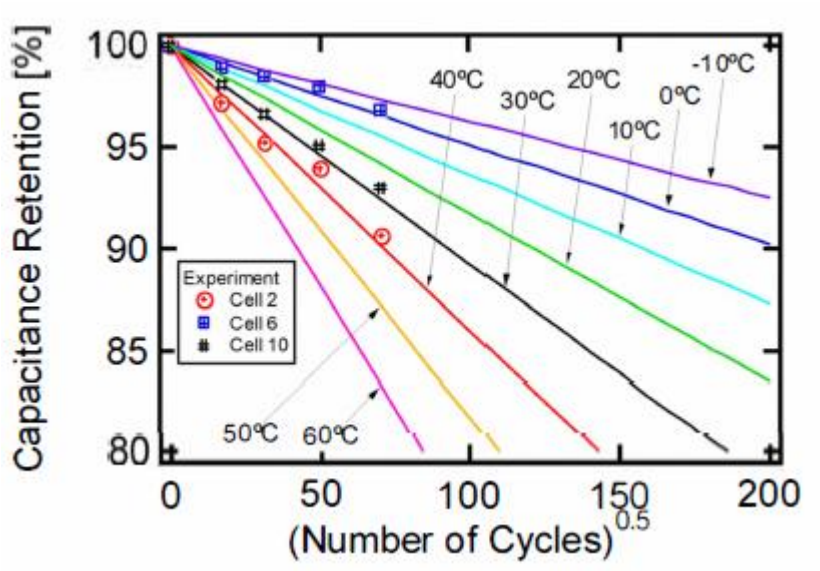

(b) As a function of square root of number of cycles.

Figure 26 Examples of cycle life prediction

2.4.3 Third Method (based on capacity fade)

As a result, the capacity loss life model is expressed as:

$$Q_{loss} = 30330 * \exp\left(\frac{-31500}{8.3145 * T} * Ah^{0.552}\right) \quad (41)$$

Using the life model in Equation (11), we are able to simulate qualitatively the capacity fade under various conditions in Figure 27, simulations of the capacity fade at different temperatures are compared to experimental data. Overall, the life model appears to be in a general agreement with the experimental data. The model slightly underestimates capacity loss at 60 ℃and overestimates capacity loss at 45℃. Their results demonstrate that at the low rates, time and temperature are the two parameters that substantially affect capacity fade and that DOD has a negligible effect on capacity fade [34].

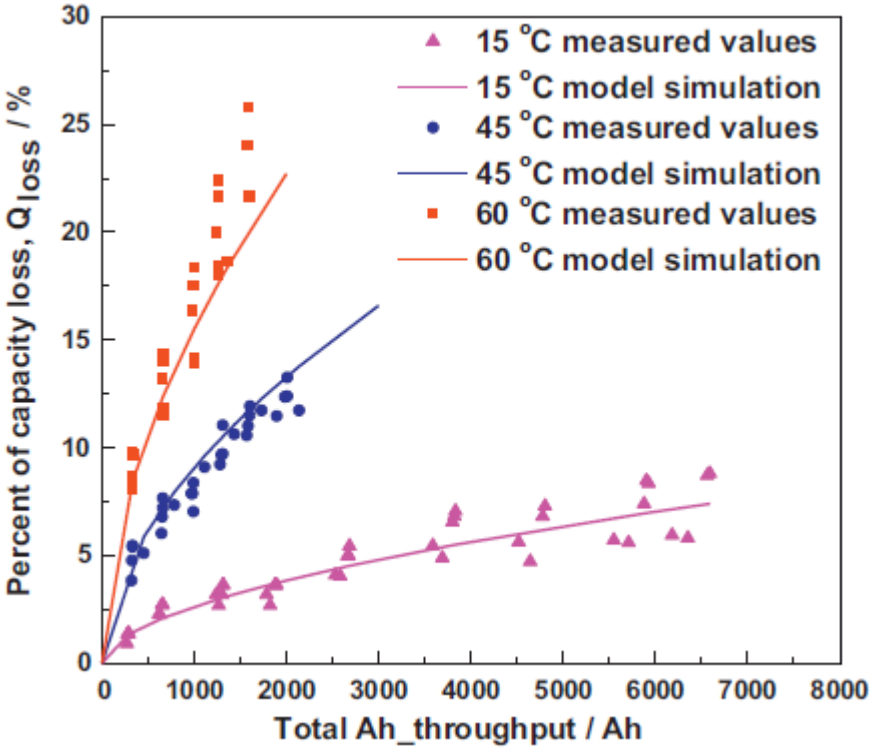

Figure 27 Simulation of cycle-life prediction model and experimental data

Consequently, their modeling results are consistent with the aging mechanism that the active lithium is consumed to repair and/or grow the SEI layer when the carbon anode is cracked due to anode degradation. In addition, there is also a C-rate effect. The Arrhenius law used in the model equation represents the kinetics of the chemical processes for the undesired side reactions such as for SEI formation. The inverse relationship of the magnitude of activation energy with the C-rate suggests that higher rates produce higher diffusion induced stress field [42] on the particles which accelerates the chemical processes that cause irreversible active lithium consumption. They have demonstrated that this rather simple life model represents qualitatively the experimental data for all the rates investigated. It is also recognized that the accuracy of the life model predictions at the high rates produce slightly more error than at the low rates. Overall, this generalized approach allows us to present quantitative projections of capacity fading behaviors for a wide range of cycling conditions [34].

2.5 International Standard

2.5.1 Life Testing

The reference test cycle shall be used to determine battery life. The battery shall be discharged until 80 % of its benchmark energy content is removed or until the end of the micro-cycle in which 80 % of the energy is removed. The battery shall then be recharged, with the recharge starting within 1 h of the end of discharge. When the recharge is complete, the discharge shall be started within 1 h. [4]

The start of discharge could be delayed in order to fit in with the normal working practices of the test laboratory. Every fifty cycles, the battery energy content shall be determined using the benchmark test cycle. It will establish the actual energy content of the battery and allow the measurement of other parameters. During this test, a continuous record of battery system voltage shall be made so that other battery system parameters may be determined. Moreover, the total number of micro-cycles, the total Wh removed and the total Wh returned shall be recorded and declared as the battery energy content at this stage of the life test program. [4]

The life test shall be terminated when the energy delivered falls to below 80 % of the reference energy content. The number of reference test cycles shall be recorded and declared as the battery life.

2.5.2 Maximum allowable deviations

The overall accuracy of controlled (or measured) values, relative to the specific (or actual) values, shall be within the following tolerances:

Switching between power levels in the micro-cycle shall be timed such that the mid-point of the transition occurs at the point allocated for the transition.

The total duration of each complete micro-cycle shall be 360 s ± 1 s. [4]

Parameters	**Range**
Temperature	±2 ℃
Power	±2 % of required value
Time	±1 % of required value
Power slew rate	1 s from one value of steady power to the next

Table 2 Deviations of the Test Procedure

2.5.3 Intended Use

Test	Intended use simulation	Requirements
Electrical test A	Storage after partial use	No leakage (NL) No explosion (NE)
Environmental tests B1	Transportation shock	No leakage (NL) No explosion (NE)
Environmental tests B2	Transportation vibration	No leakage (NL) No explosion (NE)
Climatic-temperature	Climatic-temperature cycling	No explosion (NE)

Table 3 Intended Use of Battery [3]

The international standard IEC 60086-5 shows the boundary condition of the electrical and mechanical test. For the reason that the battery will not be used only in stationary situation, we must consider the influence from the environment and climate. We should simulate different kinds of condition to make sure the battery can work in all the situations.

2.5.4 Failure Modes

A battery is conventionally considered to be dead if its available capacity drops below 80% of its nominal capacity (presumably when it was new). A failure mode usually has 2 effects:

1. Decrease in capacity, and
2. Decrease in power delivery due to internal resistance.

Considering that the experiment may encounter some unpredicted problems, the following situation in the Table 4 will be considered as a failure, and the data from this kind of tests would not be used:

Failure Modes	Surface Corrosion of Negative Electrode
	Decrepitation of Alloy Particles
	Loss of Water in the Electrolyte
	Crystalline Formation
	Cell Reversal
	High Self Discharge
	Shorted Cells

Table 4 Different kinds of failure modes

2.6 Capacity Fade result from small format batteries

2.6.1 Small Size Li-Fe battery

The Figure 28 show the normalized capacity in different DOD from 10% to 90% of a small size LiFePO4 battery, the nominal capacity is 2.2Ah. We can read from the line of DOD of 90%, the end of life (80% of the capacity) will happen at the cycle number 800. At the end of life the total Ah throughput will be 800*90%*2.2Ah=1600Ah.

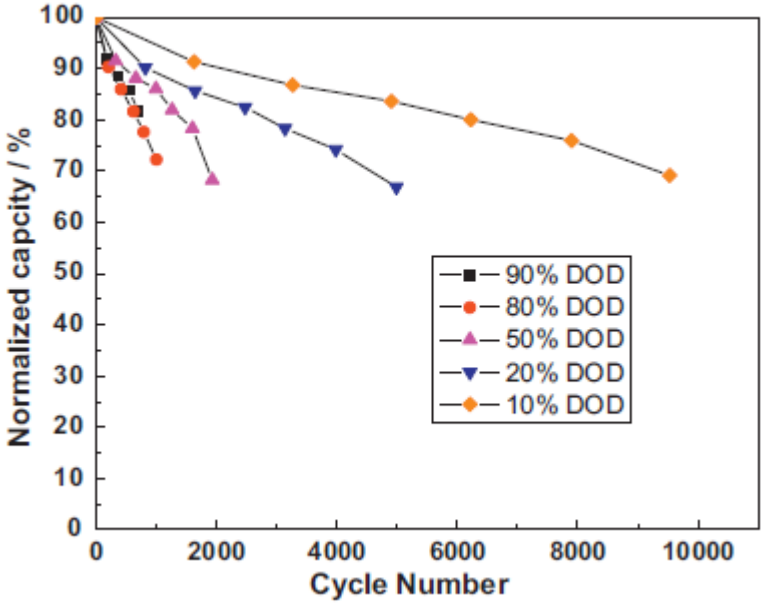

Figure 28 Capacity retention at 60 ◦C and a discharge rate of C/2 plotted as a function of cycle number, data shown for different DOD [34]

This observation is illustrated in Figure 28, where capacity retention as a function of cycle number at various DODs for the cells at 60 .C and C/2 rate is plotted. When plotted in this manner capacity fade appears to be a function of DOD. However, when the same data is plotted as a function of time as shown in Figure 29, the results indicate DOD has very little effect on capacity fade. The capacity fade rate was found to be approximately the same at each DOD indicating that the effect of cycling time is more significant than DOD. After a closer examination of all the DOD data at C/2 rate, we

concluded that the DOD effect was not important for the conditions investigated. Thus, the DOD effect was not considered for formulating a model for at low discharge rates.

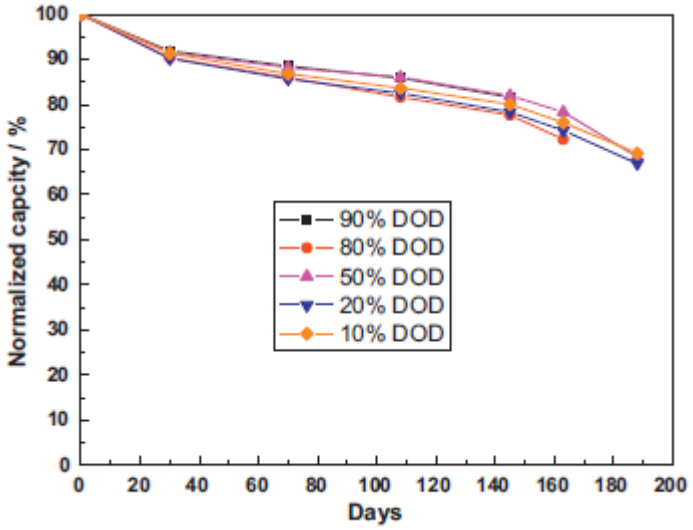

Figure 29 Capacity retention at 60 .C and a discharge rate of C/2 plotted as a function of time (days)

2.6.2 LiCo2/C Battery

In the Figure 30capacity may decline very rapidly after a first “normal” phase.

When dismantling the cells described in Figure 30 after cycling, a large deposit of Li metal was observed, this was the reason for rapid capacity decay. In the same time, a strong increase in cell resistance is observed

Due to a reduction in charging capability of the cell, the degradation mechanism can be explained by the progressive clogging of the micropores of the negative electrode by the passivation layer growth. If this reaction is not stabilized enough, the reactions products (Li2CO3, alkyl-carbonates, polymers) will depose in the microposity, thus significantly reducing the active surface area.

When induced, lithium plating itself will produce more deposit, and aggravates the phenomenon, which explains the increasing of capacity fading rate. Indeed, the electrode porosity is recognized as one of the first-order parameters controlling the capacity fade on cycling [45]. The charging rate has obviously a strong influence on this

behavior. Temperature decrease would accelerate the fading rate, lowering the limit at which the Li plating will occur, and for the same reasons increasing temperature in some limits would be beneficial. This is a tradeoff effect between lithium corrosion rate, which accelerates reduction of active area (negative effect of temperature), and concentration gradients producing high local current density (positive effect of temperature) [23].

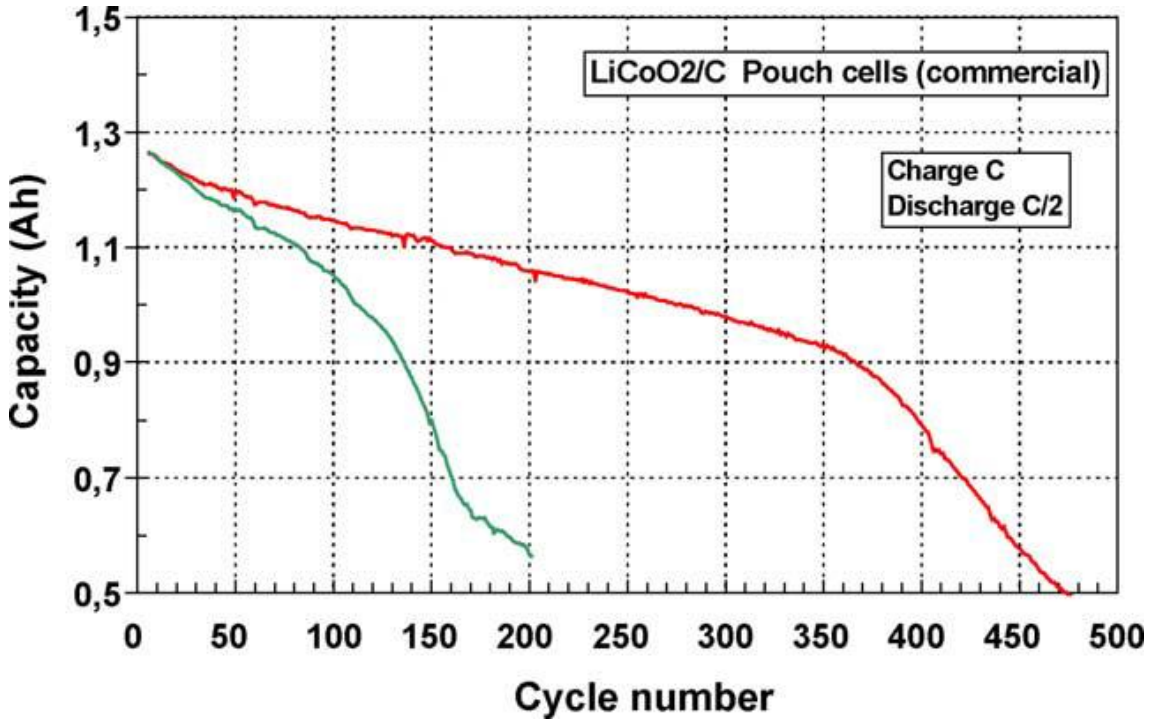

Figure 30 Example of capacity evolutions during 100% DOD cycling.

LiCoO2/graphite pouch cells, charge at C, discharge at C/2, 20 C).

Although each Li-ion chemistry may behave differently, there are few basic mechanisms, which may account for general aging phenomena in Li ion batteries. The most obvious is linked to the high reactivity of lithium from lithiated carbon, and stability of the passivating layer (SEI) is the key of the overall cell stability.

2.6.3 10Ah $LiFePO_4$-based Li-ion batteries

Two types of large format (>10 Ah) LFP cells, denoted as “Cell L” and “Cell P”, were purchased from two manufacturers, respectively.

In the life cycle tests, Cell L was first characterized at 25 Celsius with a procedure comprises 10 cycles of charge – discharge regime at C/10 and 5 cycles with C/10 charge and C/2 discharge. Cell L was then subjected to 1 C/10 cycle and 100 cycles of C/10 charge and C/2 discharge regime at 60 Celsius. The end-of-charge (EOC) cutoff condition comprises a typical cutoff voltage at 4.2V and a capacity limit of 10 Ah. At the end of the life cycle test, 10 additional C/10 cycles were carried out at 60 Celsius. Cell P was tested using a different test plan and protocol. A C/10 cycle was conducted first, followed by four cycles of C/10 charge and C/2 discharge regime. Such a five-cycle regimewas repeated at 25 and 60 Celsius. The data and presentations used in the illustration and discussion in this paper are selected from representative cells in each type that are worth discussion or comparison. Therefore, the result generally reflects the behavior of each type of cells.

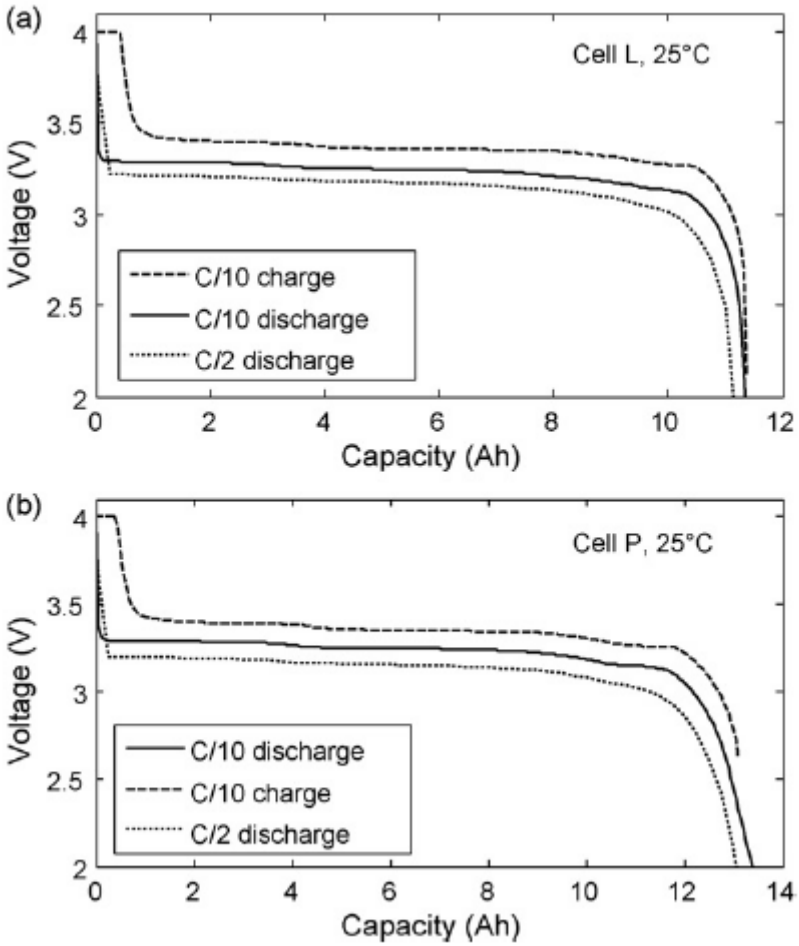

Figure 31 (a) Voltage.capacity curves for Cell L in the first 15 cycles at 25 Celsius.

(b) Voltage.capacity curves for Cell P in the first 5 cycles at 25 Celsius.

Figure 31(a) displays the voltage vs. capacity curves in the first few cycles of Cell L at 25 Celsius. Little change was observed among the first 15 cycles. The cell delivered 11.35 Ah at C/10 and 11.14 Ah at C/2.

Figure 31 (b) shows similar curves in the first 5 cycles of Cell P. The cell delivered a higher capacity with 13.38 Ah at C/10 and 13.07 Ah at C/2. Although the shape of discharge curves appears similar, Cell P released more capacity in the low voltage range than Cell L. In comparison, below 2.75 V; Cell L delivered 2.5% and 3% capacity at C/10 and C/2, while Cell P delivered 4.5% and 6.5%, respectively.

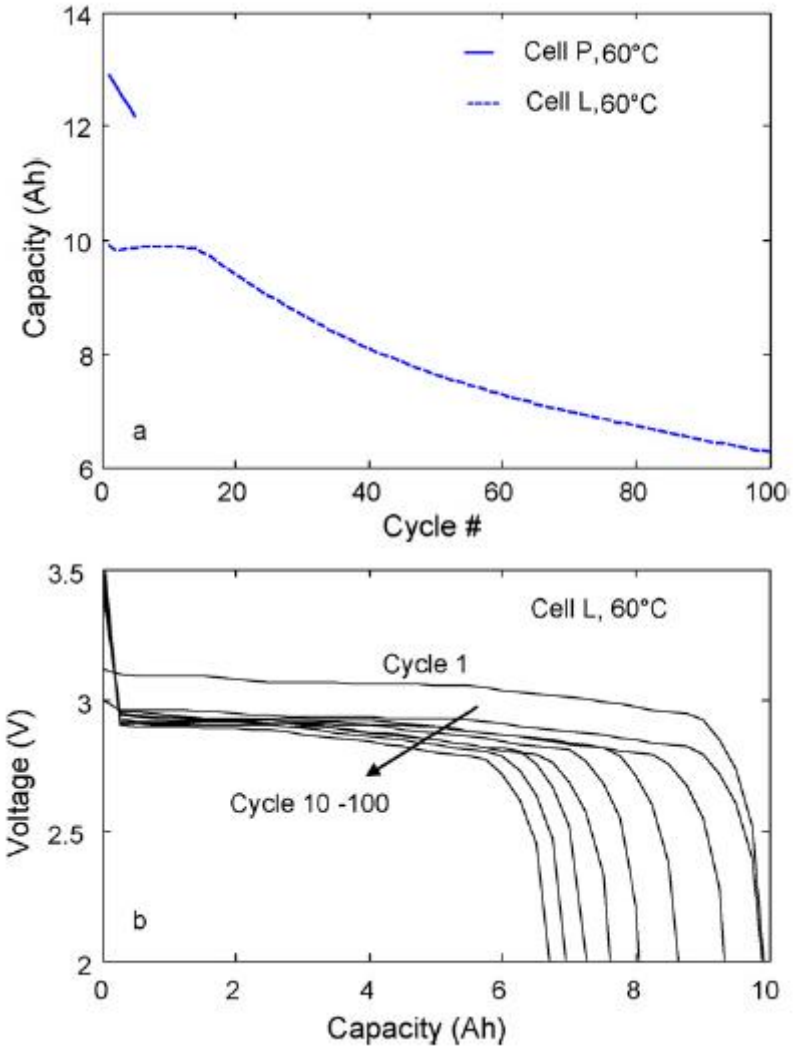

Figure 32 (a) Capacity loss with cycle number for both cells and (b) evolution of the V vs. Q curves for Cell L.

Figure 32 (a) presents capacity retention with cycle number for Cell L and P. In Cell P, the capacity loss was immediate and the cell lost 4% after 4 cycles. In Cell L, the capacity was stable for about 15 cycles before a quick degradation kicked in. Subsequently, the cell lost 37% of its capacity after 100 cycles. Figure 32(b) displays the progression of the discharge (voltage vs. capacity) curve with cycle number in Cell L at 60 Celsius. Although the plateau voltage did not show significant changes over cycling, the length of the plateau seems to have changed significantly.

After 100 cycles, Cell L was subjected to 10 extra cycles at C/10 at 60 Celsius (Figure 33). Even if the capacity retention seems to fade continuously in the C/2

regimes, it remains stable in the last 10 C/10 regimes. The stable retention in the last C/10 cycles suggests that at low rates, the cell can consistently deliver the capacity in accordance with the active material content remained in the cell. Overall, Cell L had lost about 45% of its capacity in the overall life cycle test through the C/2 regimes at 60 Celsius, according to the capacity determined by the last 10 C/10 cycles.

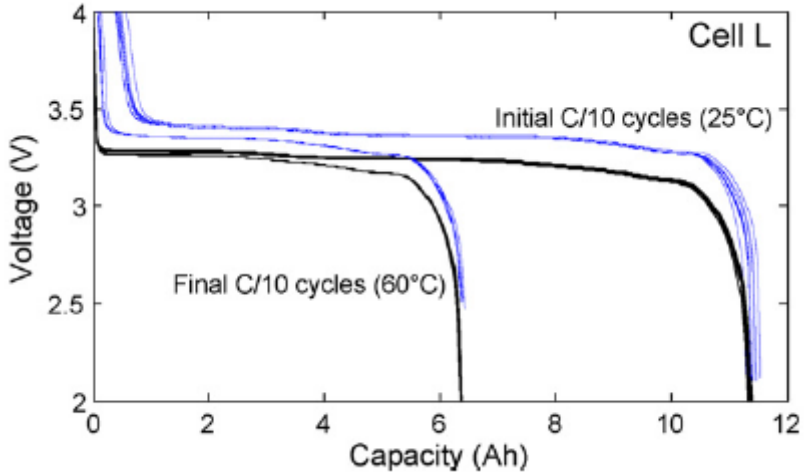

Figure 33 Initial and final C/10 cycles in the life cycle test of Cell L at 25 C

3. Experimental Set-up

3.1 Test Bench for test

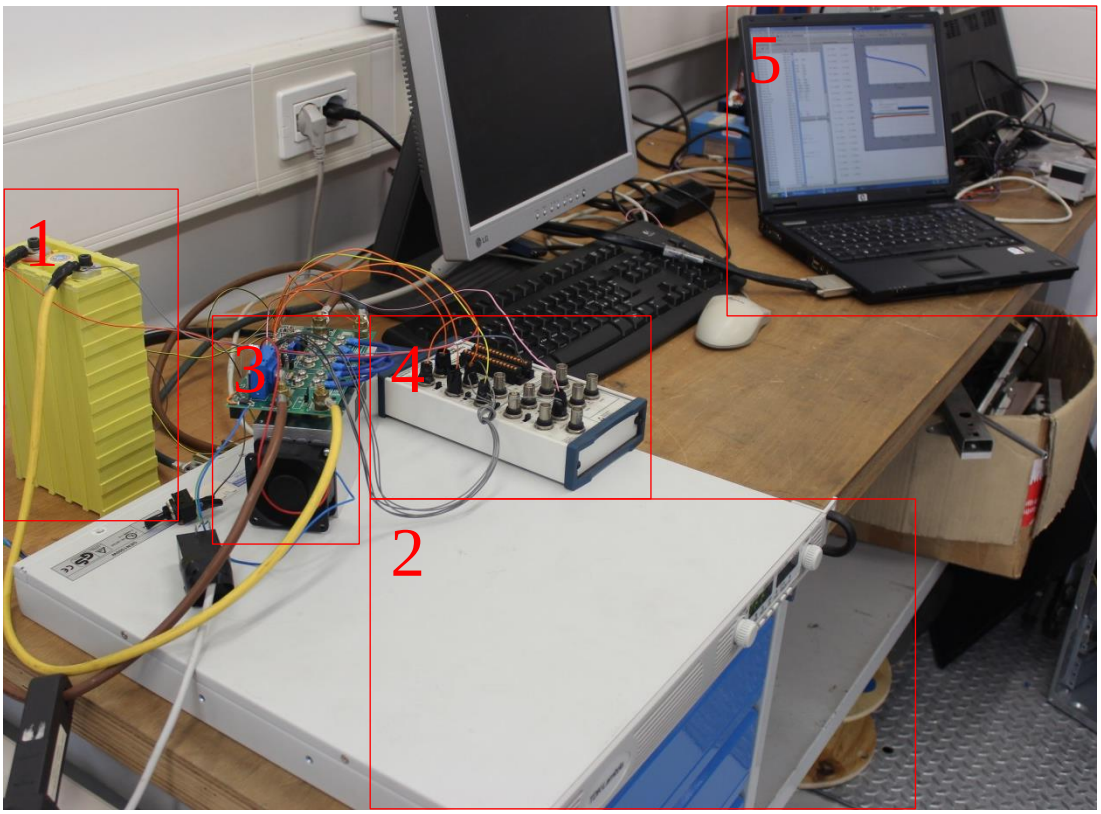

Figure 34 Battery Test Bench

1: Battery

2: Power supply

3: Load

4: Data Acquisition System

5: Computer

This is the test bench for the battery and it can be divided into 5 parts: battery, power supply, load, data acquisition system and PC. The following figures (Figure 35 and Figure 36) show the hardware structure during the charging and discharging phase.

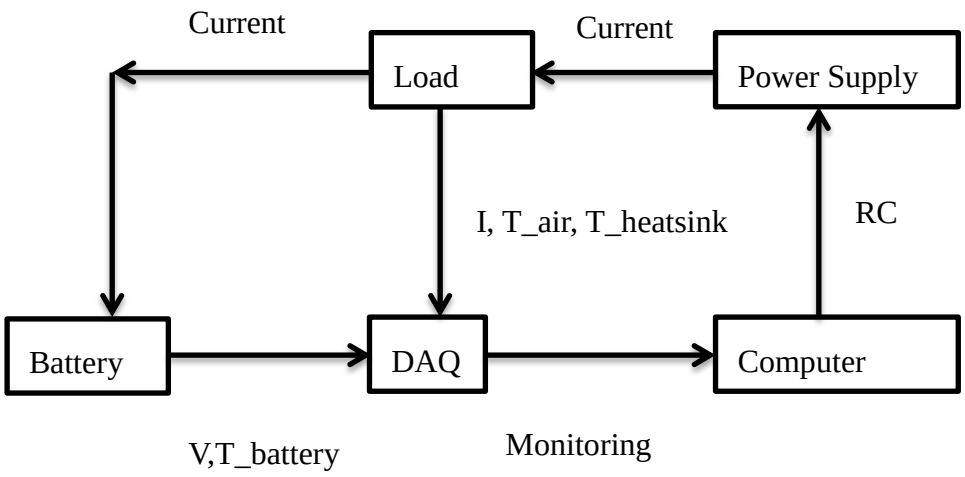

Figure 35 Connection During Charging

AO: Analog output Signal

AI: Analog input Signal

RC: Remote Control

With the application of the MATLAB, we can control all the electric components in the bench, and receive all the information of the battery. The boundary condition set in the program of the PC (Highest Voltage and Lowest Voltage of the Battery) will decide the critical time for shifting the phase. In the serial communication port (A/D convertor), we can set the sampling frequency and time-out to get the required data we want.

In the Charging phase, the computer set the current and voltage of the power supply by remote sensing. The load will measure the current going through and the temperature of air and heat sink. The data acquisition system will also record the battery temperature and the voltage of the battery continuously. At the same time, the DAQ will send the monitoring result to the PC.

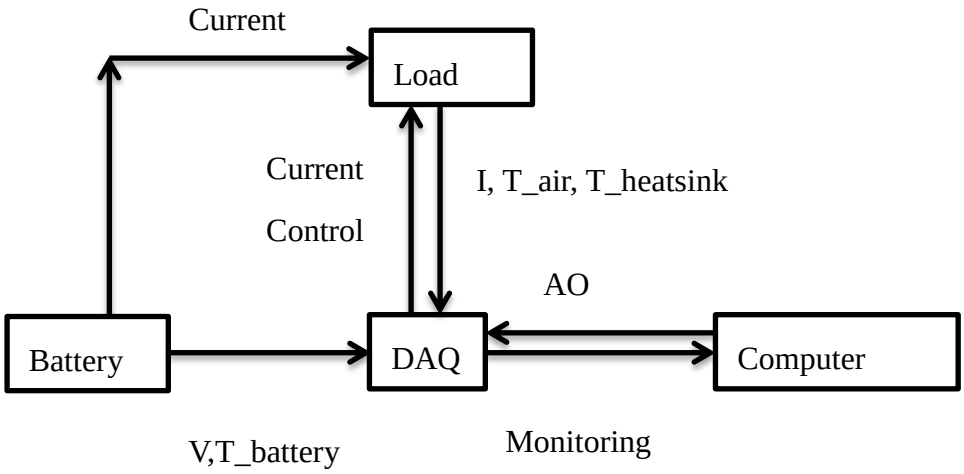

Figure 36 Connection During Discharging

During the discharging phase, most the monitoring procedure will be almost the same. But the power supply will be completely useless and we can switch off the power supply will the command. What should be pointing out is that the analog output signal should be decided carefully to control the discharged current.

3.1.1 Battery Specification

SINOPOLY LITHIUM ION BATTERY SPECIFICATIONS:

Figure 37 Battery model: TS-LFP60AHA(A) [25]

Model	**TS-LFP60AHA(A)**	
Nominal Capacity	60Ah,192Wh	
Nominal Voltage	3.2V	
Life Cycle	80%DOD	≥3000Times
	70%DOD	≥4000Times
Self-discharge Rate	≤3%	
Weight	2.3±0.05kg	

Table 5 specification of the battery

	Charge	Discharge
Cut-Off Voltage	4V	2.8V
Standard Current	0.5C,30A	0.5C,30A
Max Constant Current	3C,180A	3C,180A
Max Impulse Current	20C,1200A	20C,1200A
Operating Temperature	$-45^oC \sim +85^oC$	$-45^oC \sim +85^oC$

Table 6 Electric parameters of charge and discharge

In the Table 5, we can read the nominal voltage 3.2V and the nominal capacity 60Ah. The related power will be the production of the two that is 192Wh. For different DOD, the cycling life will be different: Increasing DOD will lead the shrinkage of the life of the lithium battery. The self-discharge rate is very small (only 3%), so we do not need to consider the influence of self-discharge on the experiment. Table 6 shows the standard parameters, current limitation and operation temperature of this type of battery. All the data here are produced by the factory of the battery, so it can be treated as the reference of the following test.

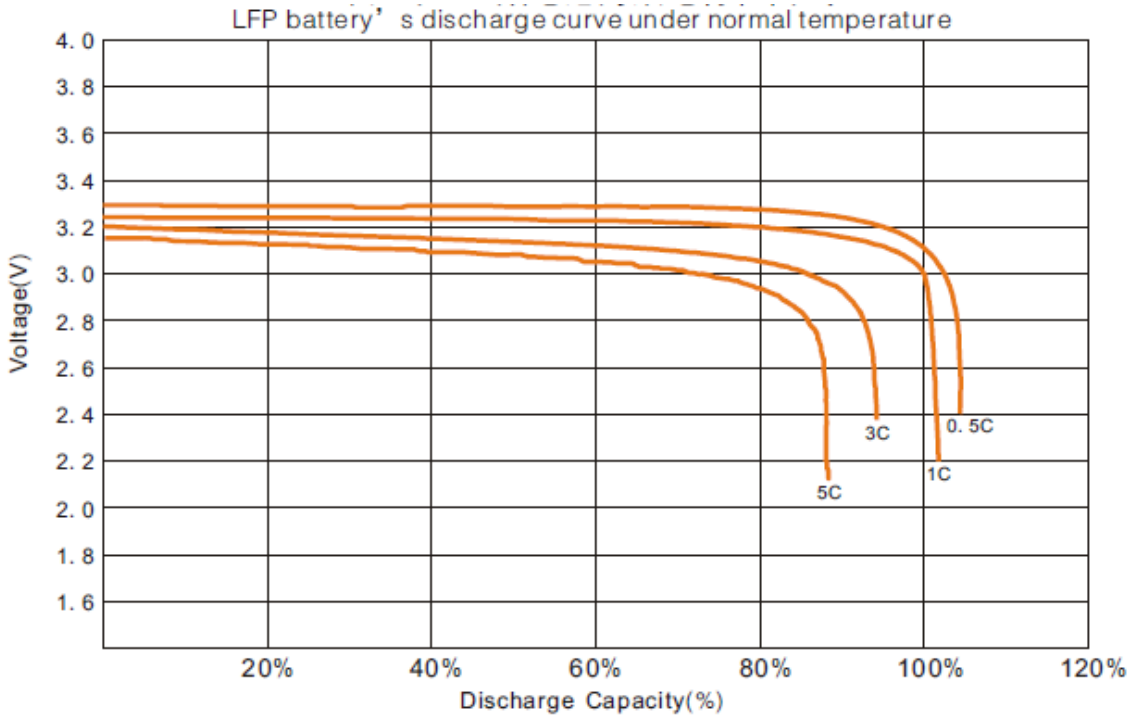

Figure 38 Discharge Curve under Normal Temperature

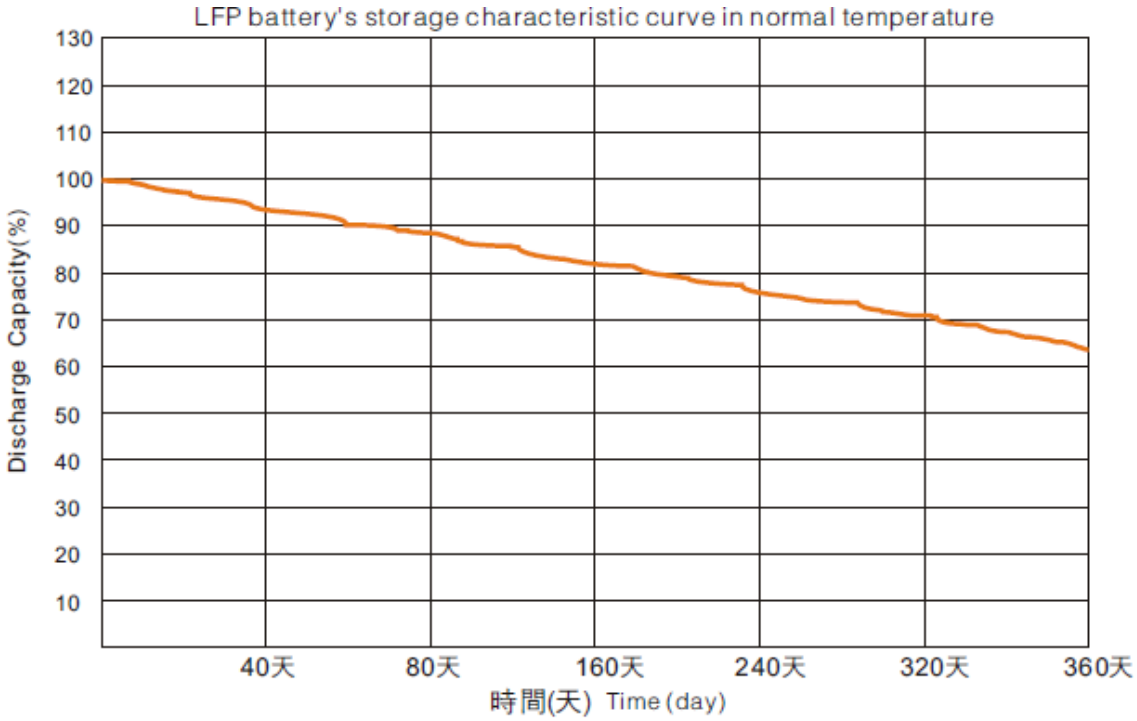

Figure 39 Battery’s storage characteristic curve in normal temperature

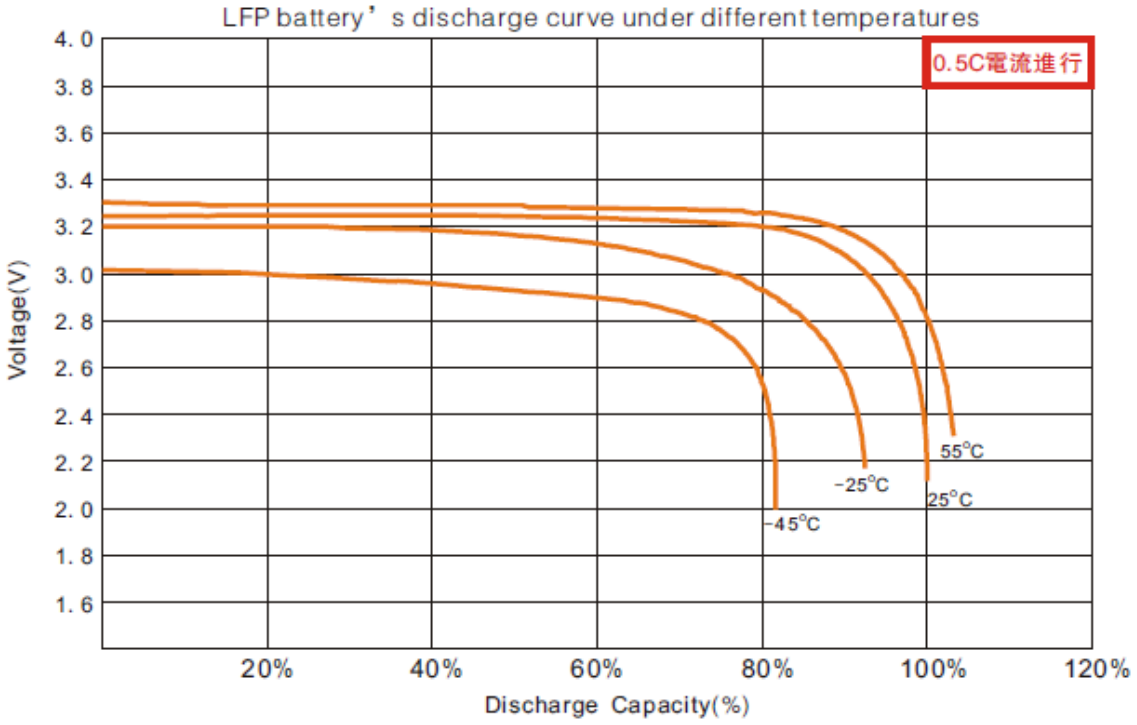

Figure 40 Battery’s discharge curve under different temperatures

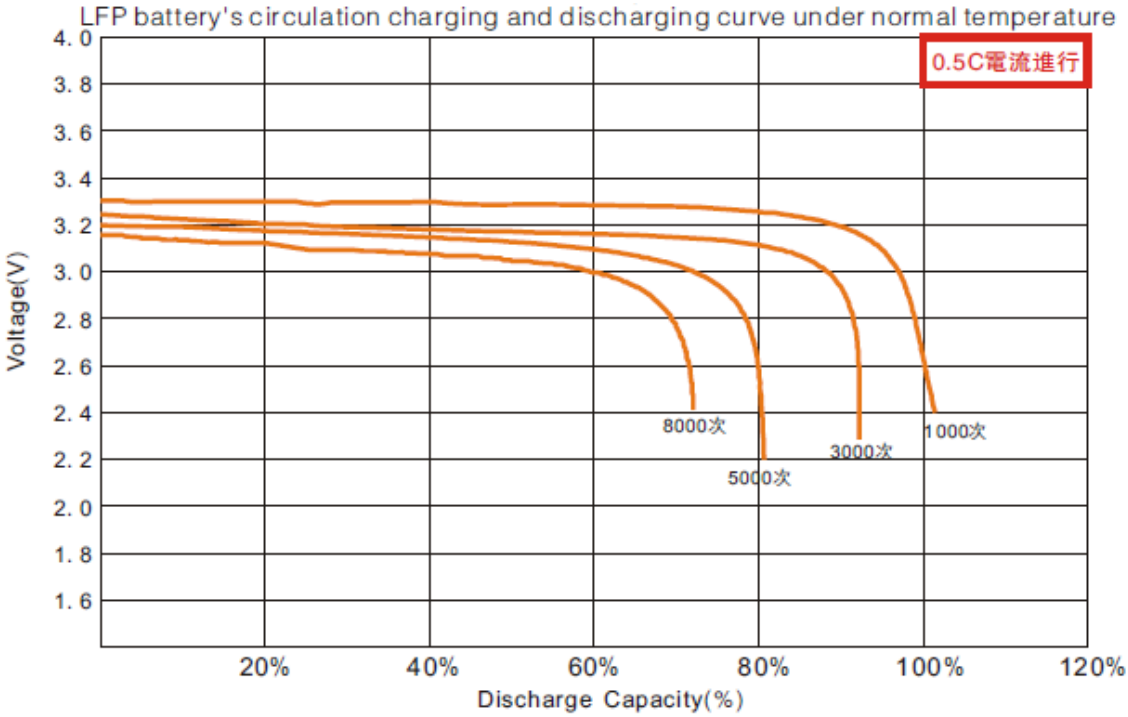

Figure 41 LFP battery's circulation charging and discharging curve under normal temperature

From Figure 38 to Figure 41, we can see different characteristics of the batteries. In the Figure 38, the voltage decreases rapidly at the beginning of the discharging, and then the trend becomes stabilized between 15Ah and 45Ah. After that, the voltage drops very quickly to the lowest point at 68 Ah. Figure 39 shows clearly the calendar aging of the battery during storage, we can find that the capacity decreases from 100% to 65% smoothly. The influence of the temperature can be read in the Figure 40, in high temperature environment, the voltage seems to be horizontal in a longer time than that of lower temperature.

3.1.2 Power Supply-Charge system

Power supply will be used to charge the battery and stabilize the current by remote control during charge phase. It connects the computer with serial communication port. The connection cable will be RS232, this kind of cable is very useful in short distance signal transmission, and it is very easy to be installed on the computer. On the screen, we can read the current and the voltage of the charging system to understand clearly the state of the experiment.

Figure 42 Different Buttons on the panel of Power Supply

3.1.2.1 Working Principle of the Power supply

The working principle of the power supply is to execute the AC-DC switching. Figure 43 shows a switching supply with electrical isolation in a simplified block diagram form. The input ac voltage is rectified into an unregulated dc voltage by means of a diode rectifier. It should be noted that an EMI filter is used at the input to prevent the conducted EMI. The dc-dc converter block in the figure converts the input dc voltage from one level to another dc level. This is accomplished by high-frequency switching, which produced high-frequency ac across the isolation transformer. The secondary output of the transformer is rectified and filtered to produce V0. The output of the dc supply in figure is regulated by means of a feedback control that employs a PWM (Pulse Width Modulator) controller, where the control voltage is compared with a saw-tooth waveform at the isolation transformer as shown or through an opto-coupler.

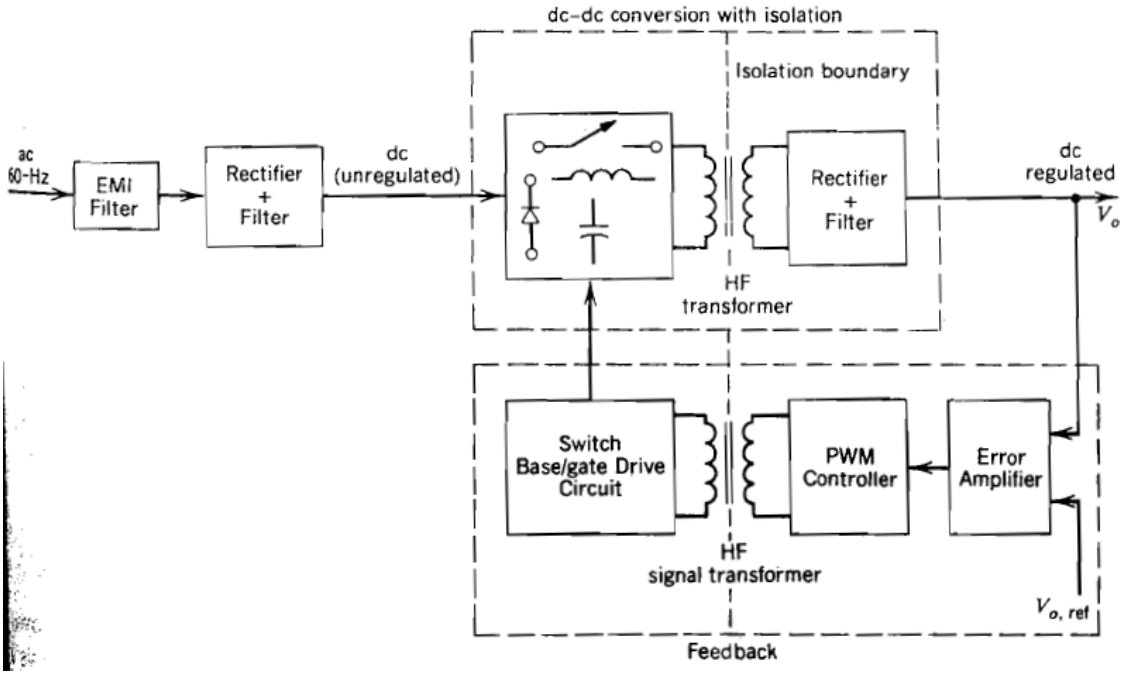

Figure 43 Schematic of a switch-mode dc power supply

3.1.2.2 PWM control

In the PWM switching at a constant switching frequency, the switch control signal, which controls the state (on or off) of the switch, is generated by comparing a signal-level control voltage with a repetitive waveform as shown in the Figure 44 (a) and (b). The control voltage signal generally is obtained by amplifying the error, or the difference between the actual output and its desired value. The frequency of the repetitive waveform with a constant peak, which is shown to be a saw-tooth, establishes the switching frequency. This frequency is kept constant in a PWM control and is chosen to be in a few hundred kilohertz range. When the amplified error signal, which varies very slowly with time relative to the switching frequency, is greater than the saw-tooth waveform, the switch control signal becomes high, causing the switch to turn on. Otherwise, the switch is off. In terms of voltage and the peak of the saw-tooth waveform, the switch duty can be expresses as

$$\mathrm{D} = \frac{t_{on}}{T_s} \tag{42}$$

The dc-dc converters can have two distinct modes of operation: (1) continuous

current conduction and (2) discontinuous current conduction. In practice, a converter may operate in both modes, which have significantly different characteristics.

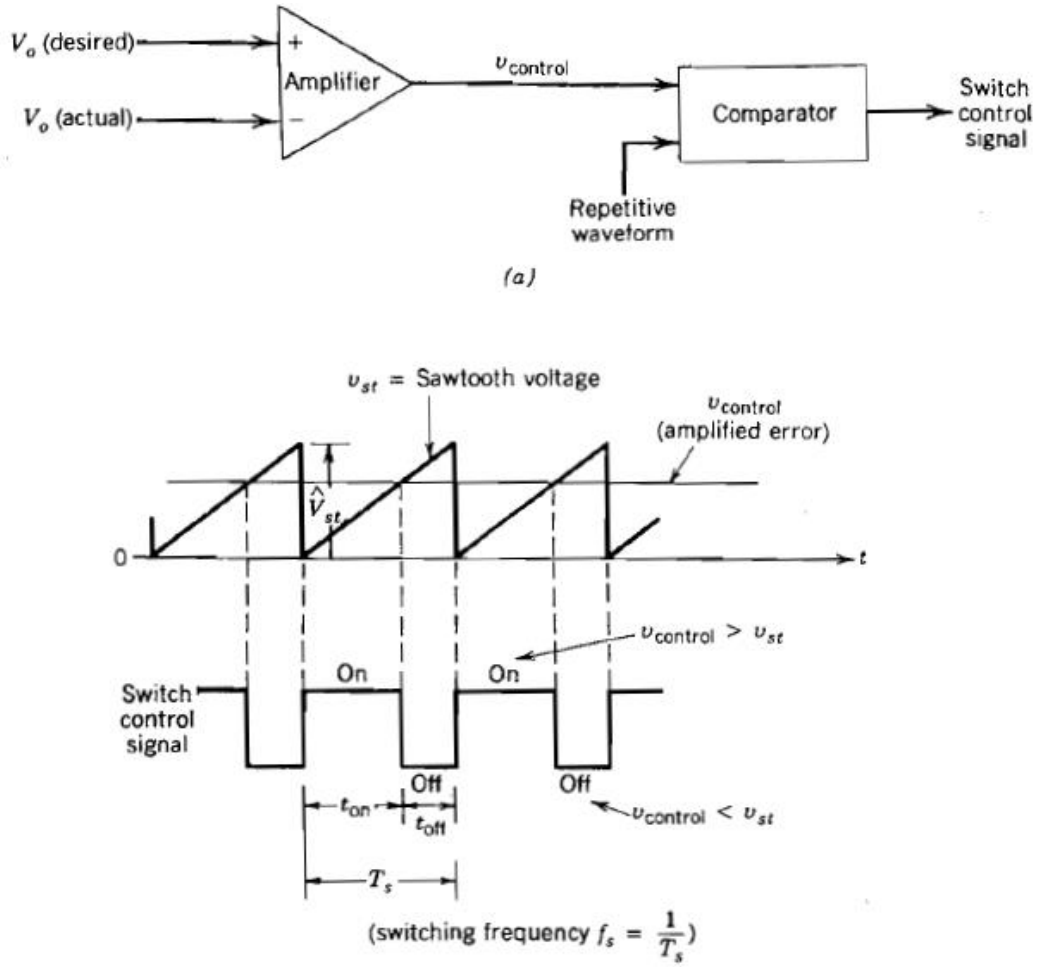

Figure 44 Pulse-width modulator: (a) block diagram; (b) comparator signals

3.1.3 Discharge system

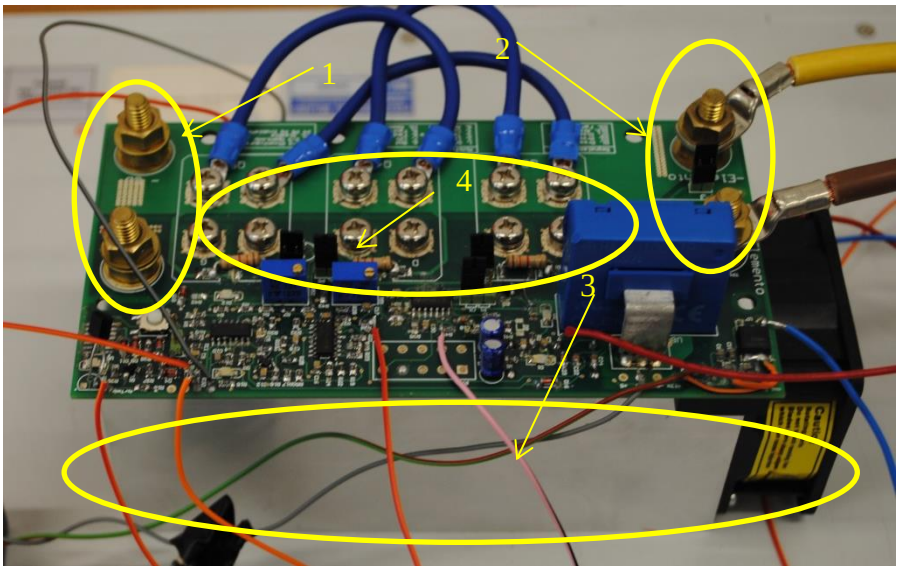

Figure 45 Discharge System

1: Connection with the battery for discharging

2: Connection with the power supply for monitoring

3: Heat sink for cooling

4: MOSFET for current control

This is the discharge system for the cycling. It can be divided into 2 parts: the heat-sink and 3 MOSFET cells. The MOSFET cells are responsible for the stabilization of the current to get a constant current condition and the heat-sink is applied to transforming the electrical energy to the heat energy and decreasing the discharger temperature.

3.1.3.1 Heat sink

Figure 46 shows the specification and size of the heat-sink, the heat-sink in my experiment is 150mm with 12V. So, we can read from the right line chart in the Figure 46, the thermal resistance is 0.175K/W. The maximum voltage is 4V at the beginning with the current 60A, so the maximum power is 80W. The temperature difference between air temperature and heat-sink will be 80W*0.175K/W=42K.

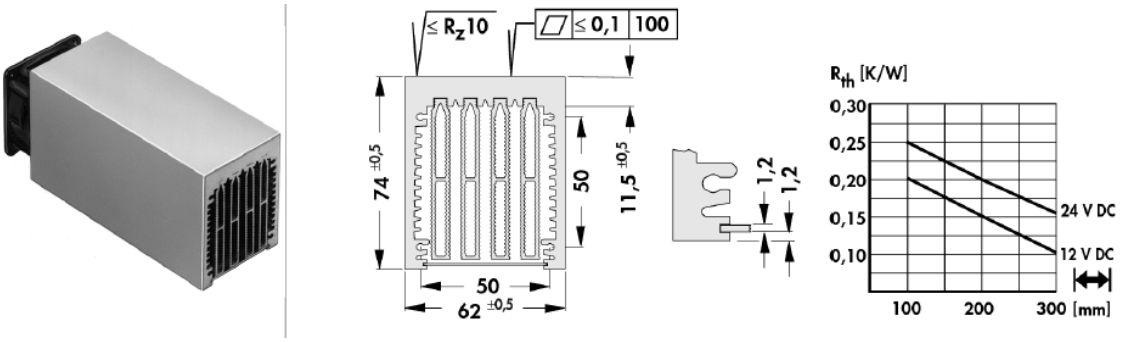

Figure 46 Specification of the heat-sink

3.1.3.2 MOSFET

The model of the MOSFET cells is IXFN 60N80P. The analog signal goes into the Gate (G point in the Figure 47). And the resistance of the MOSFET is the function of the analog signal. The lowest resistance is 0.14Ω. For example, if the voltage of the cell is 2.8V, the current run through the cell will be 2.8V/0.14Ω=20A. With 3cells, we can reach required current for discharge. In the Figure 48, we can check easily the relationship between current and the cell voltage.

The thermal resistance of the MOSFET is 0.17K/W. The power for each resistance will be 20A*4V=80W. The temperature difference will be 0.17K/W*80W=13.6K.

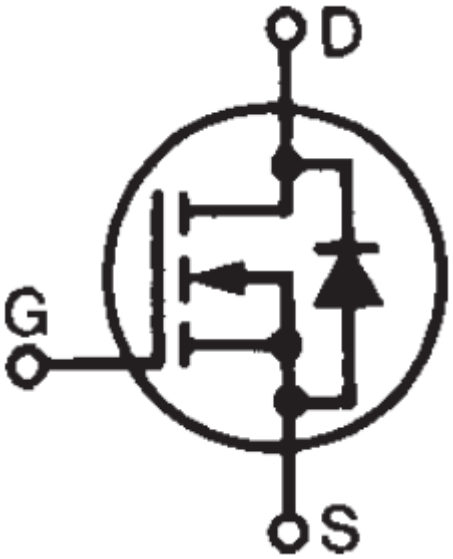

Figure 47 Structure of MOSFET

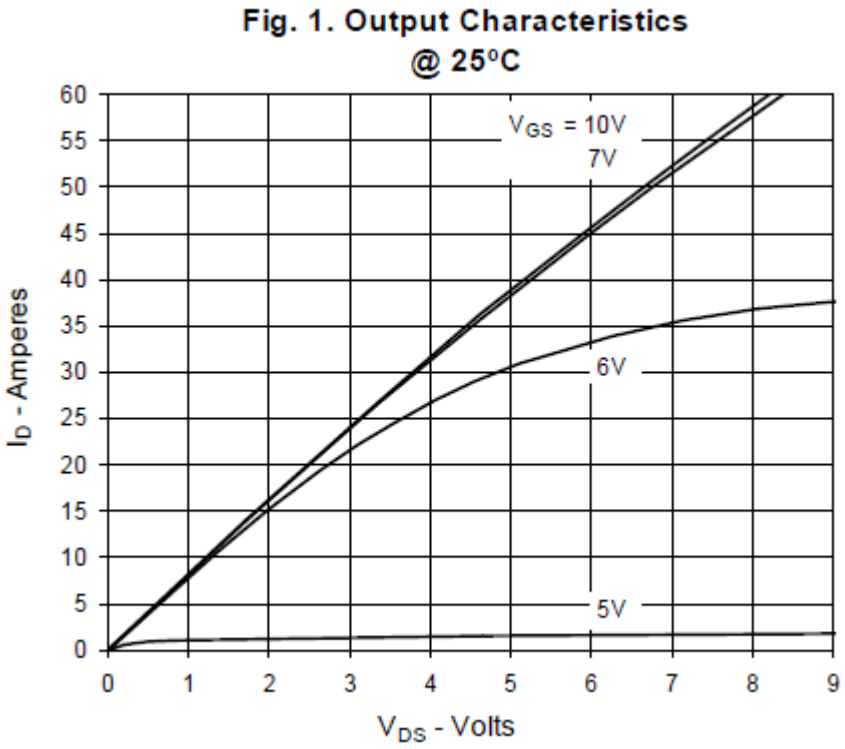

Figure 48 Output Characteristics of the MOSFET

3.1.3.3 Safety Consideration

Our experiment is executed under the condition of the 60A, with theory Joule law, a huge amount of the heat will be generated during the discharging phase. The temperature during the test must be considered as an important factor to be analysis and measured. The Figure 49 shows the resistor structure of the discharger. Resistor1-3 represent the 3 MOSFET cells the Resistor 4 represent the thermal resistor of the heat sink. From the calculation of the previous 2 chapters, we know the temperature difference of the heat sink and MOSFET cells are 42K and 13.6K. If we assume the air temperature is 25 degree. The highest temperature can be reached would be 25+42+13.6=80.6. This value is lower than temperature limitation, which is 125 degree. So we can make sure the discharger can works well during experiment from the theoretical side.

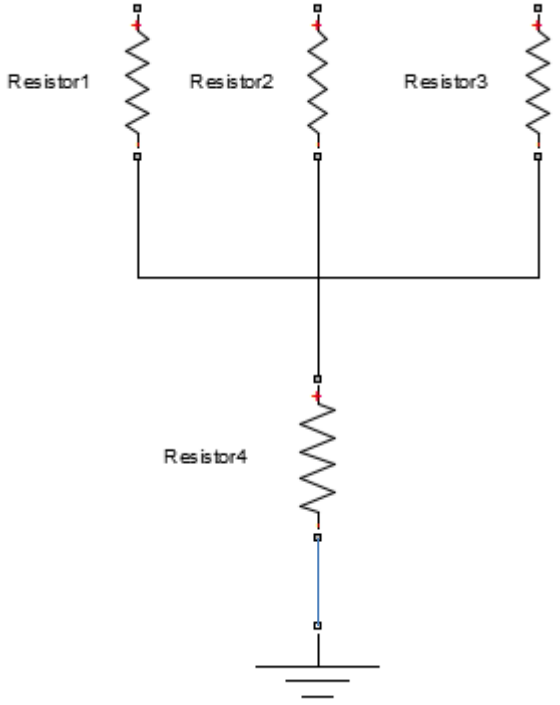

Figure 49 Thermal resistor structure of the discharge system

3.1.4 BNC Adapter for Digital and Analog Signals

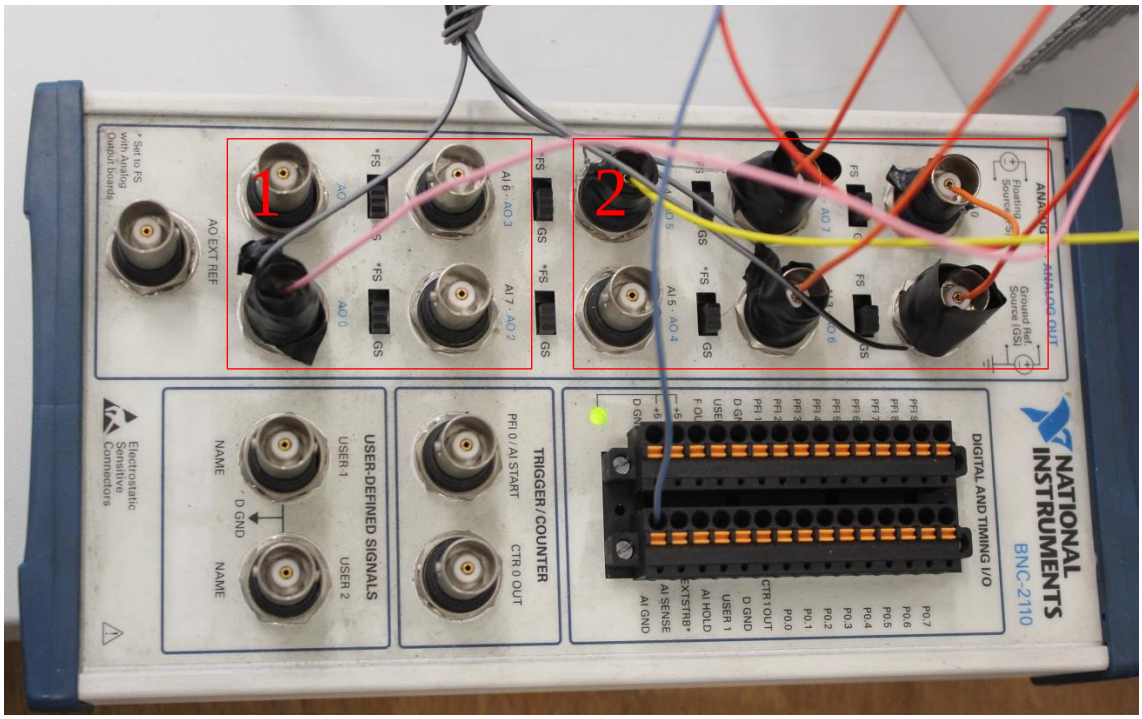

Figure 50 BNC-2110

1: Analog Output

2: Analog Input

The BNC-2110 is ideal for simplifying connections between your measurement apparatus and my DAQ device in laboratory, test, and production environments. [5]

The BNC-2110 has the following features:

• 15 BNC connectors for analog input, analog output, trigger/counter functions, and user-defined signals

• A spring terminal block with 30 pins for digital and timing I/O signal connections

• A 68-pin I/O connector that connects to multifunction DAQ devices

• Can be used on a desktop or mounted on a DIN rail

3.1.4.1 Analog Input of the BNC Adapter

Analog input is very important for the whole system, because it's the bridge between sensors and the computer. In my program 5 channels (Voltage, Current, temperature from the heat sink, air temperature, and battery temperature) are set to send analog information to the PC.

The analog signals from the 5 channels are from the sensors of system. All the signals will be sent with the unit volt. The computer will do some amplification or conversion to get the real value of the signals.

No. of Channels	Type of information
1	Voltage
2	Current
3	Temperature in heat sink
4	Air Temperature
5	Battery temperature

Table 7 Channels for Analog Input

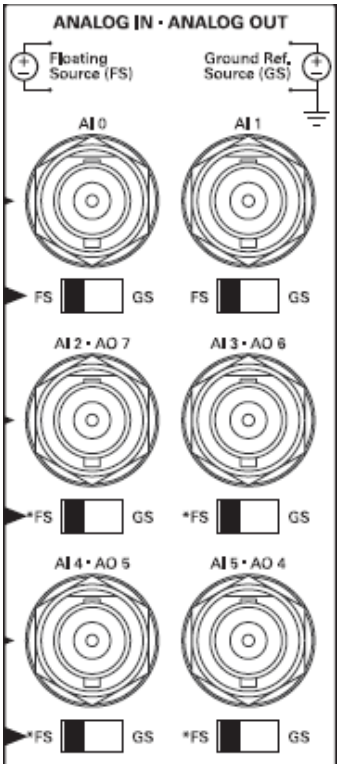

Figure 51 Analog Input of the BNC Adapter

3.1.4.2 Analog output of the BNC Adapter

Analog output signal is used to control the current of the load during the discharging: the increasing analog output signal will lead to the increasing current in the load. In my system, the AO1 will be used.

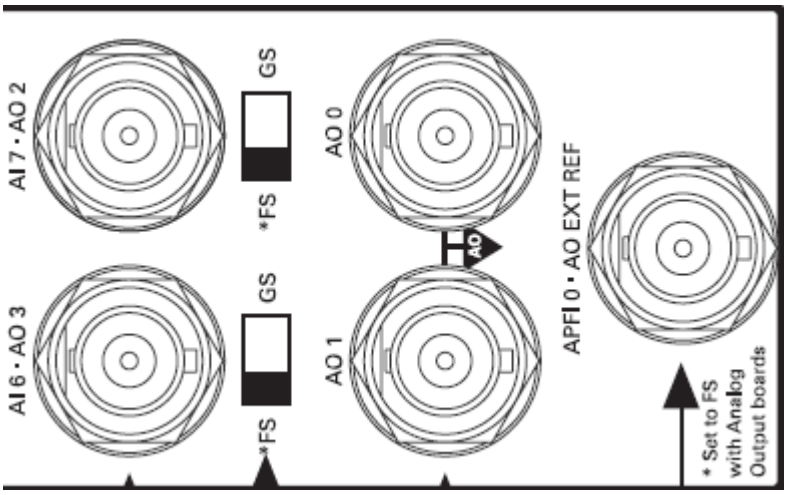

Figure 52 Analog output of the BNC adapter

3.1.4.3 Signals Conversion

No.	Original Units	New Units	Offset & Sensitivity
1	V	V	Read directly
2	V	I	I=(U-2.5)/1.35*100
3	V	K	T=(U-2.5)*100
4	V	K	T=(U-2.5)*100
5	V	K	T=(U-2.5)*100

Table 8 Signal Conversion

From the Analog input of the board, all the signals must be in volts, we need to compensate the difference by some amplification. The first one, voltage, can be read directly. The current should be changed due to some specification of the BNC board [5]. The temperature should be applied in Kelvin, so the sensitivity should be 100 and the offset should be 2.5.

3.2 Software Structure

One cycle can be divided into 4 phases: Discharge, Rest, Charge and Rest. With the application of the Matlab, we can control the boundary condition for shifting phase. This figure shows clearly the complete procedure of the test.

The n starts from 1, meaning that the test starts from the 1st cycle, and the cycle will stop when it reach the desired number of cycle N. In the discharge phase, the voltage is decreasing with the time and when the voltage reaches the boundary condition, the lowest voltage set at the beginning of the program, the internal cycle will stop, and the computer will record the real discharge stop time DST. During the Rest phase, the time of this phase RT will be set as 1 hour, so when the time reach the sum of RT and DST, the internal cycle will break and the Charging phase starts. As the same theory of discharging, the charge phase will stop when the voltage reaches the boundary condition, the highest voltage set at the beginning. After the second the rest phase, all the data will be saved in the mat file.

Symbol	Meaning
Tic	Real calculation start time
Toc	Time recorded from tic
N	total number of cycles
n	number of cycle
k	number of times for monitoring
DST	Discharge stop time
CST	Charge stop time

Figure 53 Parameters Definition

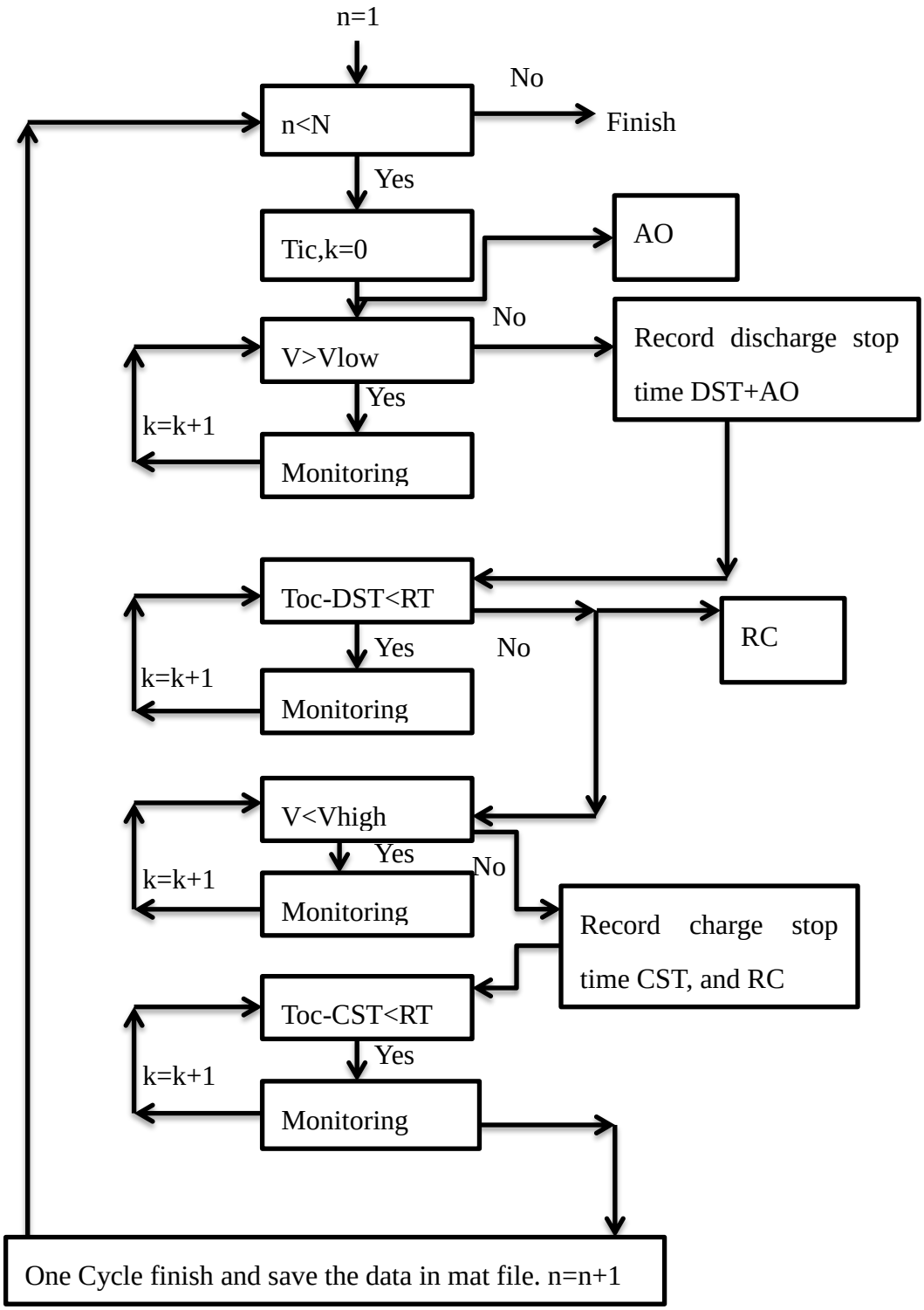

Figure 54 Logical Circuit for one cycle

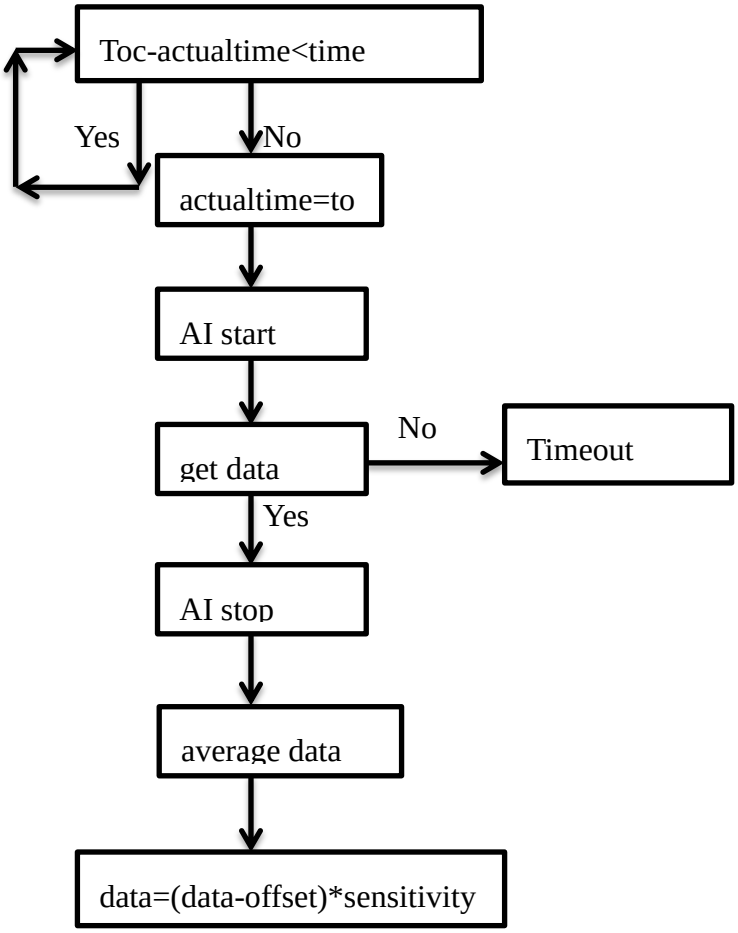

Figure 55 Logical cycle for monitoring

Each monitoring will last 5 seconds, and the data will be recorded in the first second, due to the sampling frequency is equal to 1000Hz, we can get 1000 samples in the first second, then the following 4 seconds will be used to average the 1000 samples and save the averaged value in the text file which will be used for data analysis in the following steps. The offset and the sensitivity of the devices should be taken into consideration due to the transformation of the sensors.

During the discharging, when the voltage of the battery is decreasing, the current will influenced. So we prefer to use the differential method to compensate the error between the measured current and reference current as follows:

When the measured current is quite higher than that of the reference one, the analog output will be decreased by 0.1 to shrink the gate of the current to decrease the current in the discharging system. If the measured current is closed to that of reference, the voltage will be increased or decreased by 0.02. Oppositely, if the measured current is much smaller than that of reference, we should increase the voltage by 0.1 to amplify the current in the discharging. If the current difference is between the value -1 and 1, the voltage will remain the same. In conclusion, this part of program is applied to stabilize the measured current around the reference current.

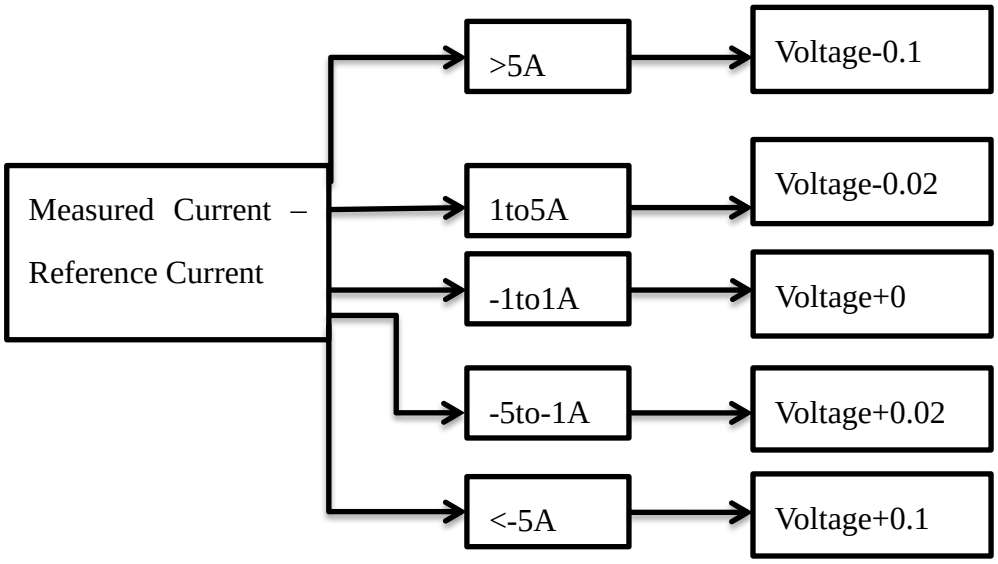

Figure 56 Current Stabilization during Discharging by Analog Output

3.3 Experimental Environment and Challenges

To obtain nice behavior, storage temperatures below 60℃ are desirable. It has to be mentioned here, that for the storage temperature of more than 65℃ used, chemical reactions are supposed to occur, that are not expected at lower temperatures. This leads to deviations from exponential behavior. Some of the cells stored at more than 65℃ even showed gassing process, leading to a fast death of cell [20].

Testing batteries can be a very tedious and long process requiring many days and hours to complete simple tests. This is due mainly to the fact that batteries are electrochemical systems that vary greatly from battery sample to battery sample. Due to this variation, it is often difficult to predict the behavior of the battery during a test, resulting in many failed tests and ruined batteries. To make matters more difficult, the battery test stations used in this work contain a switching power supply to support the requirement of charging the battery cell during testing. The switching frequency in the power supply generates noise in the electrical circuit, and because the supply must be electrically connected to the battery directly. Thus, it is easy to see that signal noise plays the part of a very challenging adversary in the task of obtaining accurate and consistent battery testing data.

4. Modeling and Data Analysis

4.1 Cycling Result

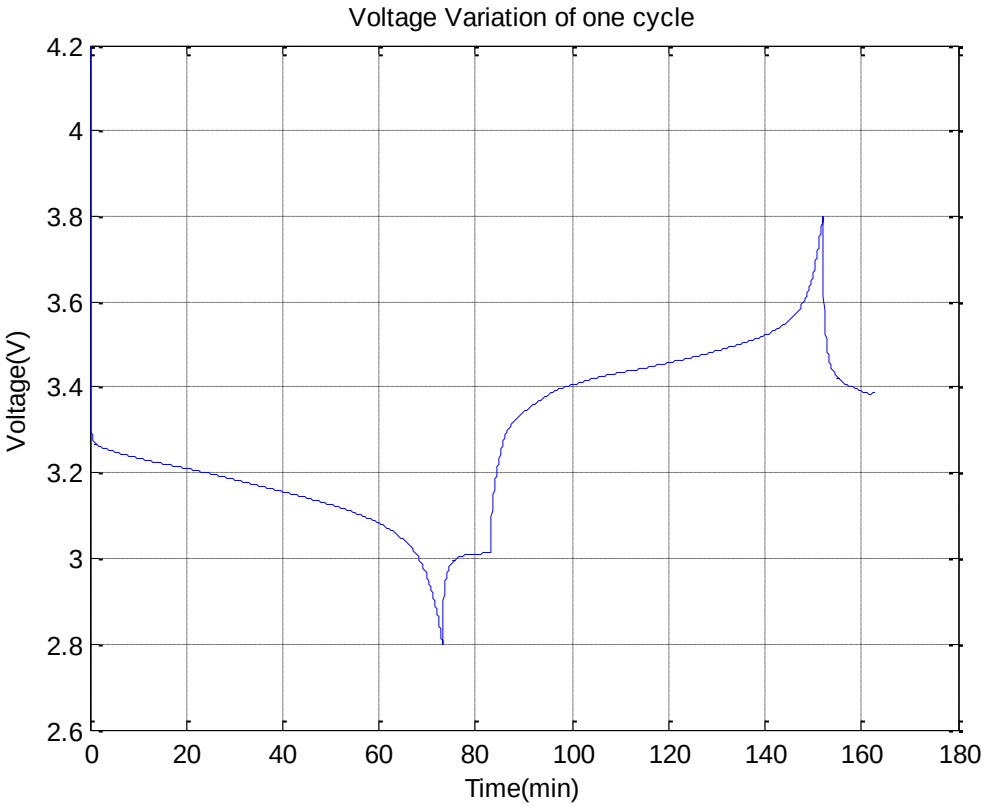

Figure 57 Voltage Variation during one cycle

This diagram shows clearly the voltage variation during one cycle, it will last 163 min, and we can read obviously 4 different state of battery: discharging, first rest, charging and second rest.

Discharge Phase starts at 100% state of charge, there was a rapid initial loss in voltage as charge was removed from the battery. Following this rapid drop, a period of nearly linear voltage loss was observed from approximately 90 to 10% SOC. After this quasi linear range, there was a steep drop in voltage until the battery reached 0% state of charge. The definition of zero percent state of charge was formed by the manufacturer's defined minimum safe voltage which was 2.8 Volts for the particular cells used in these

experiments. A similar maximum safe voltage of 3.8 Volts was also specified by the manufacturer, this formed the definition of 100% SOC. In the rest phase, the voltage recovery back from 2.8 to 3.02 Volts. After 10-minute rest, the charge phase starts. The charging phase last a bit shorter than that of discharge, from 83.5 to 152.7 minutes. The trend is similar to that of discharge, the voltage increases quickly at the first and last 10 minutes. This constant current charging protocol was followed whenever a battery was charged to 100% SOC. During the charging, the voltage stabilizes around 3.45 volts. After hundreds of cycles, the time for charging and discharging will decrease due to aging.

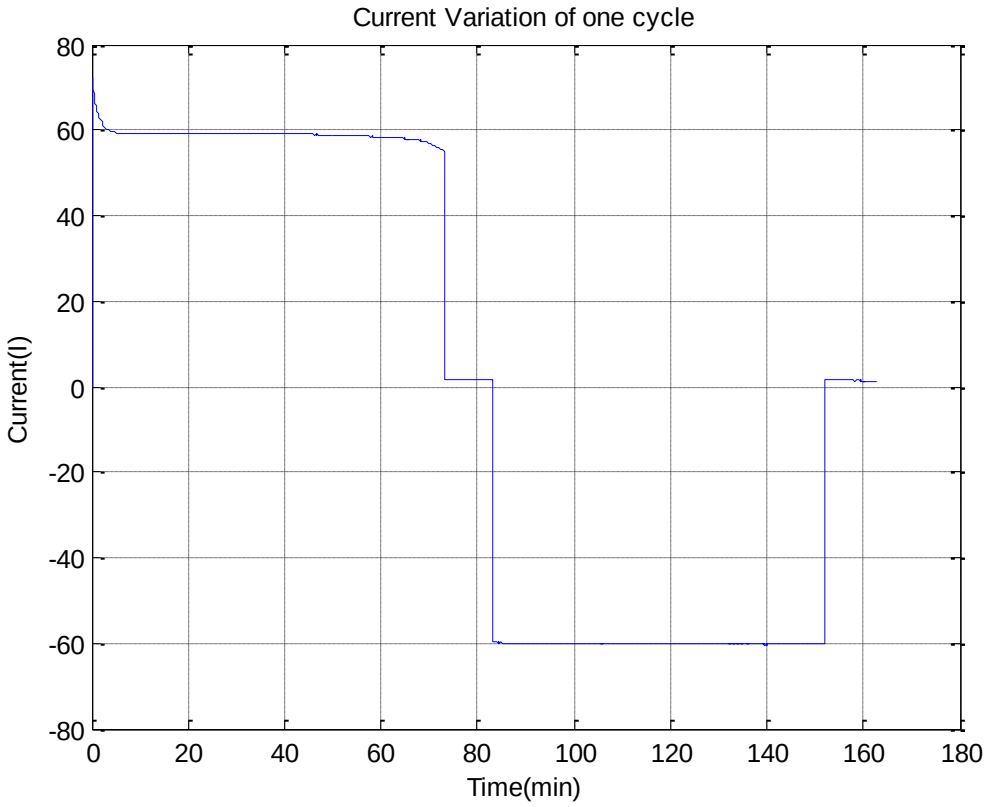

Figure 58 Current Variation during one cycle

As defined in the Matlab program, the current will be stabilized around 60 A. If the current is positive, it means the electrical current goes out of battery, oppositely, it means the power supply is charging the battery. At the end of discharging, because the voltage is very low so it can keep the current constant, this is the reason why there is a

small drop at the end of the discharging. During the 2 rest phases, there is a recovery of the voltage, so it cannot be 0. However, the electrical energy recovered is quite small, the current during rest can be regards as 0 compared with the working current.

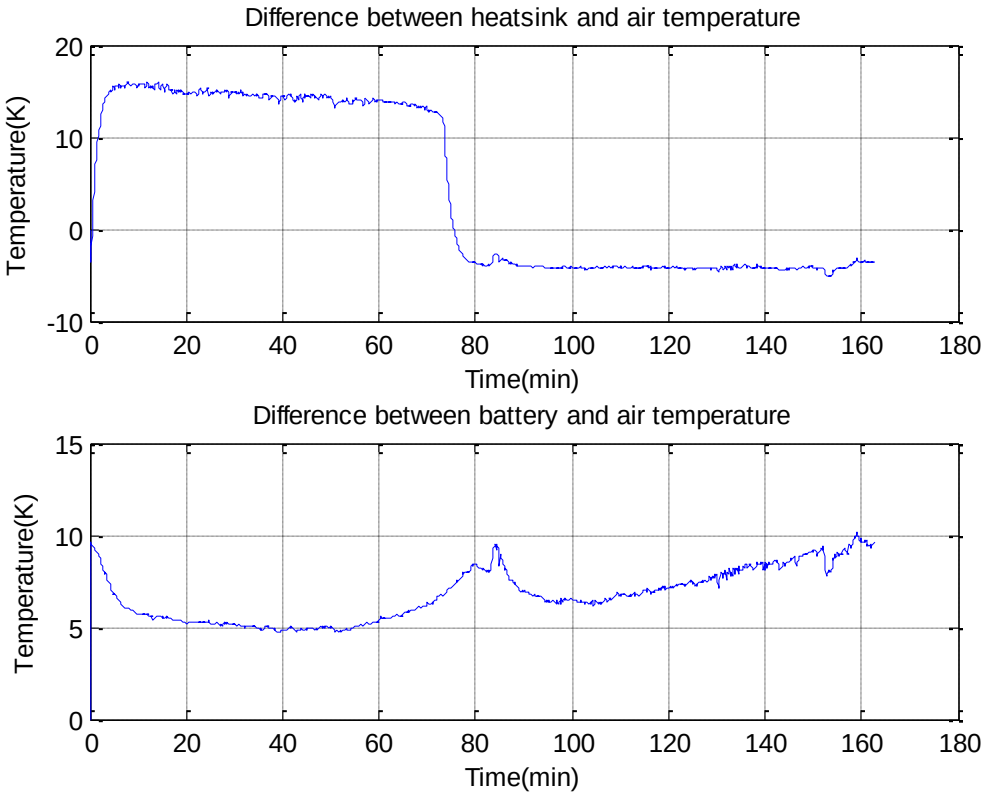

Figure 59 The temperature of the heat sink and battery

The main reason of the temperature measurement is to monitor the condition of the battery and other devices. As shown before, the current in this experiment is quite high, reaching 60A. From Joule Effect, the heat generation during the experiment should be very high. We must make sure the experiment proceeds in a safe condition.

Some trend can be seen from the temperature plot. The heat sink only work during the discharging phase, so there is a great difference between heat sink temperature and the environment temperature, which are almost 15℃. After that, the heat sink drop a bit lower than that of air temperature and keep this value until the next discharge phase.

4.2 Data Analysis

The relate energy is shown in the specification of the battery at the chapter 3,

$$\text{Relate energy } Q_r = 60\text{Ah} * 3.2\text{V} = 192\text{W.h} \tag{43}$$

And the discharged and charged energy $Q_d \; and \; Q_c$ will be

$$Q_d = \int_{tds}^{tde} V * I * dt \tag{44}$$

$$Q_c = \int_{tcs}^{tce} V * I * dt \tag{45}$$

tde: discharge end time

tds: discharge start time

tce: charge end time

tcs: charge start time

And the capacity retention ratio could be:

$$\text{r} = \frac{Q_d}{Q_r} \tag{46}$$

After calculation we can read the result of the first 160 cycles, the result of calculation is shown in the Appendix D. The Figure 60 represents clearly the capacity retention at the first 160 cycles; we can read obviously the trend of the capacity, it decreasing with the number of cycles, at the end of the line it takes only 96.5% of the initial capacity. The battery efficiency vibrates around 0.95 at the first 80 cycles, it shows a small decreasing during the following 80 cycles.

In the Figure 61, 5 different cycles are shown clearly during their discharging phase. We can find the trend that when we repeat the experiment, the time for discharging is decreasing, because the energy transferred during discharging is decreasing, under the same the current, the area of voltage $\int V \, dt$ is decreasing.

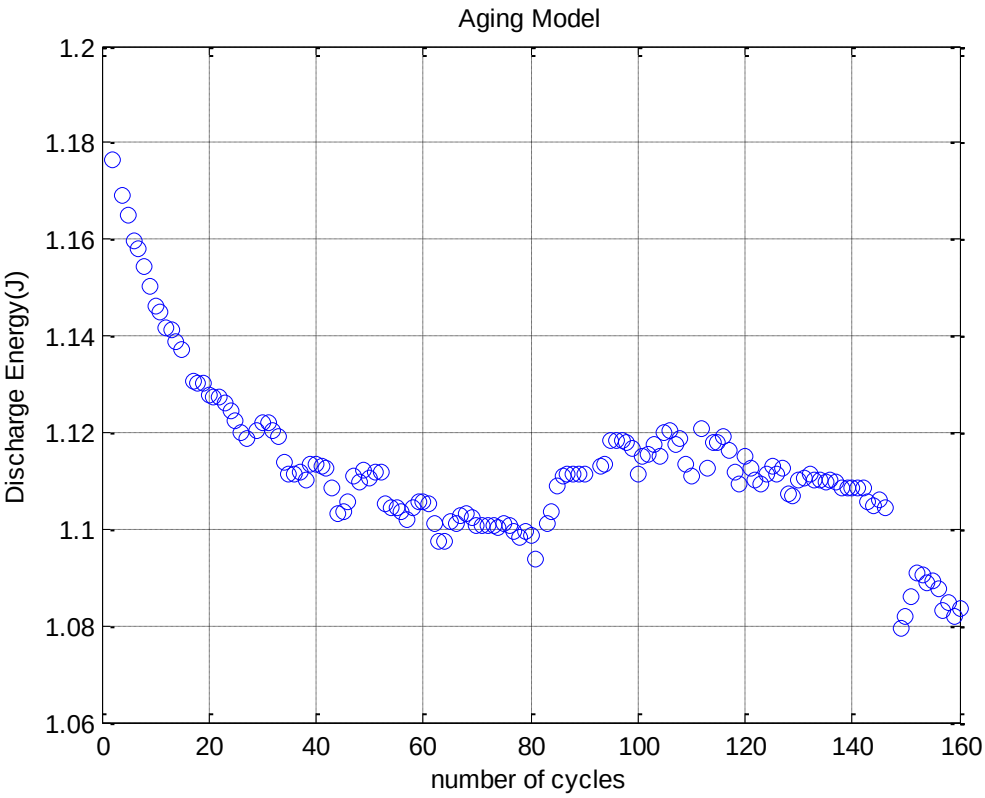

Figure 60 Capacity Retention in the first 160 cycles

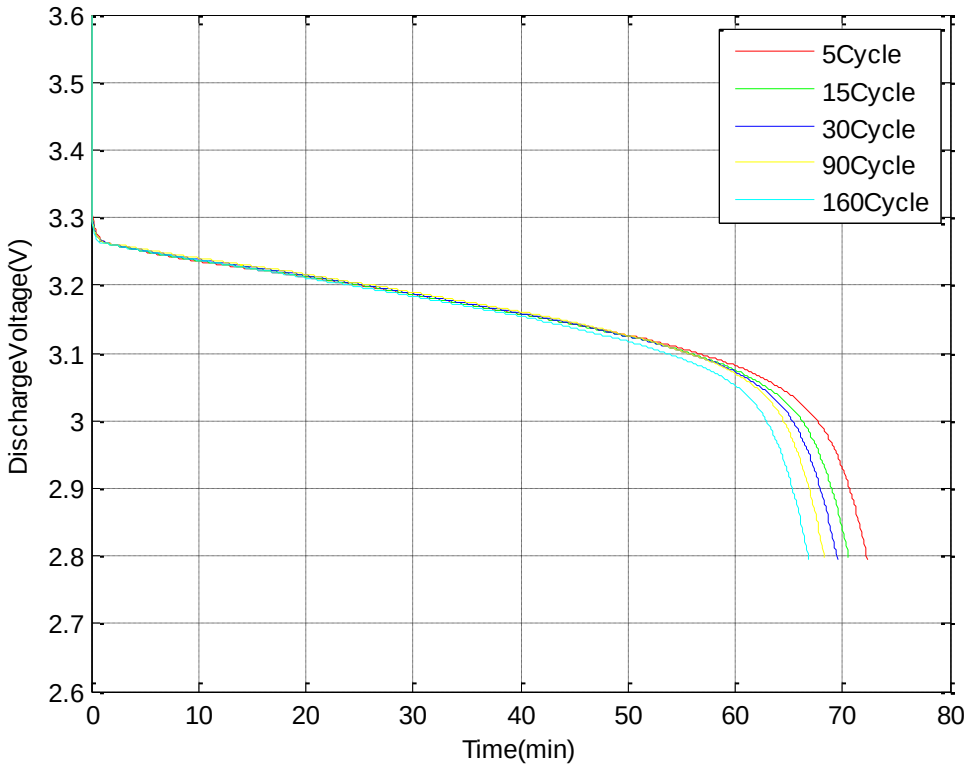

Figure 61 Discharge Curve between first 160 cycles

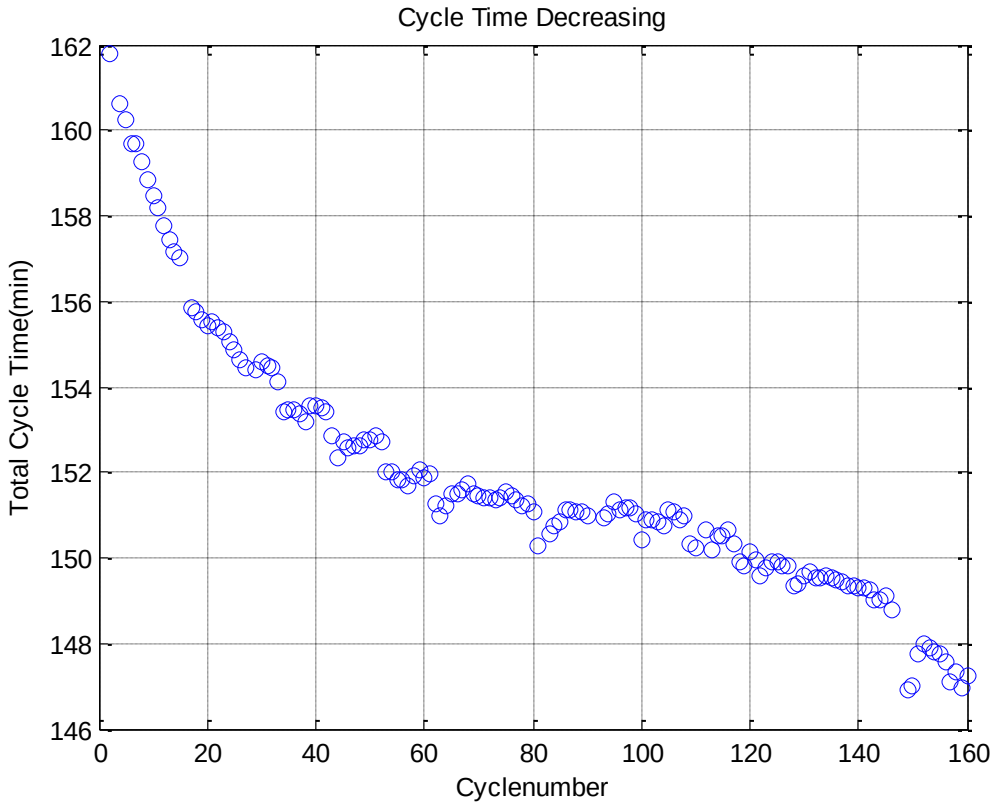

Figure 62 Decreasing of the cycle time

Figure 62 shows the time needed for cycling. We can find that the total cycle time is decreasing as increasing of the number of the cycles. The trend is very similar with that of current throughput. Because of the equation (1), we can see that the Ah throughput is proportional to the time when the current is kept almost constant.

The battery efficiency could be:

$$\eta = \frac{Q_d}{Q_c} \tag{47}$$

It represents how much energy can be stored and used from a given charge. The higher the efficiency, the higher the energy can be used. In the Figure 63, the battery efficiency can be observed that it can't be influenced or influenced obviously by the battery aging. The trend is random during the first 80 cycles, with an average value of 95%, the following 80 cycles have an average value around 94.5%.

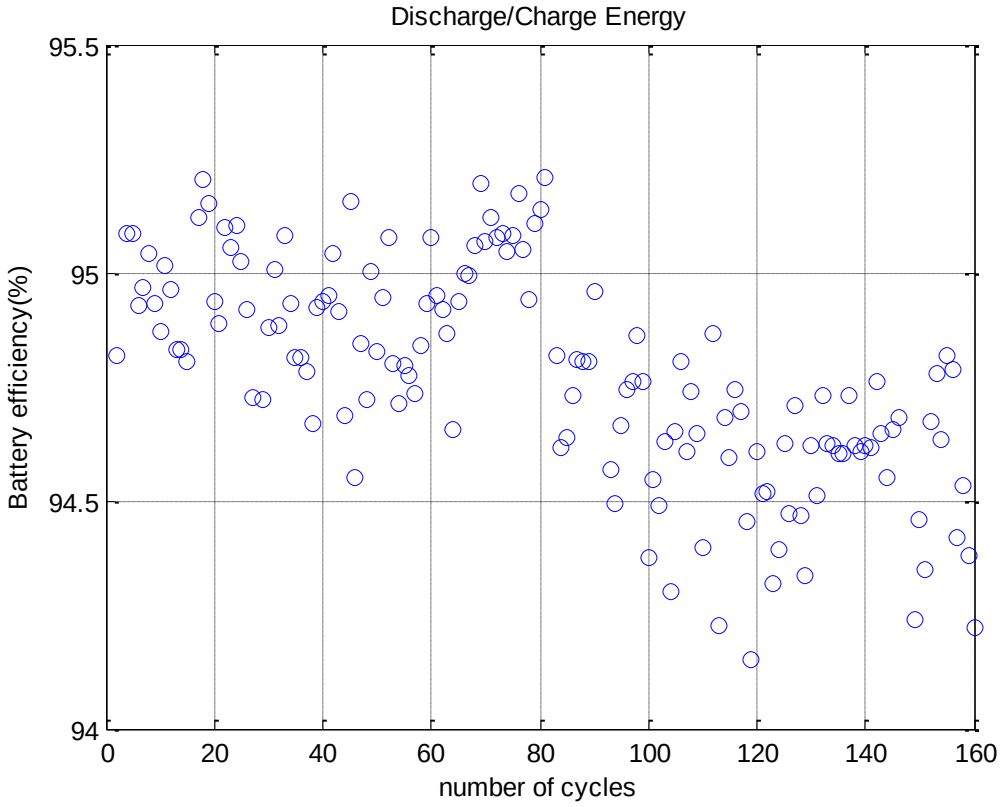

Figure 63 Battery Efficiency

4.3 Numerical Models for Fitting and Life prediction

After cycles, the creep of aging can be witnessed in the Figure 64.

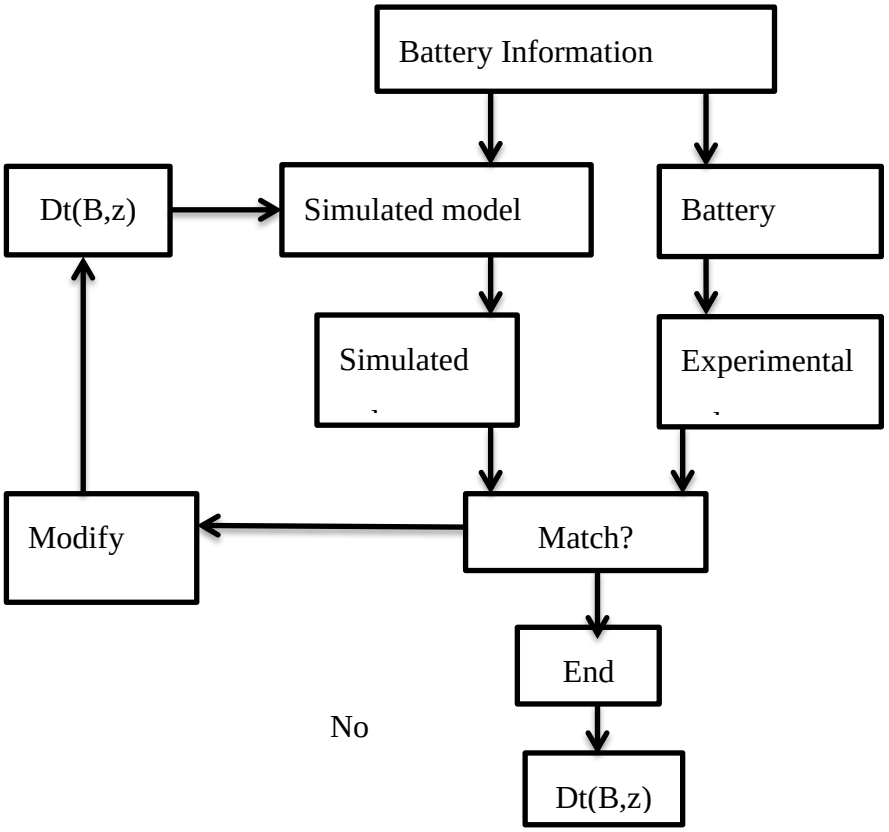

Figure 64 Flow diagram of the parameters estimation procedure

The input parameter is the number of cycles, as shown in the Figure 64, battery information such as the Ah-throughput and number of cycles will be input in both simulated battery and the battery to get the simulated voltage and the experimental voltage. Then, we calculate the difference between them to check whether they match or not.

4.3.1 First Cycling Model (based on Ah-throughput)

The current is kept constant during discharging and charging, so the electrical quantity removed in the required time is completely the same. From the equation shown in the first chapter, the state of charge will be proportional with time, so the SOC will decrease lineally during working phase as the Figure 65. On the opposite side, the DOD will increase linearly with the time. The final value of the DOD will be the Ah-throughputA_h for this cycle.

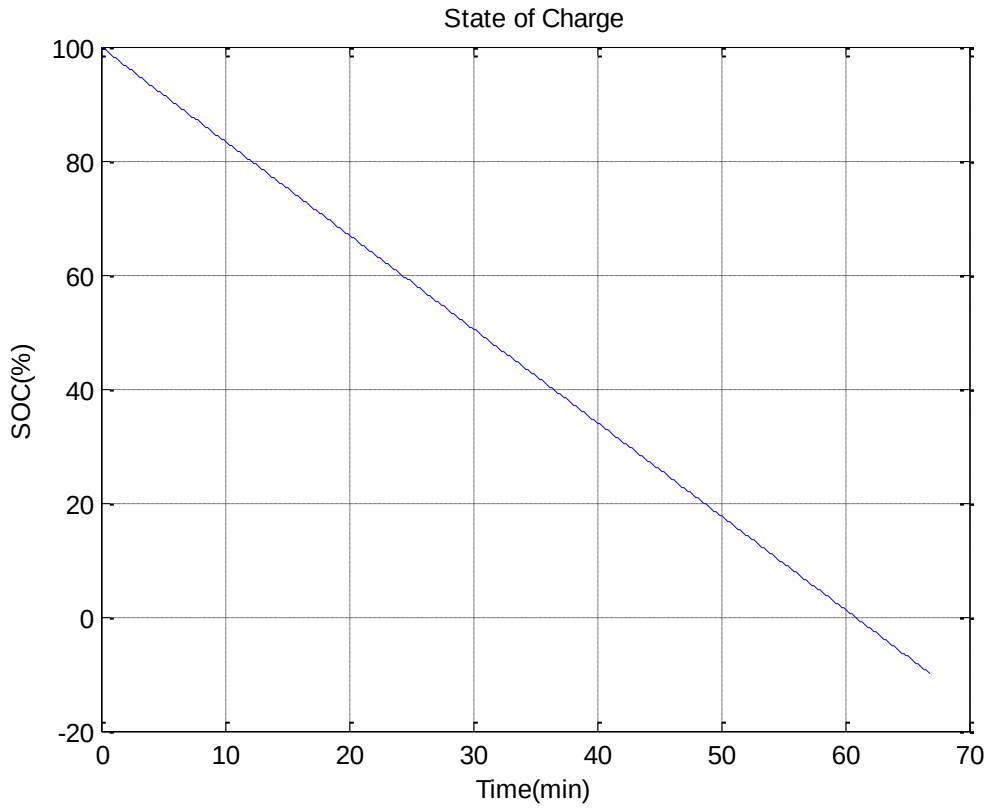

Figure 65 State of Charge of the first cycle

In the Figure 66, we can see that, during aging, the capacity is a parameter decreasing with the increasing cycles. Similar to the energy trend, the capacity decreases quickly at the first several cycles, after that, the trend slow down. We use the first value as the reference one. So the capacity starts from the 100%. And the capacity retention Q_{loss} will start from 0%.

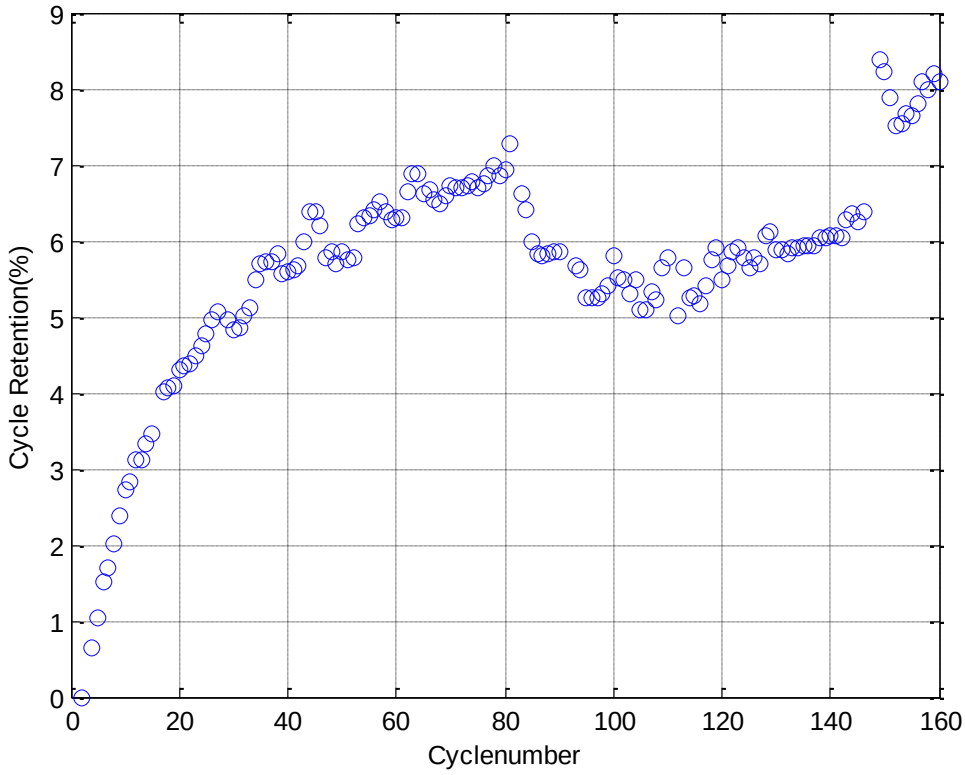

Figure 66 Capacity Retention during Aging

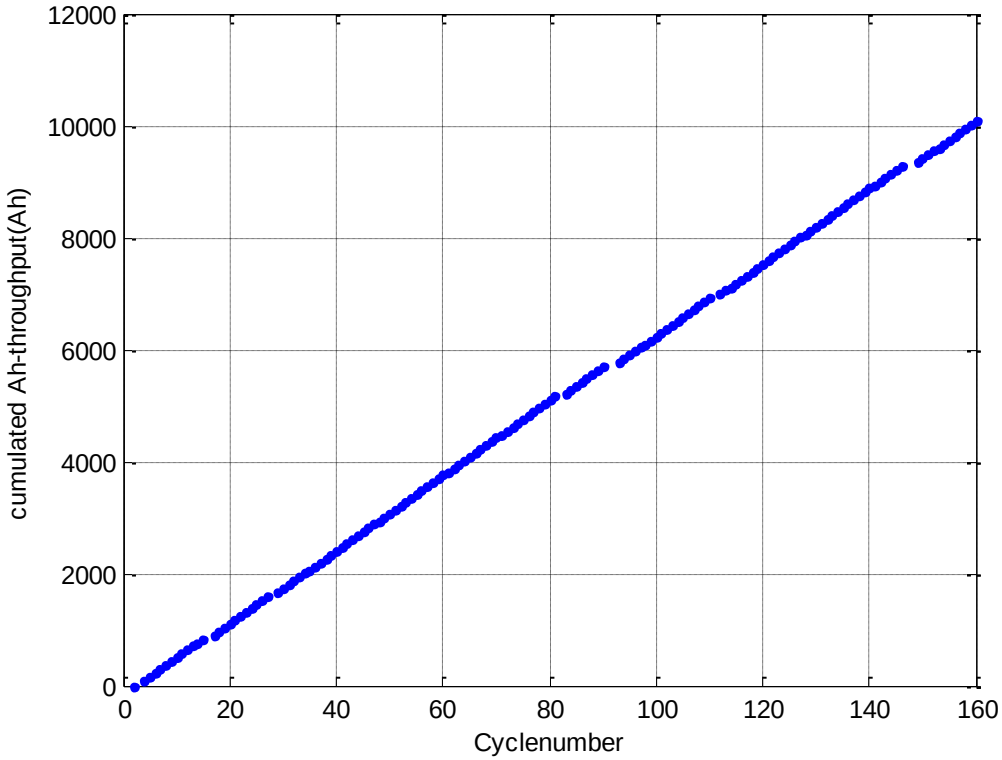

Figure 67 The Cumulated Ah-throughput

As the current stay constant during aging, we can observe the cumulated electrical quantity increases linearly with the number cycle.

Instead of using time, we chose Ah-throughput as a parameter for the life modeling. Ah-throughput represents the amount of charge delivered by the battery during cycling. At each C-rate, Ah-throughput is directly proportional to time; however, the merit of using Ah-throughput is that it allows us to quantify and correlate the capacity fading behaviors for different C-rates. The life model can be expressed as [34]:

$$Q_{loss} = B * \exp\left(\frac{-E_a}{R * T}\right) * (A_h)^z \quad (48)$$

In Equation (48), Q_{loss}, is the percentage of capacity loss, B is the pre-exponential factor, Ea is the activation energy in Jmol−1, R is the gas constant, T is the absolute temperature, and Ah is the Ah-throughput, which is expressed as Ah = (cycle number) ×(DOD) ×(full cell capacity), and z is the power law factor. Clearly, the exponent term represents that the temperature follows Arrhenius Law. For analytical purposes, we rearrange this slightly to [34]:

$$\ln(Q_{loss}) = \ln(\mathrm{B}) - \left(\frac{E_a}{R * T}\right) + \mathrm{z} * \ln(A_h)$$

E_a	31500 J/(mol)
R	8.314 J/(mol*K)
T	293 K

Table 9 Parameters for the first modeling

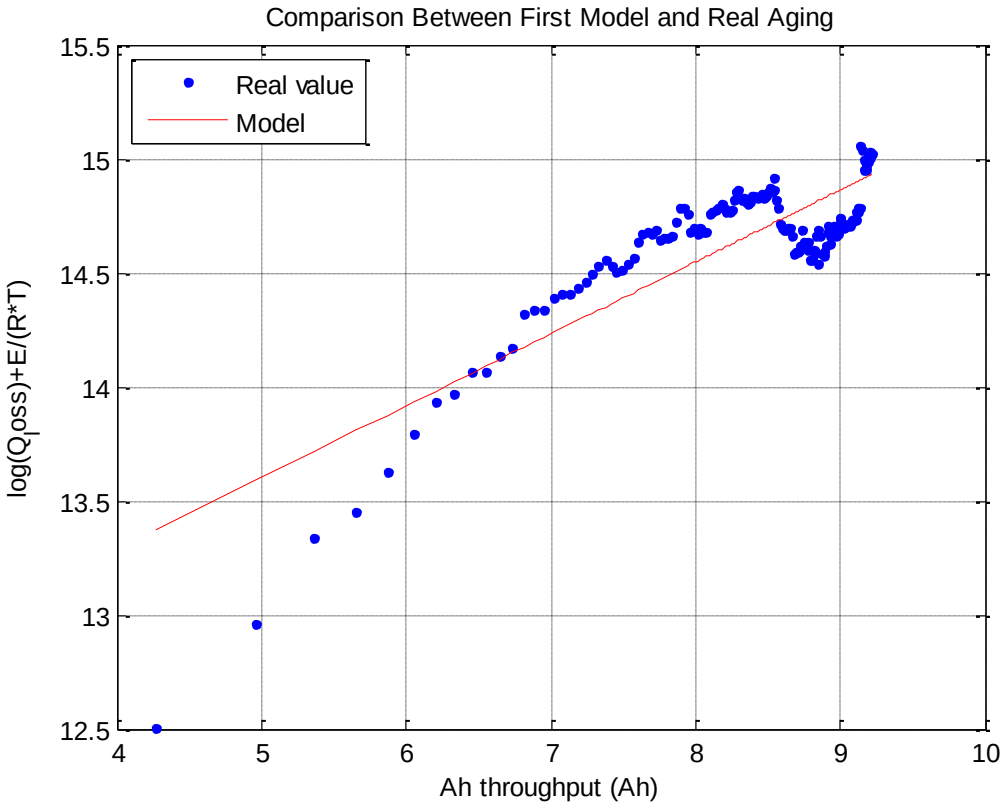

Figure 68 Comparison between second Aging Model and Real Value

The fitting parameters is z= 0.6521; ln(B)= 9.5785. If we assume the end of life will be 80% of the battery capacity, we can do the prediction of the battery life.

$$Ah_{end} = \sqrt[\frac{1}{z}]{\frac{Q_{lossend}}{B * \exp\frac{-E_a}{R * T}}} \tag{49}$$

In the following cycles, we assume the average Ah-throughput will be between the 60Ah and 65Ah. So the predicted number of cycles would be around 3400 cycles.

4.3.2 Second Cycling Model (based on capacitance)

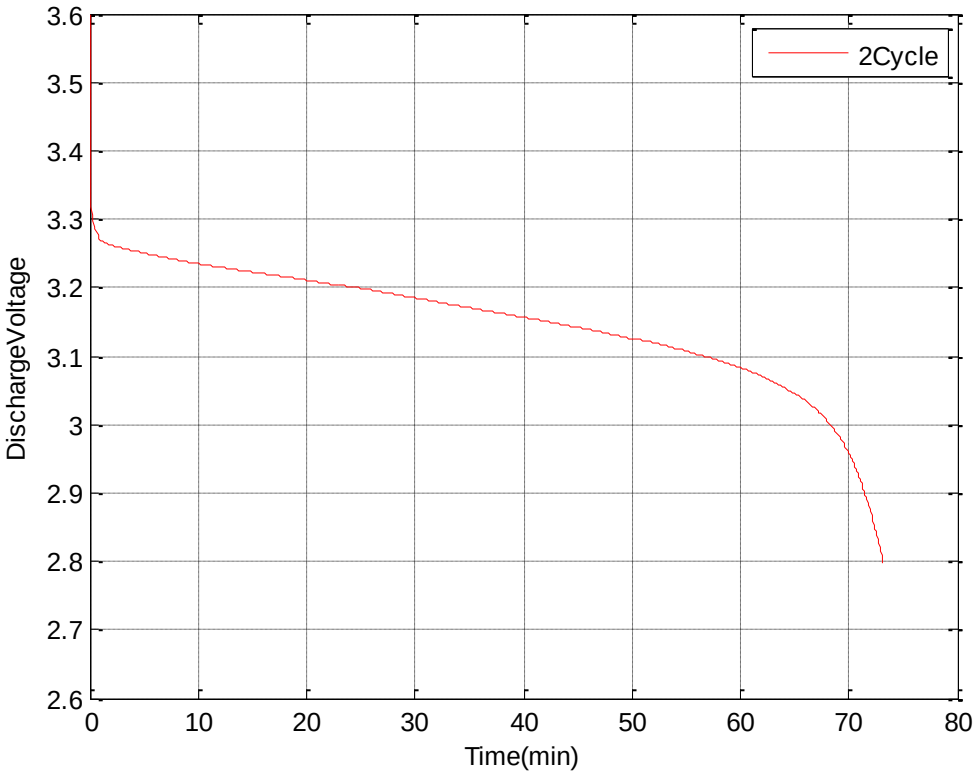

Figure 69 Voltage Change with Time

The second model is very simple compared with the first one. After discharge, we can understand the voltage varies with the time. So, we can calculate the derivative of the voltage dV/dt. The ratio of the average current (60 A) and derivative will the capacitance C (F).

The numerical model used for simulation is as follows:

$$C_T = 100 - d_T * \sqrt{N} \tag{50}$$

C_T: $Capacitance\ Retention$

d_T: $degradation\ rate$

N: Number of cycles

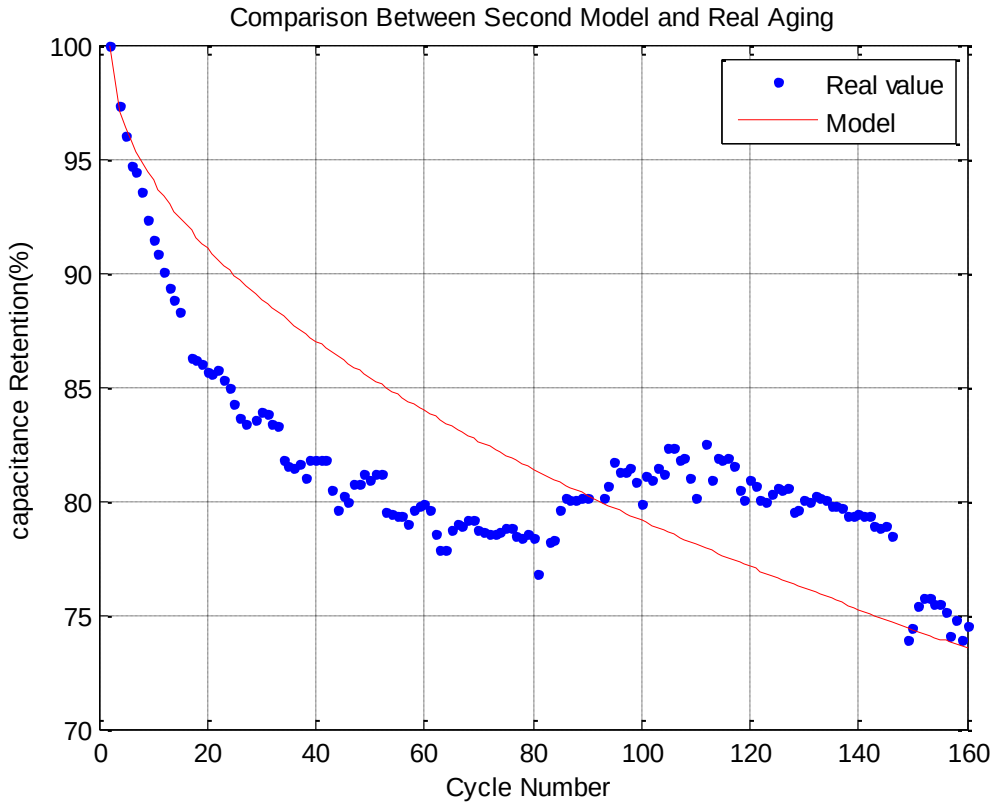

Figure 70 Comparison between second Aging Model and Real Value

The fitting parameters Dt= 2.1063

4.4. Discussion of the Results

In the real application of the electric vehicles, the energy transfer is much larger than that of daily application. From the Chapter 3, we know that literature ageing models usually referred to small cell (100mAh to 10Ah). The improvement of this thesis is to apply literature ageing models to large automotive cell. The rates current is 60 A which much higher respect to the literature paper is. During the experiment, the battery is fully discharged with the DOD is almost 100% during each cycle. So the total Ah-throughput can be 4000Ah in one week.

The aging mechanism of the TS-LFP60AHA battery depends on the life definition: we can find the speed of the capacity decreases is almost the same as that of small size batteries if we use the cycle number as the way for definition after comparison of the capacity fade shown in Figure 71 and Figure 28 (The line 90% DOD).

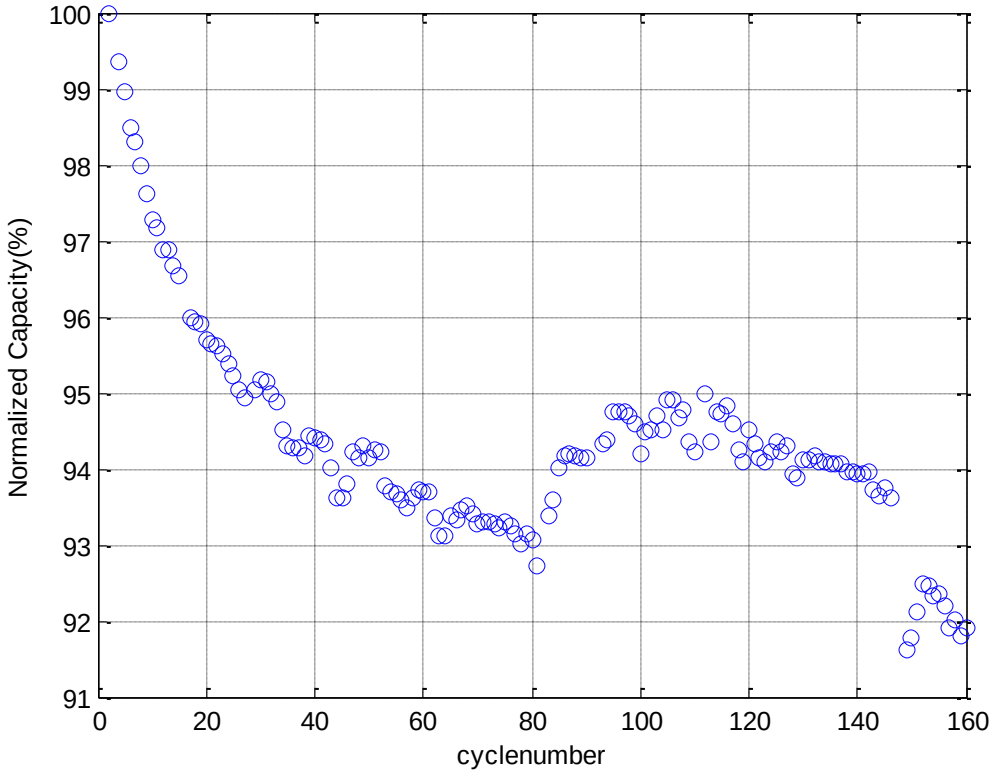

Figure 71 Capacity as a function of the cycle number

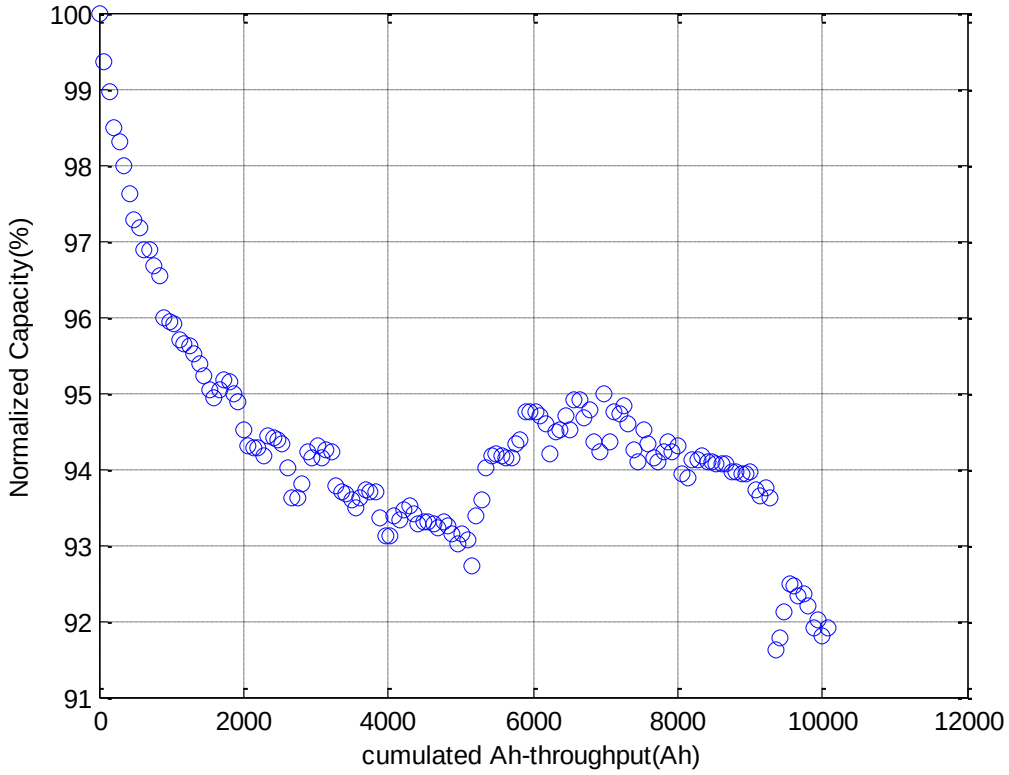

Figure 72 Capacity as a function of the cumulated Ah throughput

But if we use cumulated Ah throughput as the way for life definition, the TS-LFP60AHA Lithium-ion battery shows an excellent aging mechanism. The aging speed is quite slower than that of other batteries. In the Figure 72, we can see that the capacity decreases only 8% after reaching 10000 Ah. After prediction from the numerical models, we can find that the cumulated Ah-throughput can reach 180000 Ah when it goes to the end of life (80% of the capacity).

5. Conclusions and Recommendations

5.1 Contributions

In this work we have presented the cycling test results from a cycle life study on commercially available LiFePO4 batteries with capacity of 60Ah. The effects of test parameters (time, temperature, I, V) were investigated and described. The results show that the capacity loss is strongly affected by cycle number and Ah-throughput. Several models based on the capacity, battery efficiency, discharge ability and capacitance are developed to describe the cycle and Ah-throughput dependence of capacity fade and capacitance retention at this high current discharge-charge process under the room temperature (20 degree). In estimating capacity values, the growth rate of capacity was identified on a local basis by solving an optimization problem in which the error between estimated and calculated resistances was minimized. From the result of the fitting process, these models which are suitable for the small capacity cells also fit well in the automotive electrical propulsion cells. The capacitance retention ratio percentage decreases linearly with the root of the number of cycles and this square-root of cycle dependence is consistent with the aging mechanisms that involve diffusion and parasitic reactions leading to loss of active lithium. Concerning capacity fade, the simulation model, is able to make reliable lifetime predictions for high capacity lithium-ion cell under realistic operation condition. The predicted growth rate was then used to project the number of amp hours remaining in the life of a battery before capacity reached a predetermined threshold. Overall, we were able to establish a simple battery life model that accounts for Ah throughput (time), C-rates, and temperature and achieves qualitative agreement with experimental data. We note in closing that the model should be applicable to other lithium ion batteries as long as the aging mechanisms are similar. Experimental observations indicate a change in the decay mechanism might be operative at lower temperatures, and this remains an open question.

To be concluded, there are two major contributions of this thesis. The first is that

several models that capable of describing the ageing mechanism and making predictions of the life of a high-capacity lithium ion battery which is applied on the electrical vehicle were developed. The methodology and algorithm were developed and tested on data sets created by aging batteries under constant conditions in the Electrical Lab. Steps in the prediction process consisted of calculating battery capacity by observing battery discharge voltage under constant current steps. Although life predictions resulting from this algorithm ranged in their precision and accuracy, predictions made at the midpoint of projected battery life were generally accurate. Life predictions produced by the algorithm were promising, but varied in their accuracy and precision due to different battery internal chemistry and different working condition. The second is the analysis that came from the large scale simulations. By running the many simulation sets, a large amount of information was provided in terms of quantifying the cycle number and Ah-throughput. These large amount of data collected in this the experiment can be regarded as the reference of the following experiments and his work will bring a good start for the research of lithium-ion for electrical vehicles in Polytechnic of Milan.

5.2 Future Work

It has to be kept in mind that the results presented here are only valid for the specific cell considered in this work. The results cannot be transferred to other cells with different chemistry. In future, batteries with different kind of chemistry will be applied with the same methodology to find the best and most suitable Lithium-ion battery for the electrical vehicle.

Secondly, in our experiment, we didn't consider the influence of the temperature. All the test were completed in the room temperature and the temperature of the system especially the battery temperature fluctuated during charging and discharging, so the generation rate of the SEI (solid electrolyte interphase) will be different during one cycle. In the future, the heating chamber will be developed to fix the working temperature. As everyone knows the temperature has a very great on the aging mechanism: high temperature means accelerated aging. My work will be the reference of the future work in 60 and 0 degree.

Thirdly, which is also very important for the test, the test doesn't take consideration of the real condition. The entire test is under constant current (CC) condition. But in the real application of the electrical vehicle, the current will be different under various working condition. In the following test, the current will be varying during a complete cycle. The profile of the current should be decided carefully to make sure the experiment coincident with real situation.

Acronyms

AI: Analog input

ANN: Artificial Neural Network

AO: Analog output

BSF: Battery Size Factor

CC: Constant Current

CV: Constant Voltage

DI: Digital input

DOD: Depth of Discharge

DO: Digital output

ECM: Equivalent Circuit Model

EOL: End of Life

EV: Electrical Vehicle

EVB: Electrical Vehicle Battery

HEV: Hybrid Electrical Vehicle

LCA: Life Cycle Assessment

LIB: Lithium Ion Battery

NE: No Explosion

NL: No Leakage

OCV: Open Circuit Voltage

OVP: over voltage protection

PHEV: plug-in hybrid electric vehicle

SOC: State of Capacity

SOH: State of Health

SEI: Solid Electrolyte Interphase

UVL: Under Voltage Limit

Reference

[1] E. Prada, D. Di Domenico, Y. Creff. Physics-based modelling of LiFeP04-graphite Li-ion batteries for Power and Capacity fade predictions: Application to calendar aging of PHEV and EV. 2012 IEEE Vehicle Power and Propulsion Conference, Oct. 9-12, 2012, Seoul, Korea

[2] J. Vetter, P. Novak, M.R. Wagner. Ageing mechanisms in lithium-ion batteries. Journal of Power Sources 147 (2005) 269–281

[3] INTERNATIONAL STANDARD IEC 60086-5 Primary batteries – Part 5: Safety of batteries with aqueous electrolyte

[4] IEC 61982-3 Secondary batteries for the propulsion of electric road vehicles-
Part 3: Performance and life testing（traffic compatible，urban use vehicles）

[5] http://www.ni.com/pdf/manuals/372121f.pdf BNC 2110 Manual

[6] C.C. O'Gorman, D. Ingersoll, R.G. Jungst, T.L. Paez, "Artificial neural network simulation of battery performance", System Sciences, 1998., Proceedings of the Thirty-First Hawaii International Conference on Volume 5, 6-9 Jan. 1998, pp. 115-121, vol.5.

[7] Ahmed Fasih. Modeling and Fault Diagnosis of Automotive Lead-Acid Batteries. The Ohio State University.

[8] S. Liu, R. Dougal, J. Weidner, L. Gao. A simplified physics-based model for nickel hydrogen battery, Journal of Power Sources, Vol. 141, Issue: 2, March 1, 2005. pp. 326-339.
[9] Benjamin J. Yurkovich, B.S. Electrothermal Battery Pack Modeling and Simulation. Master's Examination Committee

[10] Alexander K Suttman. ‘Lithium Ion Battery Aging Experiments and Algorithm Development for Life Estimation’ The Ohio State University. 2007

[11] Sauer, Dirk U., and Heinz Wenzl. "Comparison of Different Approaches for Lifetime Prediction of Electrochemical Systems - Using Lead-acid Batteries as Example." Journal of Power Sources 176.2: 534-46. ScienceDirect.
Web<http://www.sciencedirect.com/science/article/pii/S0378775307016199>.

[12] Nick Picciano. Battery Aging and Characterization of Nickel Metal Hydride and Lead Acid Batteries. Master’s Thesis. The Ohio State University. 2007

[13] http://www.ecoinvent.org/database/

[14] Z. Chehab, ‘Aging Characterization of NiMH Batteries for Hybrid Electric Vehicles’. Master’s Thesis. The Ohio State University. 2006.

[15] Precision LCR Meter-800 User Manual

[16] George Feldman, Dr.Hong Shih. Electrochemical impedance Spectroscopy for battery research and development. Technical Report 31, Solartron analytical

[17] Mats Zackrisson, Lars Avellán, Jessica Orlenius. Life cycle assessment of lithium-ion batteries for plug-in hybrid electric vehicles - Critical issues. Journal of Cleaner Production 18 (2010) 1519e1529

[18] E. Pradai, D. Di Domenico, Y. Creff, J. Bernard, V. Sauvant-Moynot, F. Huet2. Physics-based modeling of LiFeP04-graphite Li-ion batteries for Power and Capacity fade predictions: Application to calendar aging of PHEV and EV. 2012 IEEE Vehicle Power and Propulsion Conference, Oct. 9-12, 2012, Seoul, Korea

[19] Lorenzo Serrao, Zakaria Chehab, Yann Guezennec, Giorgio Rizzoni. An Aging Model of Ni-MH Batteries for Hybrid Electric Vehicles. 0-7803-9280-9/05 ©2005 IEEE.

[20] Madeleine Ecker, Jochen B. Gerschler, Jan Vogel, Stefan Kabitz, Friedrich Hust, Philipp Dechent, Development of a lifetime prediction model for lithium-ion batteries based on extended accelerated aging test data. Journal of Power Sources 215 (2012) 248e257

[21] A. Cherif, M. Jraidi, A. Dhouid. A battery ageing model used in stand along PV system. Journal of Power Sources 112 (2002) 49-53

[22] Tarun Huria, Massimo Ceraolo, Javier Gazzarri, Robyn Jackey. High Fidelity Electrical Model with Thermal Dependence for Characterization and Simulation of High Power Lithium Battery Cells. 978-1-4673-1561-6/12/$31.00 ©2012 IEEE

[23] M. Broussely, Ph. Biensan, Bonhomme, Ph. Blanchard, S. Herreyre, K. Nechev, R.J. Staniewicz. Main aging mechanisms in Li ion batteries, Journal of Power Sources 146 (2005) 90–96

[24]K. Suzuki, MBI, Abstracts, in: Proceedings of the 44th Battery Symposium, Saka¨ı, 2003).

[25] http://www.sinopolybattery.com/ClientResources/201203261550172.pdf

[26] Programmable DC Power Supplies, Document: 83-530-000 Rev G, TDK-Lambda Americas Inc. High Power Division

[27] Uwe Troltzsch, Olfa Kanoun, Hans-Rolf Trankler, Characterizing aging effects of lithium ion batteries by impedance spectroscopy. Electrochimica Acta 51 (2006) 1664–1672

[28] Ferdinando Luigi Mapelli and Davide Tarsitano. Modeling of Full Electric and Hybrid Electric Vehicles Chapter7. http://dx.doi.org/10.5772/53570 INTECH

[29] NJOYA MOTAPON. Souleman. A GENERIC FUEL CELL MODEL AND EXPERIMENTAL VALIDATION. Master Thesis of ECOLE DE TECHNOLOGIE SUPERIEURE

[30] Yiran Hu, M.S. Identification and State Estimation for Linear Parameter Varying Systems with Application to Battery Management System Design. DISSERTATION of Ohio State University

[31] A. Jossen, "Fundamentals of battery dynamics", Journal of Power Sources, Vol. 154, Issue: 2, March 21, 2006. pp. 530-538.

[32] Gamry Instruments, “Electrochemical Impedance Spectroscopy Theory: A Primer.” Online. http://www.gamry.com/App_Notes/EIS_Primer/EIS_Primer.htm

[33] I. Bloom, B.W. Cole, J.J. Sohn, S.A. Jones, E.G. Polzin, V.S. Battaglia, G.L. Henriksen, C. Motloch, R. Richardson, T. Unkelhaeuser, D. Ingersoll, H.L. Case, J. Power Sources 101 (2001) 238.

[34] John Wang, Ping Liu, Jocelyn Hicks-Garnera. Cycle-life model for graphite-LiFePO4 cells. Journal of Power Sources 196 (2011) 3942–3948

[35] J. P. Fellner, G. J. Loeber, S. P. Vukson, and C. A. Riepenhoff, “Lithiumion testing for spacecraft applications,” J. Power Sources, vol. 119–121, pp. 911–913, Jun. 2003.

[36] X. Wang, Y. Sone, and S. Kuwajima, “Effect of operation conditions on simulated low-Earth orbit cycle-life testing of commercial lithiumion polymer cells,” J. Power Sources, vol. 142, no. 1/2, pp. 313–322, Mar. 2005.

[37] Masatoshi Uno, Member, IEEE, and Koji Tanaka Accelerated Charge–Discharge Cycling Test and Cycle Life Prediction Model for Supercapacitors in Alternative Battery Applications. IEEE TRANSACTIONS ON INDUSTRIAL ELECTRONICS, VOL. 59, NO. 12, DECEMBER 2012

[38] H. Yoshida, N. Imamura, T. Inoue, K. Takeda, and H. Naito, “Verification of life

estimation model for space lithium-ion cells," Electrochemistry, vol. 78, no. 5, pp. 482–488, 2010.

[39] S. Brown, K. Ogawa, Y. Kumeuchi, S. Enomoto, M. Uno, H. Saito, Y. Sone, D. Abraham, and G. Lindbergh, "Cycle life evaluation of 3 Ah LixMn2O4-based lithium-ion secondary cells for low-Earth-orbit satellites," J. Power Sources, vol. 185, no. 2, pp. 1444–1464, Dec. 2008.

[40] Y. Mita, S. Seki, N. Terada, N. Kihira, K. Takei, and H. Miyashiro, "Accelerated test methods for life estimation of high-power lithium-ion batteries," Electrochemistry, vol. 78, no. 5, pp. 382–386, 2010.

[41] Masatoshi Uno and Koji Tanaka Accelerated Ageing Testing and Cycle Life Prediction of Supercapacitors for Alternative Battery Applications. 978-1-4577-1250-0/11/$26.00 .2011 IEEE

[42] Y.T. Cheng, M.W. Verbrugge, J. Appl. Phys. 104 (2008) 6.

[43]California Motors, "Hybrid systems: glossary of terms." Online. http://www.calmotors.com/faqs_glossary.html

[44] Githin K. Prasad, Christopher D. Rahn Model based identification of aging parameters in lithium ion batteries. Journal of Power Sources 232 (2013) 79e85

[45] K. Suzuki, MBI, Abstracts, in: Proceedings of the 44th Battery Symposium, Saka¨ı, 2003).

Acknowledgements

Firstly and fore mostly, I am most grateful to my supervisor, Professor Francesco Braghin, Davide Tarsitano and Ferdinando Mapelli, whose useful suggestions, incisive comments and constructive criticism have contributed greatly to the completion of this thesis. They devoted a considerable portion of time to reading my manuscripts and making suggestions for further revisions. His tremendous assistance in developing the framework for analysis and in checking the draft versions of this thesis several times as well as his great care in this work deserve more thanks than I can find words to express.

I am also greatly indebted to all the teachers or staffs who have helped me directly and indirectly in this work. Any progress that I have made is the result of their profound concern and selfless devotion.

Thank you all very much!

Appendix A-Main Program

```
%%%%%%%%%%%%%%%%%%%%%%%%%%%%%%%%%%%%%%%%%%
%%%%%%%%%%%%%%%%%%%%%%%%%%%
% Name: Zhi Zhang
% Matricola: 780987
% Professor: Francesca Braghin, Davite Tarsitano
% Department: Mechanical Engineering
%%%%%%%%%%%%%%%%%%%%%%%%%%%%%%%%%%%%%%%%%%
%%%%%%%%%%%%%%%%%%%%%%%%%%
%% Start
if exist('s1')==1
    if length(s1.Status)==4
         fclose(s1);
    end
end                                         % Clear status.Set FEVE and SEVE registers
to zeros
clear all
close all
clc
%% Fixed Parameters Defined
global AI channels offset sens Realtime averagevalue k act_time name tp i
Sampling_frequency=1000;                    % Sampling frequency 1000Hz
Aqtime=1;                                   % Time for Acquiring Data
tp=5;                                       % For each time section ,we should have an
average value
Sampling_number=Aqtime*Sampling_frequency; % Sampling number needed to have
an average value
```

```
current=60;                                % Fixed Current 70A;the setting current should be between 40-110A ,the maximum current can be 120A
V_elementl=2.8;                            % Set the lowest voltage
V_elementh=3.8;                            % Set the highest voltage
Resttime=10;                               % minutes, Time between charge and discharge
Ncycle=1000;                               % Number of cycle we need to apply on the battery
channels=5;                                % Number of channels I need
Voltage_output=7.5;                        % Voltage controled during discharge
name={'V [V]','I [A]','heatsink temperature [ ℃]','air temperature [ ℃]','battery temperature [ ℃]'};
averagevalue=zeros(1,channels);
sens=ones(size(name))';                    % Sensitivity
sens(1)=1;                                 % A/V
sens(2)=100/.8438;                         % gradi/V
sens(3:5)=100;                             % gradi/V
offset=[0 2.5 2.73 2.73 2.73 ];            % Offset=Gain
%% Serial Port Setting
s1=serial('COM1');                         % generation of the serial port
s1.BaudRate =9600;                         % Baudrate
s1.Terminator='LF';                        % resets the terminator
s1.DataBits=8;                             % 8 bit of data
s1.Parity='none';                          % none parity
s1.StopBits=1;                             % one stop bit
s1.InputBufferSize=25;                     % input buffer size
s1.Timeout=6;                              % 6 seconds of the time out if it doesn't receive data
%% Serial Port communication
```

```
fopen(s1);                                  % Start the serail port communication
buffer=['ADR 06' 13];                       % Choose the address 6
fprintf(s1,buffer);
pause(1);
%% AnalogInput Setting
AI = analoginput('nidaq',1);                % build the object of signal
chan=addchannel(AI,[0:channels-1],name);    % Add channels-Add one channel to AI
set(AI,'SampleRate',Sampling_frequency)     % set sampling frequency as 8000Hz
ActualRate=get(AI,'SampleRate');            % Actual sampling frequency from AI
set(AI,'TriggerType','immediate')           % use matlab to start trigger,it's also possible
to start manual
set(AI,'timeout',40)
set(AI,'SamplesPerTrigger',Sampling_number)% Set sampling number ,we can use this
to deal with sample time
set(AI,'InputType','SingleEnded');

%% AnalogOutput Setting
AO = analogoutput('nidaq',1);               % build the object of signal
chan_out=addchannel(AO,0);
set(AO,'SampleRate',Sampling_frequency)     % Sampling frequency is 1000Hz
set(AO,'timeout',20)
putdata(AO,0)
start(AO) % start output analog signal

for i=1:Ncycle
%% Discharge phase
averagevalue(1)=4.2;                        % initial value set
k=1;
figure(1),subplot 211,hold on    % plot figure
```

```
nomefigure=sprintf('Cycle %04d',i);
title([nomefigure])
disp('discharge phase')
tic                                          % time beginning
act_time=toc;
% buffer=['OUT 1' 13];
% fprintf(s1,buffer);
% pause(1);
% buffer=['PV 2.5' 13];
% fprintf(s1,buffer);
while averagevalue(k,1)>V_elementl
      Monitor;
      current_measure=(averagevalue(k,2));
      error=current-current_measure;
if error>5
    Voltage_output=Voltage_output+.1;
end
if error>1&&error<=5
    Voltage_output=Voltage_output+.02;
end
if error<-5
    Voltage_output=Voltage_output-.1;
end
if error<-1&&error>=-5
    Voltage_output=Voltage_output-.02;
end
if Voltage_output>8.5
    Voltage_output=8.5;
end
```

```
%          Voltage_output=5.5;
disp([current_measure Voltage_output]);
      putsample(AO,Voltage_output)
end
stop(AO)   % stop output analog signal
figure(1)
subplot 211
plot([act_time/60 act_time/60],[V_elementl V_elementh],'color',[1 0 0],'linewidth',2)
subplot 212
plot([act_time/60 act_time/60],[-current current],'color',[1 0 0],'linewidth',2)

%% Rest phase
putdata(AO,0)
start(AO)
Discharge_stop_time=toc;
clc
disp('Rest phase')
while (toc-Discharge_stop_time)<Resttime*60
         Monitor;
end
stop(AO)
figure(1)
subplot 211
plot([act_time/60 act_time/60],[V_elementl V_elementh],'color',[1 0 0],'linewidth',2)
subplot 212
plot([act_time/60 act_time/60],[-current current],'color',[1 0 0],'linewidth',2)
%% Charger phase
buffer=['OUT 1' 13];                    % Turn On
fprintf(s1,buffer);pause(.2);
```

```
buffer=['PV 5.5' 13];                    % Voltage set 2.5 Volts
fprintf(s1,buffer);pause(.2);
buffer=['PC 60' 13];                     % Current 50 A
fprintf(s1,buffer);pause(.2);
clc
disp('Charge phase')

while averagevalue(k,1)<V_elementh
    disp(averagevalue(k,1))
    Monitor;
end
buffer=['PC 0' 13];                      % Current 50 A
fprintf(s1,buffer);pause(.2);
buffer=['OUT 0' 13];                     % Turn On
fprintf(s1,buffer);pause(.2);
stop(AO)
%% Rest phase
figure(1)
subplot 211
plot([act_time/60 act_time/60],[V_elementl V_elementh],'color',[1 0 0],'linewidth',2)
subplot 212
plot([act_time/60 act_time/60],[-current current],'color',[1 0 0],'linewidth',2)
putdata(AO,0)
start(AO)
Charge_stop_time=toc;
clc
disp('Rest phase')
buffer=['OUT 0' 13];                     % Turn Off the system
fprintf(s1,buffer);
```

```
while (toc-Charge_stop_time)<Resttime*60
        Monitor;
end
stop(AO)
clc
disp('one cycle finish')
nomefile=sprintf('%04d%05ds',i);
% nomefile=sprintf(i);
save([nomefile],'Realtime','averagevalue');
close all
end
```

Appendix B- Monitoring

```
function [values]=Monitor()
global AI channels offset sens Realtime averagevalue k act_time name tp
    k=k+1;
    if k>1
        while ((toc-act_time)<=(tp))
        end;
    end
        act_time=toc;
    start(AI);
    try
        [data1,time]=getdata(AI);              % Save the data in the data1 and time
    catch
          time=0;data1=0;
          disp('A timeout occurred')
    end
    stop(AI);
    values=zeros(size(data1));
    for ii=1:channels
        values(:,ii)=(data1(:,ii)-offset(ii))*sens(ii);
    end
        averagevalue(k,:)=mean(values);
    Realtime(k,1)=act_time;                    % Build the table to save the data
    figure(1)
    subplot 211
    minute=act_time/60;
    plot(minute,averagevalue(k,1),'o');
```

```
legend((name(1)'),2),grid on, hold on
xlabel('Time [min]')
    subplot 212
plot(minute,averagevalue(k,2:end),'o');
legend((name(2:end)'),2),grid on, hold on
    xlabel('Time [min]')
```

Appendix C- Data Analysis Program

```
clc
close all
clear all
global Temperature_Average Gas_constant Activation_Energy
file_name=0;
Cycle=0;
DischargeCurve=[1,10,16];
a_line=['r','g','b','y','c','m','k','.','o','x','+','s','d','r','g','b','y','c','m','k'];
line_index=1;
disp('The Following Cycles are Missing')
%% Read Data
while (file_name<16)

    Cycle=Cycle+1;
    while 1
        file_name=file_name+1;
         nomefigure=sprintf('%04d%05ds',file_name);
         file_exist_flag=exist([pwd '\' num2str(nomefigure),'.mat']);
          if file_exist_flag==2
              break
          else
              disp(file_name)
          end
    end
load(nomefigure)
Cyclenumber(Cycle)=file_name;
```

```
RestTime=10;
ElectricQuantity=60;
NominalVoltage=3.2;
RelatedEnergy=ElectricQuantity*NominalVoltage;
Activation_Energy=31500; % J/mol
Gas_constant=8.314472; %J/(K*mol)
Temperature_Average=293;
%% Basic Imformation
NumData=length(Realtime);
Voltage=averagevalue(:,1);
Current=averagevalue(:,2);
Heatsink_temperature=averagevalue(:,3);
Air_temperature=averagevalue(:,4);
Battery_temperature=averagevalue(:,5);
Time=Realtime;
% figure(1)
% subplot 211
% plot(Time/60, Voltage)
% title('Voltage Variation of one cycle')
% xlabel('Time')
% ylabel('Voltage')
% grid on
% subplot 212
% plot(Time/60,Current)
% title('Current Variation of one cycle')
% xlabel('Time')
% ylabel('Current')
% grid on
%
```

```
% figure(1)
% subplot 211
% plot(Time/60, Heatsink_temperature-Air_temperature)
% title('Difference between heatsink and air temperature')
% xlabel('Time(min)')
% ylabel('Temperature')
% grid on
% subplot 212
% plot(Time/60,Battery_temperature-Air_temperature)
% title('Difference between battery and air temperature')
% xlabel('Time(min)')
% ylabel('Temperature')
% grid on
%% Phase Identification
j=1;
while Voltage(j)>2.8
        j=j+1;
end
Time_Discharge=Time(1:j);
Discharge=Voltage(1:j);
Discharge_Current=Current(1:j);
Discharge_Heatsink_temperature=Heatsink_temperature(1:j);
Discharge_Air_temperature=Air_temperature(1:j);
Discharge_Battery_temperature=Battery_temperature(1:j);
k=j;
% for time=1:length(Time_Discharge)-1

C(time)=-Discharge_Current(time)/(Discharge(time+1)-Discharge(time))*(Time_Disch
arge(time+1)-Time_Discharge(time))/3600;
```

```
% end
% Capacitance(Cycle)=mean(C(400:end));
for time=1:length(Time_Discharge)-1
C(time)=-(Discharge(time+1)-Discharge(time))/(Time_Discharge(time+1)-Time_Disch
arge(time))*3600;
end
Capacitance(Cycle)=mean(Discharge_Current)/mean(C);
while Time(j)-Time(k)<RestTime*60
    j=j+1;
end
Time_FirstRest=Time(k+1:j)-Time(k+1);
FirstRest=Voltage(k+1:j);
FirstRest_Current=Current(k+1:j);
FirstRest_Heatsink_temperature=Heatsink_temperature(k+1:j);
FirstRest_Air_temperature=Air_temperature(k+1:j);
FirstRest_Battery_temperature=Battery_temperature(k+1:j);
k=j;
while Voltage(j)<3.8
    j=j+1;
end
Time_Charge=Time(k+1:j)-Time(k+1);
Charge=Voltage(k+1:j);
Charge_Current=Current(k+1:j);
Charge_Heatsink_temperature=Heatsink_temperature(k+1:j);
Charge_Air_temperature=Air_temperature(k+1:j);
Charge_Battery_temperature=Battery_temperature(k+1:j);
Time_SecondRest=Time(j+1:NumData)-Time(j+1);
SecondRest=Voltage(j+1:NumData);
SecondRest_Current=Current(j+1:NumData);
```

```
SecondRest_Heatsink_temperature=Heatsink_temperature(j+1:NumData);
SecondRest_Air_temperature=Air_temperature(j+1:NumData);
SecondRest_Battery_temperature=Battery_temperature(j+1:NumData);
figure (2)
set(gca,'ylim',[2.6,3.6]);
grid on
DischargeCurve=sortrows(DischargeCurve')';
for i=1:length(DischargeCurve)
    if file_name==DischargeCurve(i)
        plot(Time_Discharge/60,Discharge,a_line(line_index),'Markersize',1)

        line_index=line_index+1;
        hold on
    end
end
%
% figure(2)
%
% subplot 211
% plot(Time_Discharge/60,Discharge)
% xlabel('Time(min)')
% ylabel('Discharge Voltage')
% title('Discharge')
% grid on
% subplot 212
% plot(Time_Charge/60,Charge)
% xlabel('Time(min)')
% ylabel('Charge Voltage')
% title('Charge')
```

```
% grid on
%
% figure(3)
% grid on
% subplot 211
% plot(Time_FirstRest/60,FirstRest)
% xlabel('Time(min)')
% ylabel('First Rest Voltage')
% title('First')
% grid on
%
% subplot 212
% plot(Time_SecondRest/60,SecondRest)
% xlabel('Time(min)')
% ylabel('Second Rest Voltage')
% title('Second Rest')
% grid on
%% SOC and DOD
SOC_Discharge=zeros(length(Time_Discharge),1);
DOD_Discharge=zeros(length(Time_Discharge),1);
for i=1:length(Time_Discharge)-1
    Power=(Time_Discharge(i+1)-Time_Discharge(i))*Discharge_Current(i)/3600;
    DOD_Discharge(i+1)=DOD_Discharge(i)+Power;
end
SOC_Discharge=(ElectricQuantity-DOD_Discharge)/ElectricQuantity*100;
Ah_thoughput(Cycle)=DOD_Discharge(end);
% figure (4)
% plot(Time_Discharge/60,SOC_Discharge)
% title('SOC')
```

```
% xlabel('Time')
% ylabel('SOC')
% grid on
SOC_Charge=zeros(length(Time_Charge),1);
DOD_Charge=zeros(length(Time_Charge),1);
for i=1:length(Time_Charge)-1
    Power=-(Time_Charge(i+1)-Time_Charge(i))*Charge_Current(i)/3600;
    DOD_Charge(i+1)=DOD_Charge(i)+Power;
end
SOC_Charge=(ElectricQuantity-DOD_Charge)/ElectricQuantity*100;
% figure (4)
% plot(Time_Charge/60,SOC_Charge)
% title('SOC')
% xlabel('Time')
% ylabel('SOC')
% grid on
%% Energy Analysis
Energy_Discharge=0;
for i=1:length(Time_Discharge)-1
Energy_Discharge=Energy_Discharge+(Time_Discharge(i+1)-Time_Discharge(i))*Dis
charge_Current(i)/3600*Discharge(i);
end
Energy_Charge=0;
for i=1:length(Time_Charge)-1
Energy_Charge=Energy_Charge+(Time_Charge(i+1)-Time_Charge(i))*Charge_Current
(i)/3600*Charge(i);
end
Ratio_DC(Cycle)=-Energy_Discharge/Energy_Charge;
% disp('the ratio between discharged energy and charged energy')
```

```
% disp(Ratio_DC)
Ratio_DR(Cycle)=Energy_Discharge/RelatedEnergy;
% disp('the ratio between discharged energy and Related energy')
% disp(Ratio_DR)
end
for i=1:length(DischargeCurve)
        str{1,i}=([num2str(DischargeCurve(i)),'Cycle']);
end
figure(2)
legend(str);
xlabel('Time(min)')
ylabel('DischargeVoltage')
figure(4)
plot(Cyclenumber,Ratio_DR)
xlabel('number of cycles')
ylabel('capacity Retention')
title('Aging Model')
grid on
%% Numerical Modeling 1
CapacitanceRatio=Capacitance/Capacitance(1)*100;
Strarting=rand(1,1)*100;
options=optimset('MaxFunEvals',10000);
Estimates1=fminsearch(@myfit,Strarting,options,Cyclenumber,CapacitanceRatio);
figure(5)
plot(Cyclenumber,CapacitanceRatio,'o')
hold on
R_real=100-Estimates1*(Cyclenumber-1).^0.5;
plot(Cyclenumber,R_real,'r')
legend('Real value','Model')
```

```
xlabel('Cycle Number ')
ylabel('capacitance Retention(%)')
title('Comparison Between First Model and Real Aging')
grid on
%% Numerical Modeling 2
Ratio_DD=abs(100-Ratio_DR/Ratio_DR(1)*100);
cum_Ah_thoughput(1)=Ah_thoughput(1);
for i=2:length(Ah_thoughput)
    cum_Ah_thoughput(i)=Ah_thoughput(i)+cum_Ah_thoughput(i-1);
end
cum_Ah_thoughput=cum_Ah_thoughput-cum_Ah_thoughput(1);
Strarting=rand(2,1)*100;
options=optimset('MaxFunEvals',10000);
Estimates2=fminsearch(@myfit2,Strarting,options,
log(cum_Ah_thoughput(2:end)),log(Ratio_DD(2:end)));
figure(6)
plot(log(cum_Ah_thoughput(2:end)),log(Ratio_DD(2:end))+Activation_Energy/(Gas_c
onstant*Temperature_Average),'o')
hold on
plot(log(cum_Ah_thoughput(2:end)),Estimates2(1)*log(cum_Ah_thoughput(2:end))+lo
g(Estimates2(2)),'r')
legend('Real value','Model',2)
xlabel('Ah thoughout ')
ylabel('log(Q_loss)+E/(R*T)')
title('Comparison Between Second Model and Real Aging')
grid on
```

Appendix D-Fitting Program of 2Models

```
function sse=myfit(params,Input,Actural_Output)

dT=params(1);

Fitted_Curve=100-dT*(Input-1).^0.5;

Error_Vector=Fitted_Curve-Actural_Output;

sse=sum(Error_Vector.^2);

function sse=myfit2(params,Input,Actural_Output)

global Temperature_Average Gas_constant Activation_Energy

z=params(1);

B=params(2);

Fitted_Curve=log(B)-Activation_Energy/(Gas_constant*Temperature_Averag
e)+z*Input;

Error_Vector=Fitted_Curve-Actural_Output;

sse=sum(Error_Vector.^2);
```